THE RELATIONSHIP BETWEEN STRUCTURAL PARAMETERS AND MECHANICAL PROPERTIES OF CACTUS SPINES

A Senior Project

Presented to the Faculty of the Materials Engineering Department

California Polytechnic State University, San Luis Obispo

In Partial Fulfillment

of the Requirements for the Degree

Bachelor of Science, Materials Engineering

Authors:

Jorge Martinez, Theresa Stewart, Pamela Szeto

June 2017

ABSTRACT

Considering an increasing interest in renewable, biodegradable resources that exhibit excellent mechanical properties, 24 species of cactus spines were investigated using three-point bend testing, X-ray diffraction (XRD) for structural parameters, and scanning electron microscopy (SEM) to analyze fracture surfaces. Additionally, a density of about 1.3 g/cm^3 was measured for each spine utilizing the displacement method, closely matching existing data from literature. The flexural modulus varied greatly between species, ranging from 1.22 GPa (*Echinocactus polycephalus*) to 43.58 GPa (*Stenocereus thurberi*). In addition, flexural strength and strain to failure was also measured for each spine. XRD analysis of the spines was used to find the degree of crystallinity and the multifibrillar angle (MFA). The degree of crystallinity for most species ranged from 20-60% with two species ranging above 65%. MFA, which is a measurement of the divergence of the fiber angle from the central axis of the spine, ranged from 1-2.5°; this showed a consistent high degree of alignment of the cellulose fibers, despite the wide range and relatively low values of crystallinity. Examining the trends between mechanical properties, degree of crystallinity, and MFA showed no significant correlation, but it is possible that the crystallinity and MFA have a combined effect on these properties rather than individual effects. It was seen, however, that there is a trend of decreasing resiliency in larger spines due to an increased number of defects. Comparisons were made with engineering materials, such as fiberglass, and it was found that the resiliency of most cactus spines was comparable or superior to those materials.

Keywords:

Cactus spines, crystallinity, multifibrillar angle, flexural strength, flexural stiffness, three-point bend test, fracture surfaces, natural composites, arabinan-cellulose composites, resiliency, materials engineering

ACKNOWLEDGEMENTS

We would like to thank our advisor, Dr. Trevor Harding, for his guidance on this project and for supplying samples for testing. Additionally, we would like to thank the other students who have contributed to testing for this project in the past and the development of testing procedures, as well as the faculty of the MatE department for training and access to the equipment.

TABLE OF CONTENTS

LIST OF FIGURES

LIST OF TABLES

1.0 INTRODUCTION

1.1 | Background

Need For Renewable Resources

With the increasing problem of pollution, there is a need for finding sustainable and environmentally friendly biodegradable materials. Non-renewable resources are depleting at a faster rate than they are produced. Conventional materials require large amounts of energy from extraction to production and do not degrade, thus increasing waste in the landfill. Additionally, many materials in use today, especially polymers, cannot be disposed of in an environmentally friendly way. Commodity polymers, which make up 98% of all polymers used in daily life, are based on non-renewable fossil fuels and do not degrade in nature.

Global production of petroleum-based plastics is continuously rising each year and since they are not renewable they constantly end up in landfills and oceans. According to the United Environmental Program it is estimated that between 22 percent to 43 percent of plastic used worldwide is disposed of in landfills. In addition, approximately 10 to 20 million tons of plastic end up in oceans each year [1]. There is a focus on minimizing pollution by recovering plastic through recycling but it is not sustainable because plastic production rates outweigh their recycling rates. Poor environmental regulations may also lead to incineration of plastics for their energy in power plants, leading to toxic air pollution. There is a need to reduce unnecessary plastic consumption, find more environmentally friendly alternatives, improve product packaging to use less plastic, and if possible, replace the product with more sustainable materials.

Biodegradable Materials

Currently, there is a drive within the scientific community to produce more sustainable alternatives to replace conventional materials. The largest potential for this is seen in polymers, for which a variety of biodegradable and bio-based polymers have been either synthesized or modified from natural materials. The goal is to find biodegradable (degrades quickly in nature) and bio-based (produced from natural, renewable resources) materials that do not require toxic chemicals to produce and have properties that can compete with conventional materials.

Some materials are biodegradable and come from renewable sources, however, they may not be ideal choices due to other competing factors. For instance, corn-based materials such as polylactic acid are renewable, but not highly sustainable because corn is also a food product, thus both markets compete with one another. Additionally, bio-materials cannot be sustainable if they are being depleted faster than they are being produced. Finding a material that satisfies these requirements is difficult, but not impossible.

1.2 | Natural Composites

One potential area of interest in sustainable materials is natural composites. Natural composites occur in both animals and plants, and like synthetic composites, obtain significantly improved properties by the arrangement of different natural polymers. One family of natural composites that has been studied due to its structural properties is the family of wood materials.

Wood materials have high strength in tension and compression since they consist of fibers embedded in a matrix. Specifically, the strength in wood materials comes from the arrangement of cellulose fibers surrounded by hemicellulose and lignin that bind fibers together. These cellulose fibers in wood are also seen in cotton, however, binding agents are not present in cotton, therefore making it much weaker.

In addition to wood, a similar material that may be of interest as a structural and natural composite is a cactus spine. Cactus spines also get their strength from cellulose fibers, but unlike wood, spines contain 50% arabinan, whereas wood contains 25% lignin and a remaining 25% from non-structural polysaccharides [2, 3, 4]. So far, very little research has been conducted on the structure and properties of cactus spines, and what research that has been done, has only been conducted on two species of cacti.

1.3 | Plant Spines in Nature

Plant spines are dry, hardened structures that are present in a variety of plants [5], but are most well known as the sharp needles in most species of cacti. Spines are an important structural element in cacti as well as other plants, and also serve a number of other biological roles, such as water absorption, seed dispersal, camouflage, and protection from herbivores [6, 7].

Spines are a specially evolved form of a leaf with a reduced surface area designed to reduce the amount of water lost due to evaporation [8]. Unlike regular leaves, spines have no guard cells, stomata, hypodermis, chlorenchyma, or vascular tissue [9, 10]. Additionally, cactus spines use only the arabinan form of hemicellulose as a binding agent [2]. This separates spines from wood materials, which use different forms of hemicellulose and lignin as binding agents. Spines grow from an axillary bud which vacillates and elongates into the spine shape. A fully-grown spine can be divided into three regions: the basal meristem, the zone of elongation, and the apical zone composed of dead mature lignified fibers [10, 11].

Cactus spines vary greatly by species in their size, number, color, and texture. Across and within the species, the shape of the spine can range from being curved, straight, or hooked (Fig. 1). Similarly, the cross-section of the spine is either circular or not [10]. Additionally, some spines are coated in “hair-like” trichomes, which function similarly to cactus spines, while others are not (Fig. 2). With so much variation between spines of different species, more studies are needed to understand how the properties and structures vary across species.

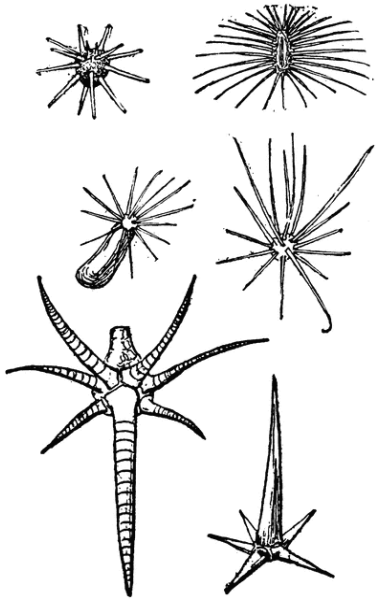

Figure 1. Drawings of cactus spines (right) showing the variety in shape and size [12]. Note that even within species spines from different parts of the plant will have different lengths or degrees of curvature.

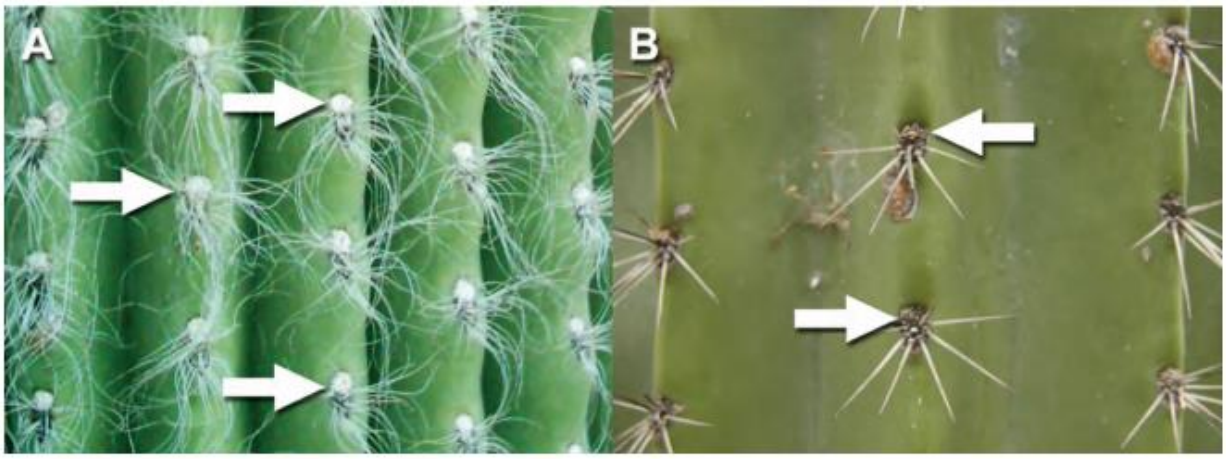

Figure 2. Photos of cactus spines a) with trichomes and b) without trichomes [13].

1.4 | Components of Natural Composites

Most natural composites are composed of four main components: cellulose, hemicellulose, lignin and pectin, and often contain varying amounts of ash.

Cellulose

Cellulose is a semicrystalline organic compound (Fig. 3) of linear polysaccharide chains that is commonly found in the cell walls of green plants, algae, and some bacteria. Cellulose fibers generally compose up to 40-50% (woods) to 90% (cotton) of plants in nature. Cellulose is insoluble in water and most organic solvents, despite being hydrophilic. Like most other natural polymers, cellulose is biodegradable. The degree of polymerization of cellulose varies depending on its source, but is

typically between 300 and 1700 for woods. In most plants, cellulose exists as a composite with binding agents such as hemicellulose, lignin, and pectin, and contains both crystalline and amorphous regions. Through chemical treatments, the amorphous binding agents as well as the amorphous regions of cellulose can be removed to produce highly crystalline cellulose nanowhiskers [14].

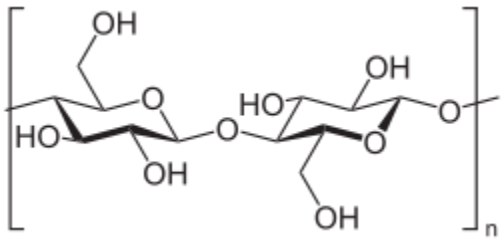

Figure 3. Cellulose ($C_6H_{10}O_5$) molecule.

Hemicellulose

Along with cellulose, hemicelluloses appear in plant cell walls as matrix polysaccharides. Unlike cellulose, hemicellulose is a branched, amorphous polymer with a low degree of polymerization and a low molecular weight. Additionally, while cellulose contains only one sugar monomer, hemicellulose may contain glucose, xylose, mannose, galactose, rhamnose, and arabinose (Fig. 4), as well as most of the D-pentose sugars and some of the L-pentose sugars [15].

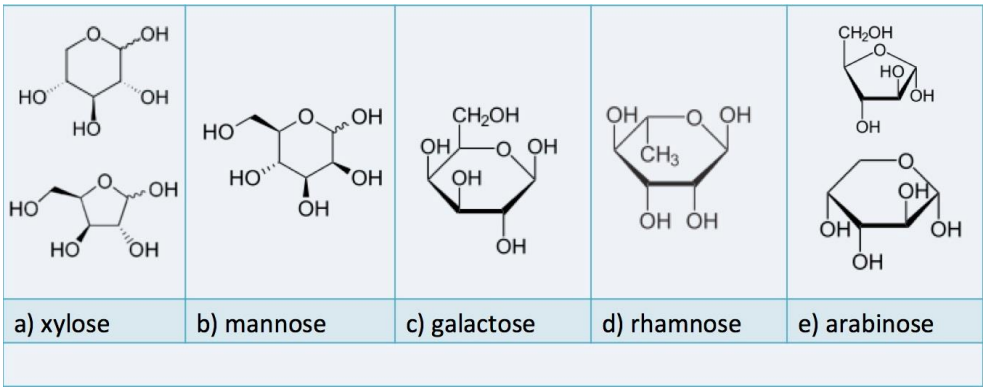

Figure 4. Monomer sugars in hemicellulose [16]

The different hemicelluloses present will vary for different types of plants. In softwood, the most common hemicelluloses are galactoglucomannan, glucomannan, and arabinoglucoronoxylan. Hardwood, on the other hand, contains mostly xylan [17].

Arabinan (Fig. 5) is a form of hemicellulose found in beet fibers and gums. Arabinan is a combination of arabinose and galactose monosaccharides.

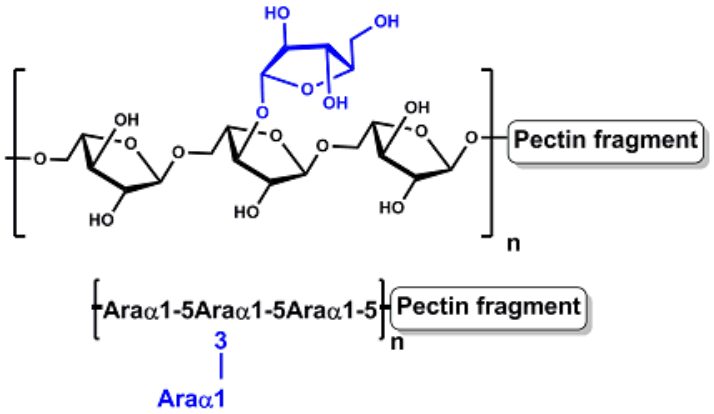

Figure 5. Arabinan molecule [18].

Lignin and Pectin

Lignin and pectin are complex organic polymers that exist in plants. Lignin (Fig. 6) is a structural element present in wood and bark that adds rigidity to the cell wall and helps to reduce rot [19].

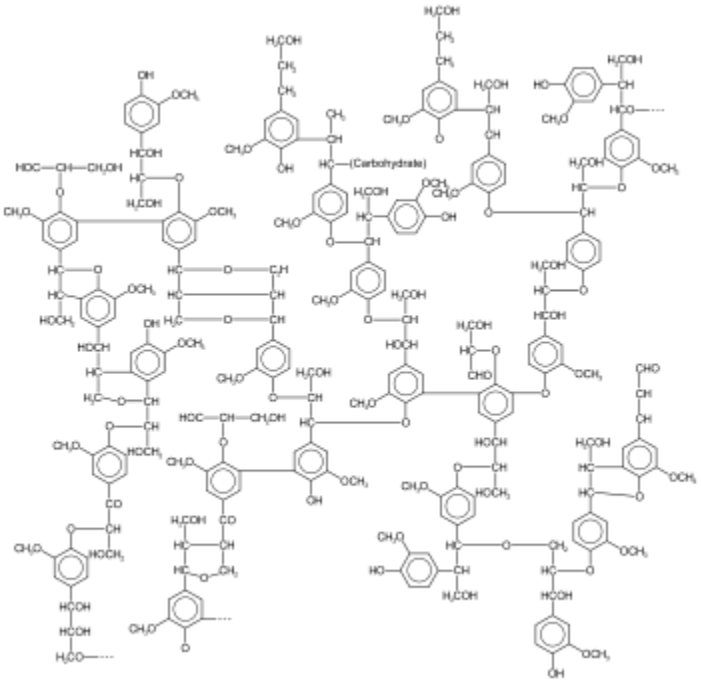

Figure 6. Example of a lignin molecule.

Pectin is a gelatinous heteropolysaccharide that is present in the middle lamella and primary cell walls of plants and is commonly used in the production of jams and jellies [20].

1.5 | Mechanical Properties

Opuntia Ficus-Indica

So far, there have been only four published papers discussing the mechanical properties of cactus spines. The first paper, published by Malainine et al. in 2003 [3], examines the effect of humidity on the tensile modulus, strength, and elongation of *Opuntia Ficus-indica (OFI)* spines. This article showed

that the modulus of *OFI* spines decreased from about 6.09GPa at 0% relative humidity (RH) to about 4.05GPa at 75% RH. However, the tensile strength and elongation increased from 84.1MPa and 2.5% to 99.4MPa and 5.0%. A second paper was published on *OFI* spines by Gindl and Keckes in 2012 [4] that compared their mechanical properties in bend testing to those of spruce wood. In this article, it was found that while the modulus of elasticity was comparable to that of spruce wood, the bending strength was much higher than expected. The bending modulus and strength of dry *OFI* spines in this article was found to be 33.5 ± 5.15 GPa and 779 ± 87.7 MPa, respectively (28.0 ± 3.66 GPa and 609 ± 48.1 MPa respectively for green spines which have a higher moisture content). This indicates a much higher strength for *OFI* spines than was previously suggested in the study by Malainine et al. The tests on green and dry spines performed by Gindl and Keckes also indicate that there is a significant increase in the bending modulus and strength when the spines are dried, but a decrease in ductility of the spines.

In addition to mechanical properties, Gindl and Keckes also determined the density of *OFI* spines using two different methods. The first method assumed an elliptical cross section, and calculated the density using the measured mass and volume of small pieces of cactus spine, giving a value of 1.3 g/cm^3. The second method estimated the density of cactus spines to be 1.5 g/cm^3 based on the information that the spines are composed of cellulose and arabinan (a form of hemicellulose), which would mean its density could be interpreted based on the density of wood. Using these values for density, Gindl and Keckes calculated the specific strength and modulus of *OFI* spines to compare them to that of spruce wood, and found that while the modulus of elasticity was comparable, the bending strength of *OFI* was over twice as high as that of spruce wood.

Echinocactus Grusonii

In addition to *OFI*, there have also been two published articles that describe the mechanical properties of *Echinocactus grusonii*. The first, published by Huang and Guo in 2013 [10], performed nanoindentation (using atomic force microscopy, AFM) and tensile tests on *E. grusonii* spines and compared them to various woods, crops, bamboo, and *OFI* spines. The nanoindentation tests were performed in both the longitudinal and transverse directions on dry and fresh spines (Fig. 7). When compared to woods, crops, and bamboo (Table 1), it was found that in the transverse directions, spines had a lower modulus than woods and crops, but was similar to that of bamboo. In the longitudinal direction, however, the spines were stronger than all of the reference materials. Huang and Guo also tested the tensile properties of *E. grusonii* spines, and compared them to those of bamboo and *OFI* spines. Here, they found that *E. grusonii* had a dry tensile strength of 140 ± 23 MPa and modulus of 17.4 ± 3.6 GPa. Compared to *OFI* spines in three-point bend testing, *E. grusonii* spines are much weaker in terms of both strength and modulus, but when compared to bamboo, *E. grusonii* was well within the range of strength, and had a stiffness that reaches the upper limit of the highest recorded properties for bamboo.

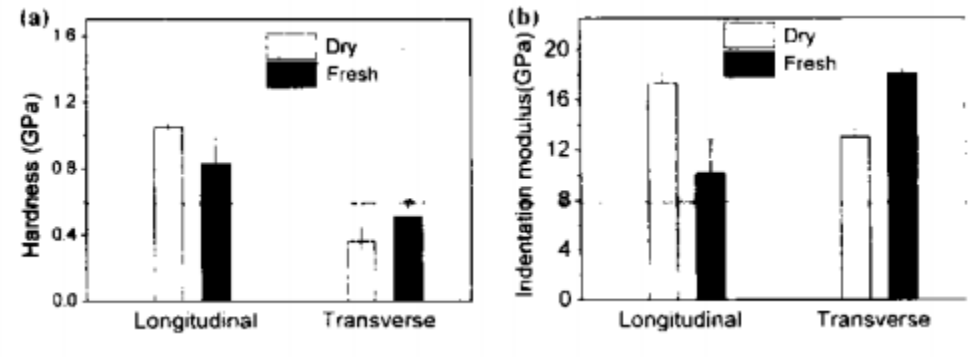

Figure 7. a) Hardness and b) indentation modulus of dry and fresh *E. grusonii* cactus spines [10]

Table 1: Comparison of nanomechanical properties of woods, crops, bamboo and *E. grusonii* spines [10]

Species	Indentation Modulus (GPa)[1]	Hardness (GPa)[1]
Hardwood (transverse)	16.9-24.6	0.44-0.56
Softwood (transverse)	14.2-18.0	0.34-0.53
Crops (transverse)	16.3-20.8	0.48-0.85
Bamboo (transverse)	10.4-19.0	0.44-0.47
Bamboo (transverse)	5.91	0.39
Bamboo (longitudinal)	16.01	0.36
E. grusonii spine (transverse)	18.1 (13.8)[2] 13.0 (9.2)[3]	0.51 (19.6)[2] 0.36 (33.3)[3]
E. grusonii spine (longitudinal)	10.1 (26.7)[2] 17.3 (19.1)[3]	0.83 (27.7)[2] 1.05 (46.7)[3]

[1] Values in parentheses represent coefficient of variation (CV) in percentage
[2] Fresh spine
[3] Dry spine

The second paper published on *E. grusonii* spines, published by Huang et al. in 2014 [9], tests the nanoindentation modulus of natural spines as well as the properties of a single spine fiber cell (SFC) without adhesives. Here, it was found that the indentation modulus of SFCs was 0.487 ± 0.086 GPa, which is about 36 times lower than the indentation modulus of a full spine.

Tensile and Three-Point Bend Testing

Tensile testing was performed on cactus spines to determine the tensile strength of *E. grusonii.* In tensile testing, the sample is loaded in the longitudinal direction to find its tensile strength before fracturing. In the tests performed by Huang et al. in 2013, *E. grusonii* spines were prepared for tensile testing by straightening curved spines using glue and clamps to hold the spine in place. After the spine was straightened out and dried, it was filed into the standard dog-bone shape in order to fit into the tensile testing machine. The resulting stress versus strain curve of the dried spine resembled the curve of a brittle material since the slope was nearly linear until fracture. In addition, when the tension load is applied to the sample, initially, the slope of the curve is not completely linear due to slacking and the sample set up. From the stress vs. strain curve, the ultimate tensile strength and Young's modulus, using the slope of the linear curve, can be found.

Another test that can determine the strength of a sample is the three-point bend test. In this test, the sample is loaded at the center in the transverse direction to find its bending strength before

fracturing. Three-point bend testing was done by Gindl and Keckes in 2012 on fresh and dry *OFI* spines to find the bending strength and modulus of elasticity. For bend testing, an elliptical cross section was assumed for all samples and the spine was placed onto the apparatus where the smaller diameter or curved end of the spine was oriented vertically or parallel to the loading nose. In order to compare the results of the bend test to other materials, such as wood, the bending strength and modulus were normalized. Since mechanical properties, such as bending strength and modulus, for wood and spines increase with increasing density, all properties were normalized by dividing the strength or modulus by the density of the specimen. This resulted in a specific bending strength and specific modulus for each specimen.

Both of these tests determine the strength of the spine, but one is much easier to do than the other. Tensile testing requires the sample to be processed into a dog-bone shape before it can be placed into the clamps for testing. Also, dried spines cannot easily be processed into that shape unless they are straightened first. On the other hand, bend testing does not require any additional processing of the sample before testing, which is a significant difference between these two tests. Having to shape the spine beforehand adds unnecessary time in sample preparation. In addition, cactus spines are fairly small in size, thus it is actually quite difficult to process them into a dog-bone shape required for tensile testing. In bend testing, the sample only needs to be placed correctly on the testing apparatus according to the ASTM standard D790–10 [22]. Without the additional processing, better mechanical properties of cactus spines can be measured using three-point bend testing.

Specific Strength

In order to compare *OFI* and *E. grusonii* spines to other materials, a CES selection graph was produced for each spine species. CES EduPack is a program that is used for material selection and learning about material properties and processes. The tensile strength and the density of the spine were plotted to obtain the specific strength of each spine which was then compared to the specific strengths of other materials. For *OFI,* the average tensile strength was 774.05 MPa and the average density was 1396.4 kg/m^3, which resulted in an average specific strength of 0.554 MPa-m^3/kg [4]. The *E. grusonii* spine had average tensile strength of 138.1 MPa and was assumed to have the same density as the *OFI* spine, resulting in a specific strength of 0.0989 MPa-m^3/kg.

On the CES graph (Fig. 8), a slope line was placed on the bubble of the spine to determine which material(s) had a similar specific strength as the cactus spine. The materials that fall along the slope line correspond to having the same specific strength as the cactus spine, whereas materials that fall below the line have a lower specific strength. Since *E. grusonii* has a much lower specific strength than *OFI*, the plot was made in level 2 of CES, where there are less materials for comparison which makes it easier to narrow down material options. From the graph, *E. grusonii* had a comparable specific strength as glass fiber reinforced polymer (GFRP) with an epoxy matrix, aluminum nitride, and zirconia. In level 2 of CES, no materials were comparable to *OFI*, so level 3 was used instead since there are more materials available for comparison.

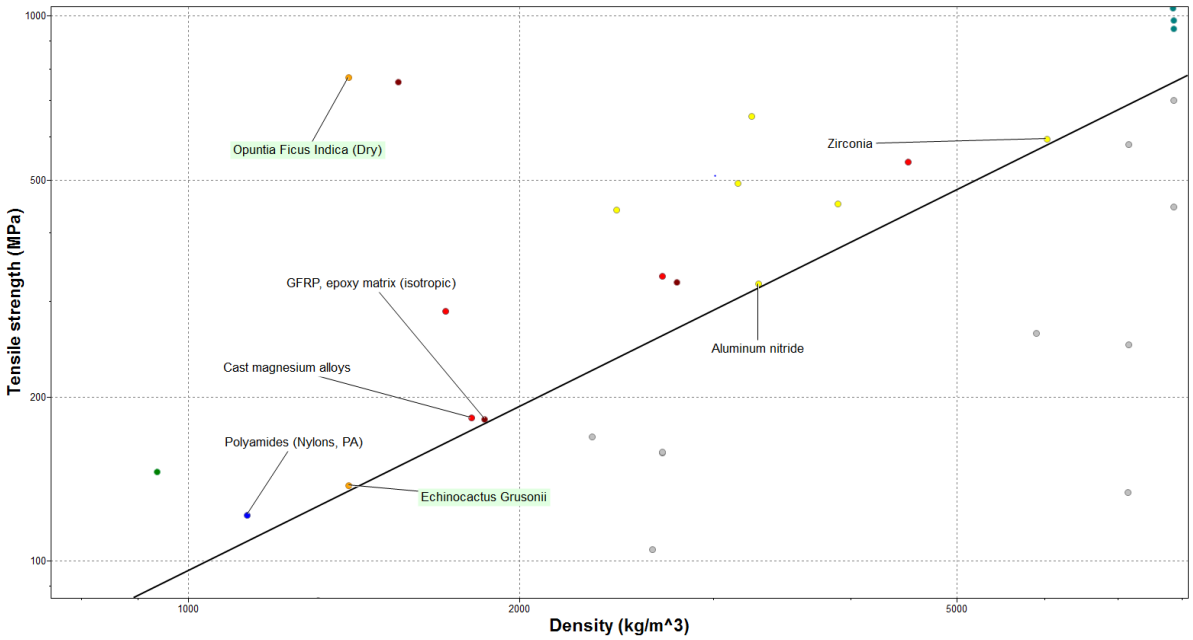

Figure 8. CES Level 2 graph (zoomed in) of average tensile strength and density values where the slope line represents materials with similar specific strength as *Echinocactus grusonii*.

In level 3, there were no materials that exactly matched the specific strength as *OFI*, so materials that had close values to *OFI* were shown instead (Fig. 9). The chosen materials had lower specific strengths than *OFI* and these included polyimide/carbon fiber, aluminum silicon carbide (Al-47%SiC, aluminum matrix with silicon carbide particles), and Nextel fiber (Al-65%A_2O_3). It is important to notice that *OFI* has a specific strength much higher than many other materials, which are represented by the gray bubbles.

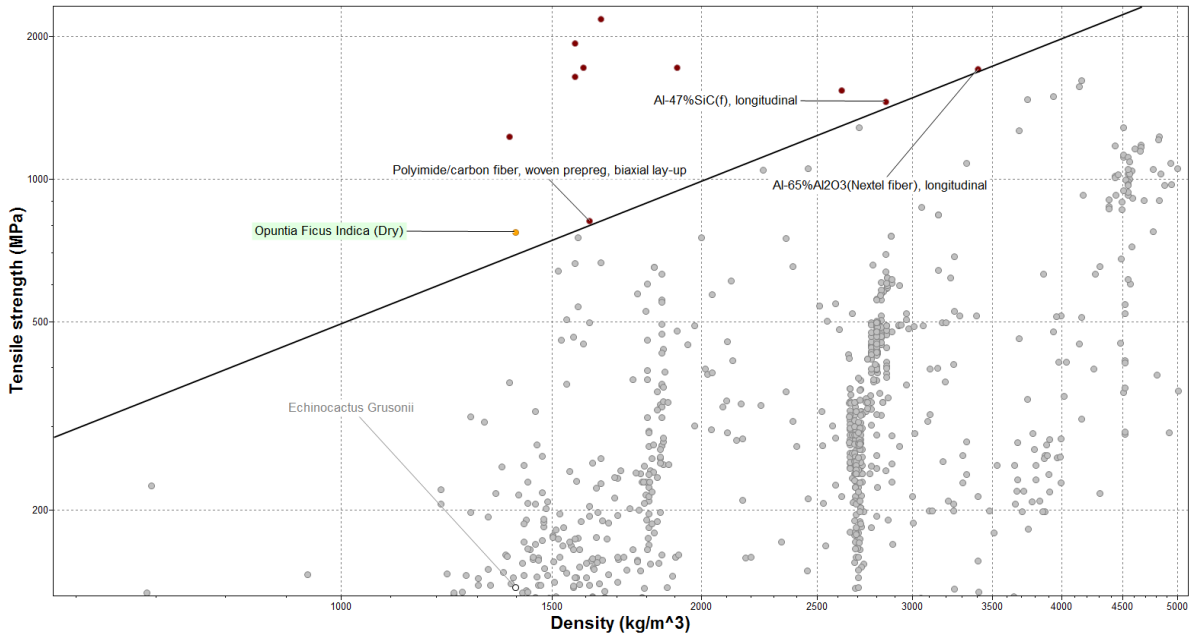

Figure 9. CES data comparisons for *Opuntia Ficus-indica* in CES Level 3.

1.6 | Structure

Opuntia Ficus-Indica

The article by Malainine et al. [3] investigated the structure of *OFI* spines using transmission electron microscopy (TEM), scanning electron microscopy (SEM), electron analysis and X-ray diffraction (XRD) analysis. Using elemental analysis, they determined that the spine was composed of 47.9% cellulose and 48.4% hemicelluloses (arabinan), with small amounts of other constituents. Using TEM and SEM, Malainine et al. were able to see the high alignment of fibers along the spine axis and the compact arrangement of cells at the spine's cross-section (Fig. 10). The high orientation of the fibers was confirmed using electron and x-ray diffraction.

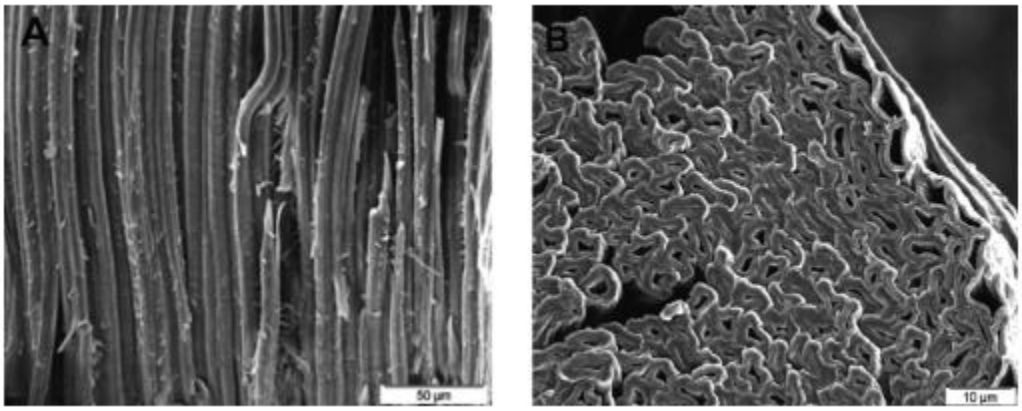

Figure 10. SEM micrographs of cactus spine a) parallel to spine axis and b) perpendicular to spine axis [2]

Gindl and Keckes' work on *OFI* spines compared the structures of cactus spines and wood using wide angle x-ray diffraction, Azimuthal integrated scattering intensity distribution along the cellulose (200) direction, and the radial integrated scattering intensity distribution. The results of the second and third tests are shown in figure 11. The sharp peaks in the Azimuthal intensity distribution curves indicates a high degree of cellulose orientation within the spines. The degree of orientation was calculated on a scale from 0 (random orientation) to 1 (perfect uniaxial orientation), and was found to be 0.57 for spruce wood, and 0.58 for cactus spines. Combining this information with the knowledge that both cactus spines and spruce wood are composed of nearly 50% cellulose, the similarity in modulus can be explained. The significantly higher bending strength of *OFI,* however, can be explained by the radial scattering intensity distribution curve, which showed a much sharper, more intense peak for the *OFI* spine than for spruce wood. This sharper peak indicates a higher degree of crystallinity, which was then calculated at an angle (2θ) of 33°. It was found that the degree of crystallinity was 57% for *OFI* spines, and 34% for spruce wood, therefore explaining the much higher bending strength of *OFI*.

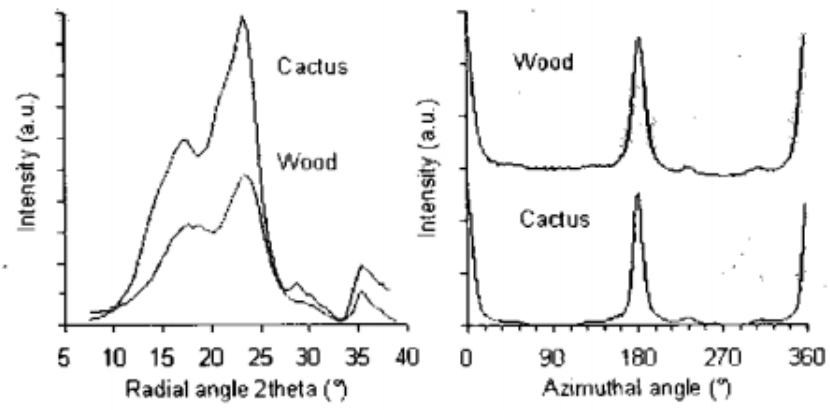

Figure 11. Left: radial integrated scattering intensity distribution for cactus spine and wood; Right: Azimuthal integrated scattering intensity distribution along cellulose 200 reflection. [4]

In addition to the degree of crystallinity, a paper published in 2004 by Vignon et al. [2] found that the strength of cactus spines can be traced to their composition. Using optical microscopy, SEM, TEM, wide angle X-ray analysis, and ^{13}C NMR analysis, the composition and structure of *OFI* was determined to be a 50:50 composite of cellulose fibers within an arabinan matrix. The strong interactions between cellulose and arabinan at the nanometric level significantly increase the mechanical properties of the spines compared to those of other cellulose and hemicellulose composites.

Echinocactus Grusonii and X-Ray Diffraction

According to Huang et al., *Echinocactus grusonii* spines are made of highly aligned spine fiber cells (SFCs) which range from 0.32 to 0.57 mm in length and 4.6 to 6.0 microns in width. The SFCs represent a layered composite structure that has a primary wall (P) and secondary wall (S) with three different sublayers, and cells are separated by medium lamella (M) (Fig. 12). Every SFC layer is mainly composed of cellulose fibers and arabinan, with small amounts of pectin and lignin. Cellulose is commonly found in the form of microfibrils which are longitudinally organized throughout the spine. The remarkable stiffness of spines is believed to come from the organization of the cellulose within the spines. An investigation done by Huang et al. on the microstructure and mechanical properties of SFCs involved the analysis of the multifibular angle (MFA), the degree of crystallinity measured as the crystallinity index (CI or %C), and the presence of binding agents to act as cellulose fibers. As seen by the results of mechanical testing, removing those binding agents significantly reduced the mechanical properties of the spine.

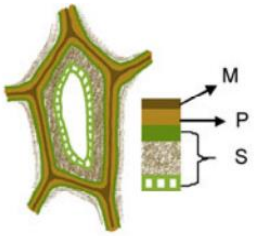

Figure 12. Cell structure of cactus spines showing the arrangement of cell walls. [9]

XRD (X-Ray Diffraction) was implemented to determine the degree of crystallinity and fiber arrangement of spines. A typical *Echinocactus grusonii* spine showed the presence of two diffraction peaks occurring at 2θ angles of 22.5° and 31.2° in which each corresponds to a crystal reflection of cellulose, since cellulose is the only component in spines that contains crystalline regions. Since cellulose fibers in the cactus spine are semi-crystalline, the CI representing the relative amount of crystalline material in the spine may be calculated.

In equation 1, $I_{22.5}$ yields the maximum intensity of the main peak for the crystalline region and $I_{18.5}$ is the safe amorphous region. The higher the CI, the less amorphous regions there are within the spine sample. MFA is another structural parameter that is defined as the angle between the direction of the cellulose microfibrils in the SFC wall. MFA may be calculated using equation 2.

$$MFA = 0.6 \times T \qquad \text{(eq. 1)}$$

The only parameter in equation 2 is T which is defined as the "distance between the two intersections of the two tangents drawn at the points of inflection in the XRD curve and the angle axes." A sample XRD graph showing how T is determined is shown in figure 13. Low MFAs indicate that the microfibril fibers in the SFCs tend to align parallel to each other in their longitudinal directions thus optimizing the mechanical strengths of the spines.

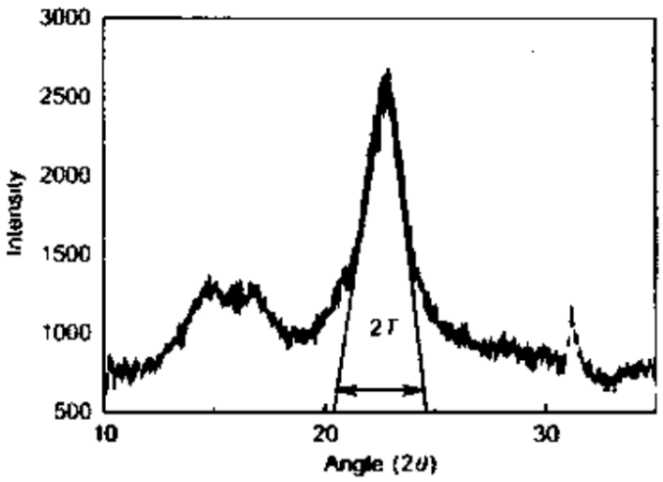

Figure 13. X-Ray Diffraction analysis of *Echinocactus grusonii* spine which shows two crystal reflections. The main peak is located at 2θ of 22.5° and the smaller peak at 2θ of 31.2°. [9]

By reviewing and synthesizing past research done on two cactus species, properties such as bending strength, MFA, and percent crystallinity can be measured and determined for spines from other species of cactus. So far, no study has examined the relationship between CI and MFA and the mechanical properties of spines over many different species.

2.0 METHODS AND PROCEDURES

Six samples from each of 24 species of cactus spines from 13 genera were tested. A full list of species is shown in Appendix A. Density measurements of each species were taken using the volume displacement method. With the assumption that all spines from a species should have the same density, every spine within the species was collected and weighed on a digital scale (read to at least 0.001 g) to determine mass. Then, a 10-mL graduated cylinder was filled with water and the initial level of the water was read at increments of approximately 0.01 mL. Once the spines were put into the graduated cylinder, the final level of the water was recorded and the difference between the final and initial water level was calculated to determine the volume. The density of a cactus spine was defined as the mass over the volume.

2.1 | Scanning Electron Microscopy

In order to view the fracture surface and cells present of a cactus spine, Scanning Electron Microscopy (SEM) was performed. The ESEM FEI Quanta 200 was utilized in low vacuum (LV) mode due to the cactus spines being biological materials. The spine was mounted to a carbon dot on a vertical sample holder with the fracture surface showing upright (Fig. 14). For low vacuum mode imaging, the large-field detector (LFD) was then inserted prior to placing the mounted sample in the chamber. A working distance of 5 mm was used for the height of the sample on the stage using a metal jig. The xT microscope software was used to input the SEM parameters listed in Table 2 along with the conditions used for high vacuum imaging. If higher resolution images were needed, high vacuum (HV) mode was chosen instead which meant that the spines had to be gold sputter coated. For gold sputtering, multiple mounted cactus spines were placed into the Cressington Sputter Coater at the same time. Gold sputter coating the spines helps reduce charging of the specimen in high vacuum mode and at high voltages. High resolution images of the fracture surfaces of each cactus species were taken at magnifications of 50x, 1000x, and 2000x. The different magnifications allowed for comparison and analysis of the cactus spines. Flatter areas of the fracture surface were focused on to show a more representative structure of the whole spine.

Figure 14. Sample SEM mounting.

Table 2: Conditions used for Low and High Vacuum SEM Imaging

Mode	Pressure (Pa)	Voltage (kV)	Spot Size	Detector	Working Distance (mm)
LV	90	12.5	4.0	LFD	5
HV	2×10^{-3}	20	4.0	ETD	10

2.2 | X-Ray Diffraction

The Siemens D5000 Diffractometer was set up with the 0.6 mm detector slit and 2 mm divergence slit to determine the degree of crystallinity and multifibrillar angle of each species. In the EVA software, testing parameters of 30 mA current, 40 kV voltage, 0.075° increment, 2°/min scan speed, start at 17°and stop at 27° were inputted prior to the start of the test. For sample preparation, one spine from a species was mounted using clay onto an aluminum sample holder (Fig. 15). The flat side

of the spine was also leveled with the top of the sample holder. Excess clay showing under the spine was scraped away to minimize the amount of background noise that shows up in the scan.

Figure 15. Mounted cactus spine sample ready for XRD with excess blue clay around the spine removed.

Once the XRD scan was completed, the intensities of 2θ angles at 18.0° and 22.6° were determined by dropping peak arrows at each corresponding point on the graph, which outputted the number of counts (I). These counts were then used in equation 2 to calculate the degree of crystallinity (%C):

$$\%C = \frac{I_{22.6} - I_{18}}{I_{22.6}} \times 100\% \qquad \text{(eq. 2)}$$

The multifibrillar angle (MFA) for each species was measured using equation 1, which is described in Section 1.6. In addition, multiple XRD runs for the same species were done for data validation and accuracy.

2.3 | Three-Point Bend Testing

For determining the mechanical properties of cactus spines, three-point bend testing was done for each species. Six spines from each species was tested using the Instron Mini 55 while following the ASTM D790-10 standards since cactus spines are composite materials. A load cell of 500 N and a strain rate of 1 mm/min was used for all bend tests. Before testing, the thickness and width at the center, and total length of each spine was measured using calipers. A span to depth ratio of 16:1 was used for this test, and the span length for each species was calculated using the smallest thickness in order to use the most conservative value. When placing the spine onto the span supports, the spine was centered with the loading nose and centered from all directions. The support span length should cover at most 80% of the spine with a 10% overhang of the length on each side (Fig. 16). If the spine was curved, then it was placed onto the support spans with the spine facing concave up.

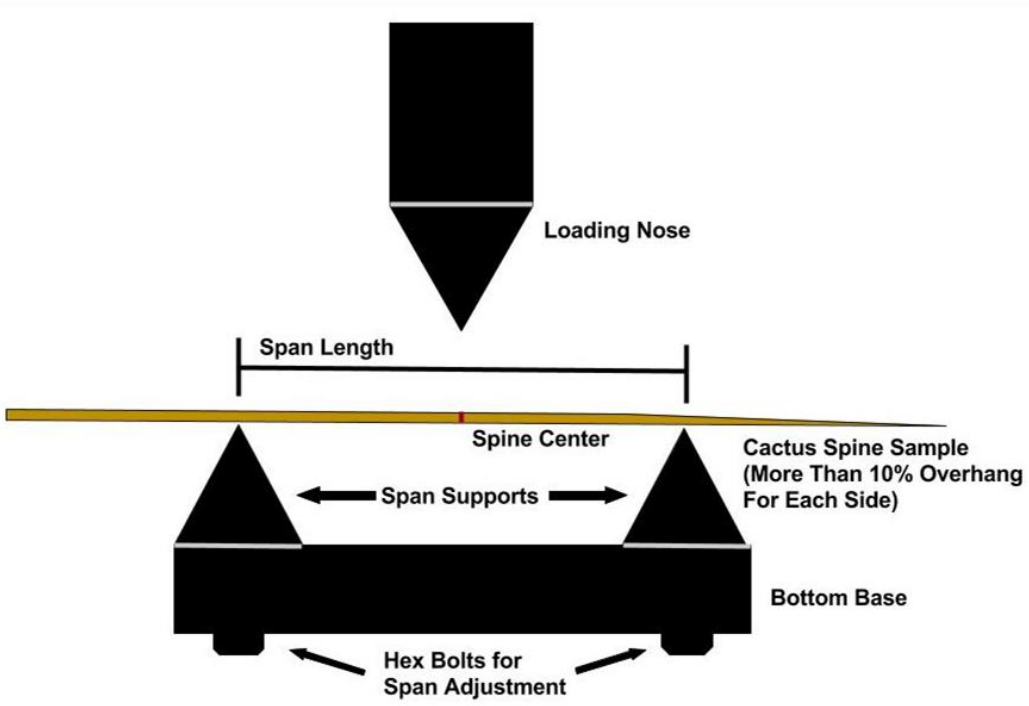

Figure 16. Three-point bend testing apparatus diagram indicating span length and position of a spine sample.

Before the test was started, the average spine thickness and width of each species were inputted into the Bluehill 3 software. Then, the loading nose was lowered down until it was just above the spine, but not touching it. The load was balanced first, then the extension was zeroed. Once all six spines of a species were tested, then a new data set was made for the next set of spines.

From the bend testing, the Maximum Flexure Extension, Modulus (E), Peak Local Maximum, and Flexure Stress at Maximum Flexure Extension were outputted. It was assumed that the cactus spines had a uniform structure and a rectangular cross-section when values were calculated since there was not an accurate method to find the cross-sectional area of a spine.

3.0 Results and Discussion

3.1 | Structure

Fracture Surfaces

SEM images for each species were taken at the three magnifications previously described, and are available in Appendix B. On the fracture surfaces, two fracture regions are visible from a bending mode fracture: a region in compression where the loading nose contacted the spine, and a region in tension at the opposite side. In roughly circular spines, such as *Echinopsis spachiana* (Fig. 17), the crack propagates through half of the spine in the manner shown in figure 17B until it reaches the region in compression, where the spine will either break entirely or bend.

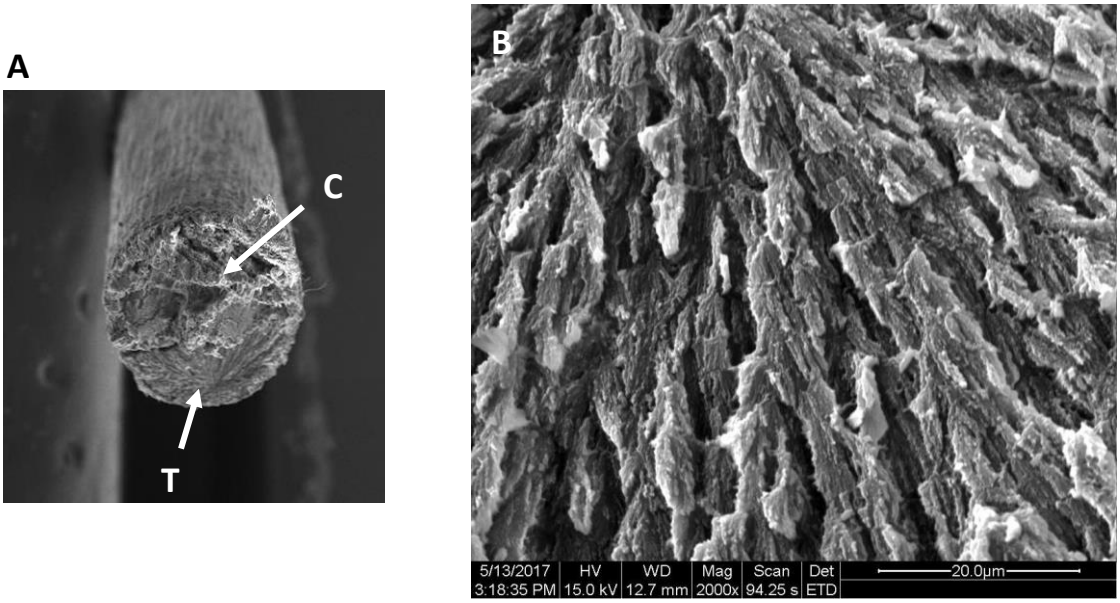

Figure 17. A) Diagram of fracture regions in tension at 50x (T) and compression (C), B) SEM image of tension region in *Echinopsis spachiana* showing the progression of the fracture from a point just below the surface of the spine.

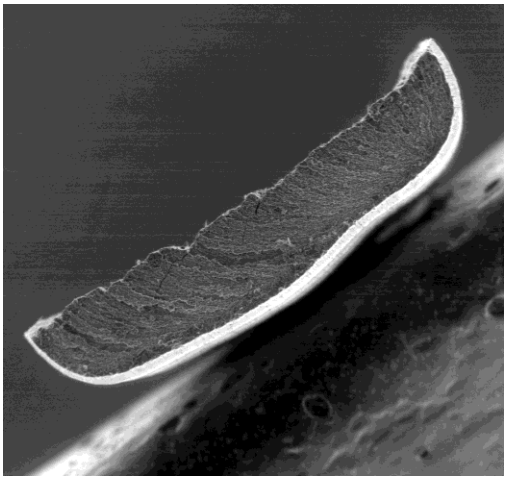

Figure 18. Fracture surface of an *Echinocactus grusonii* spine at 50x.

Larger spines, such as *Echinocactus grusonii* (Fig. 18), seemed to exhibit a different fracture surface due to their large width-to-thickness ratio and thicker epidermis, or outer layer. Like in the rounder samples, the fracture began in the region in tension, and indicates a directionality of the fracture progression. However, unlike the smaller samples, there is no visible compression region. Instead, the crack propagates through the entire thickness of the sample until it reaches the surface of the spine, where the epidermis breaks off from the inside of the spine along the center of the region in compression.

In the compressed region of the spine, the rapid fracture leaves a surface where the cell structure can be seen. In structures such as those of *Stenocactus crispatus* and *Echinocereus englemanii* (Fig. 19A and 19B, respectively), the secondary cellulose walls are visible along with the lumina, which are the hollow regions on the inside of the cell. It can be seen from these images that these tube-like fiber cells are compressed and appear to be highly oriented parallel to the spine axis. In some other species, such as *Astrophytum ornatum* and *Grusonia emoryi* (Fig. 19C and 19D, respectively) these identifiers are not as easily visible, but some of the same traits can still be seen. For example, the circled region in figure 19C shows a narrow, but visible lumen.

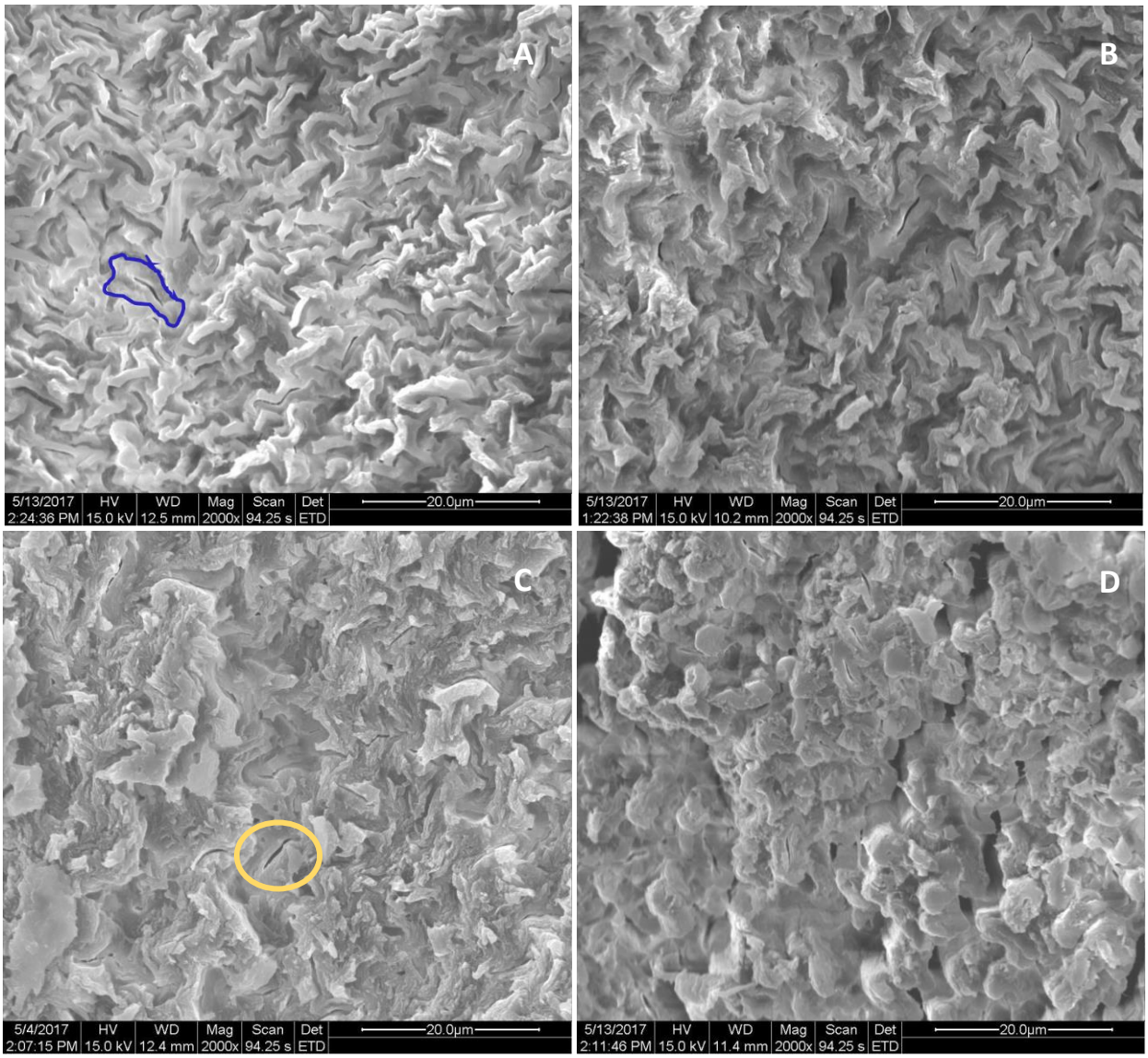

Figure 19. SEM images showing cell structures in A) *Stenocactus crispatus* with an outlined SFC, B) *Echinocereus englemanii,* C) *Astrophytum ornatum,* and D) *Grusonia emoryi.*

Multifibrillar Angle

From each species, an X-ray scan between 17-27° was taken in order to focus on the characteristic cellulose peak at 22.6°. These scans are available in Appendix C, and in each scan, the cellulose I peak is visible indicating the presence of cellulose I in each species. The full scan, shown in figure 20 for *Echinopsis terschekii,* does not show any useful information past this range, which is to be expected since cellulose is the only crystalline component in the spines.

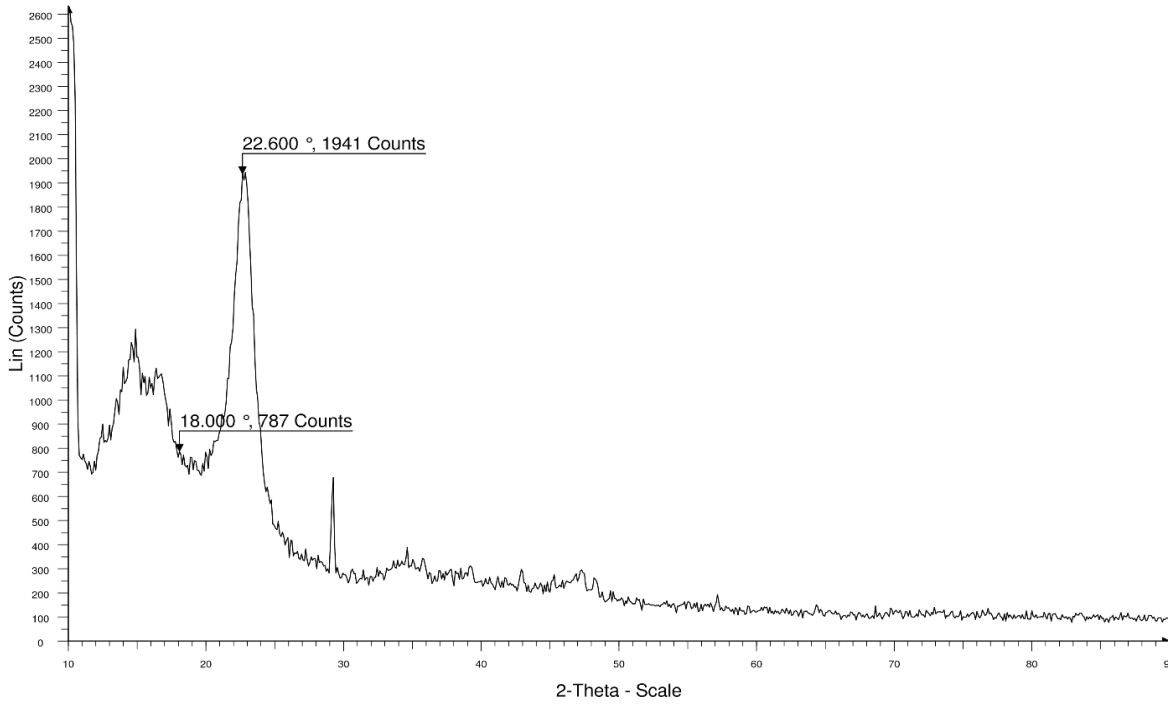

Figure 20. Full scan of an *Echinopsis terschekii* spine.

Using these graphs, a visual estimation of the slope was used to calculate the MFA of each spine, as shown in figure 21. Because this method was performed using a visual examination of the graph, there was a large margin of error for each value of MFA. In order to account for the range of error, a large and small estimate of the MFA was made for each species. In the case of *Echinopsis terschekii,* the MFA ranged from 1.23-1.53°.

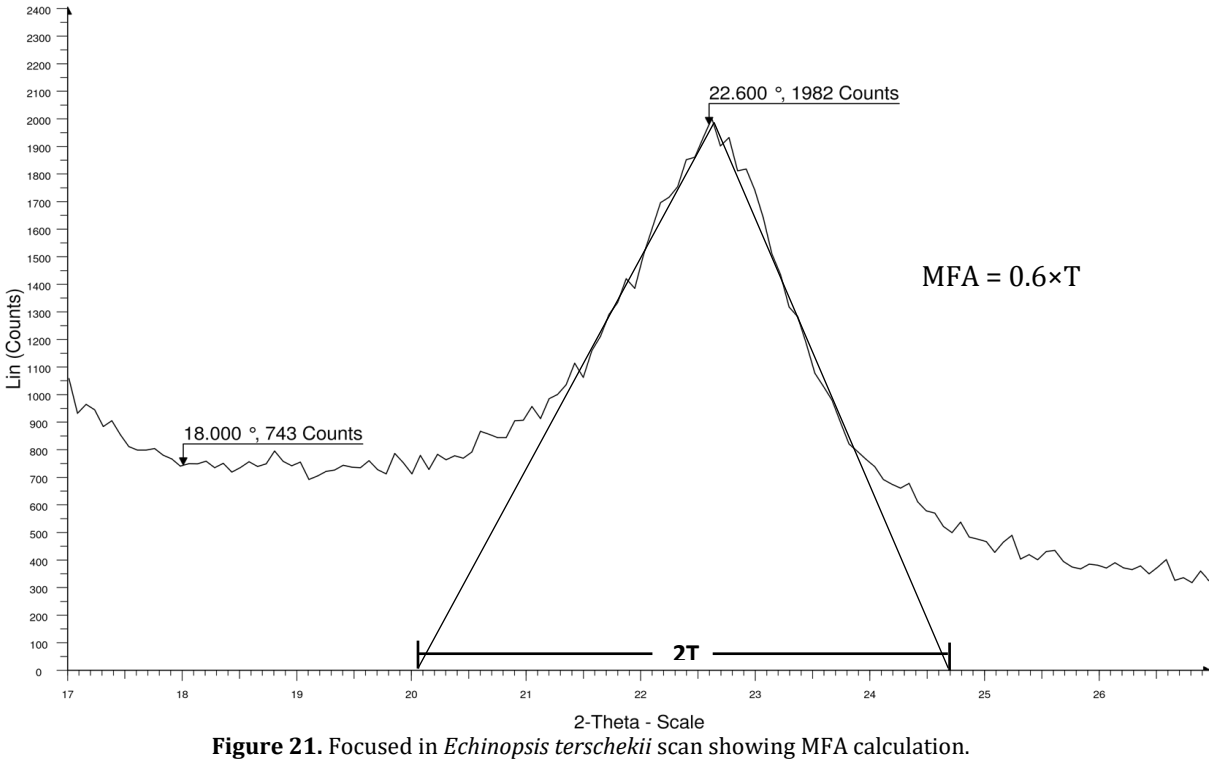

Figure 21. Focused in *Echinopsis terschekii* scan showing MFA calculation.

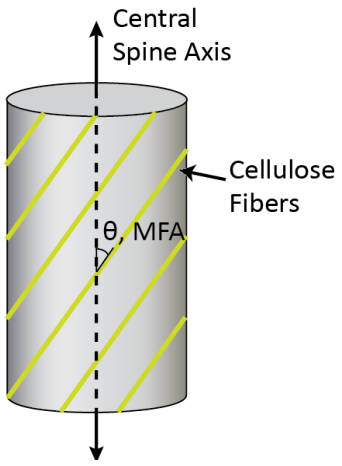

Figure 22. The MFA describes the average angle of deviation of the cellulose fibers away from the central axis of the spine.

The MFA for all species was found to range from 1.11-2.52° when the variability was accounted for. This small range as well as the overall low values for the MFA indicates the high orientation of the fibers (Fig 22). The calculations of MFA performed by Huang et. al on *Echinocactus grusonii* found a minimum MFA of 1.3° [9], which is well within the range of values obtained for this experiment. The obtained values for MFA were much lower than the MFA of bamboo, which ranges from 9-44° [10]. This result helps to explain the high mechanical properties of the cactus spines when compared to other plant materials, but due to the small range of the MFA, little information can be obtained about the relationship between MFA and the mechanical properties.

Structural Properties

Unlike the MFA, the degree of crystallinity of the cactus spines was found to have a great amount of variation. The average value of the %C was 46.38% with a standard deviation of 11.86%, but some species had a %C below 30%. The wide range of values for the crystallinity of spines indicates that cactus spines cannot be characterized for their high crystallinity, especially since other woods, such as bamboo, can have degrees of crystallinity up to 79% [10].

The density of the cactus spines ranged from 1.1-1.5 g/cm^3, which was the expected range for a wood-like composite. Precise measurements of the density were difficult to make because the resolution of the graduated cylinder was only 0.1ml, and a difference in volume of 0.01 ml leads to a difference in density of about 0.04 g/cm^3. The density could also have been affected by the adsorption of water in the spines.

3.2 | Mechanical Properties

Three-point bend testing was conducted for all cactus spine species to collect flexural mechanical data and analyze mechanical properties. The resulting stress-strain curves and the calculated mechanical properties are available in Appendix D. There were different levels of variation across the species as they were being tested, and each level of variation appeared to be consistent throughout each species. The normal and ideal variation that is expected follows a curve that is approximately linear, such as in *Echinopsis spachiana* (Fig. 23). This behavior was expected since cactus spines are natural occurring biomaterials, thus varying from sample to sample.

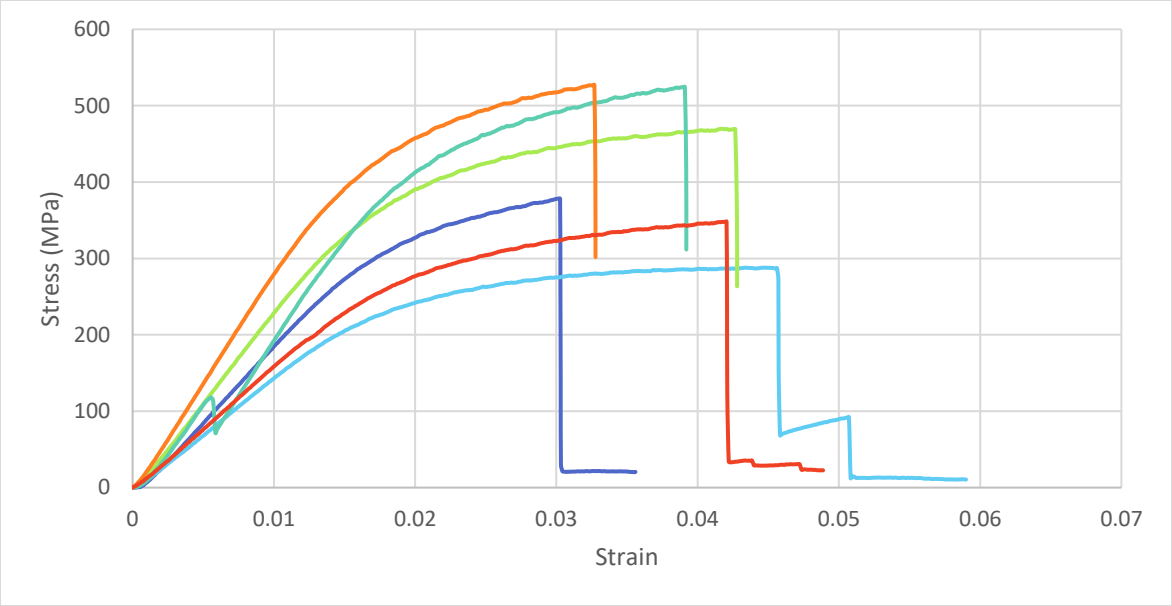

Figure 23. *Echinopsis spachiana* ideal stress-strain curves calculated from mechanical testing raw data.

A more dramatic variation in data collection was observed in other species, such as *Astrophytum ornatum* (Fig. 24). There are some theories that may possibly explain this behavior, but they are not complete conclusions. These may include cellulose fiber breakage, movement of the spine such as rolling or shifting, or effects from the cross-sectional shape of the spines. Due to this odd behavior, the flexural strength of the species (calculated from three-point bend testing raw data) is inaccurate. However, calculating the flexural stiffness of each species is much more accurate since only the slope of the first portion of the graph is used. If this behavior was due to movement of the spines while being tested, then a light resin may be applied on the edge of the support pins to minimize this issue. Averages for strain-to-failure, flexural strength, and flexural stiffness were calculated from each set of three-point bend tests (Table 3).

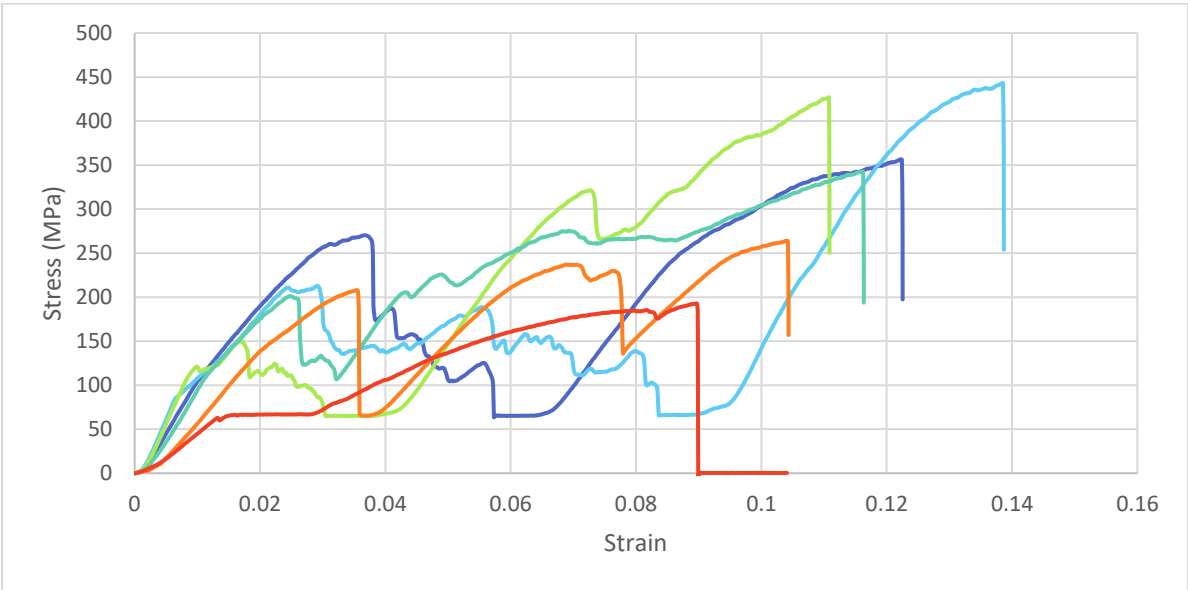

Figure 24. *Astrophytrum ornatum* atrocious stress-strain curves from mechanical testing raw data. The explanation for this particular behavior is unknown but could be due to fiber breakage or sample movement.

Table 3: Average Mechanical Properties of Cactus Species

Cactus Species	Strain-to-failure (%)	Flexural Strength (MPa)	Flexural Stiffness (GPa)
Astrophytum Ornatum	11.145	293.41	5.094
Echinocactus grusonii	4.164	240.87	8.512
Echinocactus polycephalus	4.214	111.96	2.528
Echinocereus boyce-thompsonii	2.180	250.26	22.782
Echinocereus englemanii	5.091	226.6	11.910
Echinocereus triglochidiatus	4.975	250.26	10.878
Echinopsis spachiana	3.715	389.71	19.675
Echinopsis terschekii	2.581	183.46	9.220
Ferocactus chrysacanthus	5.834	213.3	5.120
Ferocactus cylindraceus	5.572	236.95	7.528
Ferocactus emoryi	3.305	230.05	7.755
Ferocactus pilosus	2.755	313.81	13.187
Ferocactus viridescens	3.131	491.08	27.668
Ferocactus wislizenianus	3.897	287.47	16.587
Grusonia emoryi	7.707	204.14	4.582
Myrtillocactus geometrizans	8.437	119.43	2.877
Oreocereus celsianus	5.185	270.87	6.650
Pachycereus pringlei	2.627	206.37	2.627
Sclerocactus parviflorus	8.659	301.26	5.553
Sclerocactus polyancistrus	2.381	191.37	18.599
Stenocactus crispatus	6.719	220.18	6.825
Stenocactus multicostatus	9.874	129.55	5.356
Stenocereus thurberi	3.491	331.86	20.218
Tephrocactus alexanderi	3.447	212.55	16.867

Resiliency

The resiliency for each species was calculated from their flexural strength and flexural modulus. This property is a measure of how much energy a material may withstand prior to yielding (Eq. 3).

$$Resiliency = \frac{(Flexural\ Strength)^2}{2 \times Flexural\ Modulus} \quad \text{(Eq. 3)}$$

For most cactus spines that were tested, their resiliency compared to that of 4340 low alloy steel and unidirectional glass fiber reinforced polymers (Fig. 25). The data was also consistent with previous studies on the *Opuntia Ficus-indica* species by Gindl-Altumtter and Keckes. Data for *Echinocactus grusonii* from Huang and Guo was lower than the rest of the samples that were tested since they followed a tensile testing procedure. For cactus spines, a tensile testing sample is particularly difficult

to set up, thus all mechanical testing data was collected through three-point bend testing. This difference must be considered when comparing the mechanical properties.

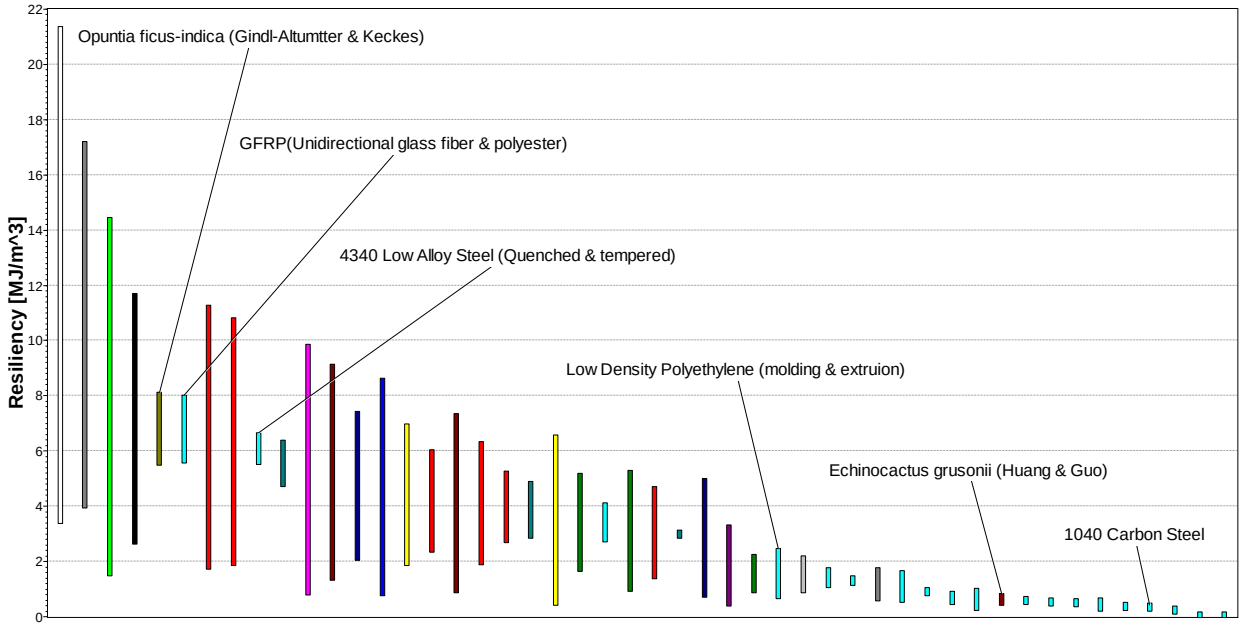

Figure 25. Resiliency variances of several cactus species. Each color represents a different genus, except teal which represents engineering materials such as GFRP, 4340 low alloy steel, and 1040 carbon steel.

3.3 | Understanding Variation in Data

Resiliency and Spine Size

An interesting phenomenon was observed when the relative size of the cactus spines is correlated with their resiliency. This trend showed that an increase in spine size leads to smaller resiliency values. Specifically, this relationship can be seen directly by analyzing the *Ferocactus* genus (Fig. 26). This effect is caused by the increased number of defects present in larger spines which lower the mechanical properties.

Figure 26. Six species from the *Ferocactus* genus showed an increase in resiliency with decreasing spine size. From left to right: *wislizenianus, emoryi, cylindraceus, pilosus, chrysacanthus*, and *viridescens.*

Radial and Central Spines

In several species there exists two different types of spines, central and radial spines (Fig. 27). Depending on which type of spine is used, the shape, size, and color of spines from the same species can be significantly different. No discretion was made between samples from radial and central spines, and neither was any consideration given to the age and location of the spine on the cactus.

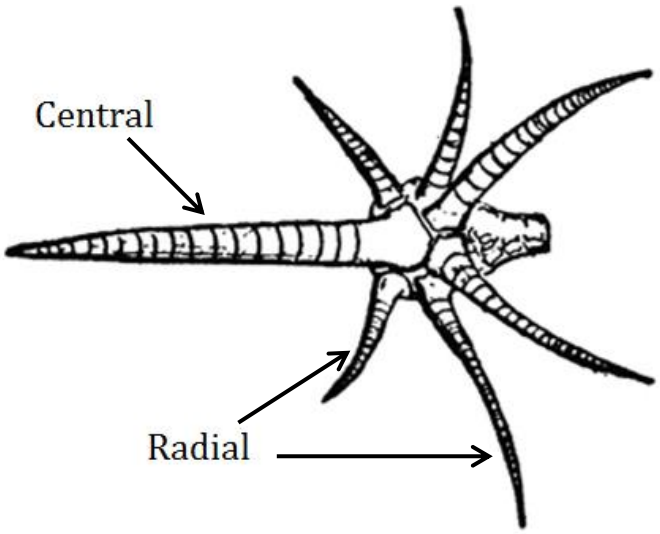

Figure 27. The difference between central spines and radial spines in a species.

Modulus, Multifibrillar Angle, and Degree of Crystallinity

The average modulus of all species was compared to their MFA and degree of crystallinity. A 3-D model was drawn from this data which showed a weak relationship between the modulus and MFA (Fig. 28). The rest of the properties did not show a relationship that was conclusive. A table of the R^2 values of the effect of each parameter on the modulus showed the same conclusion (Table 4).

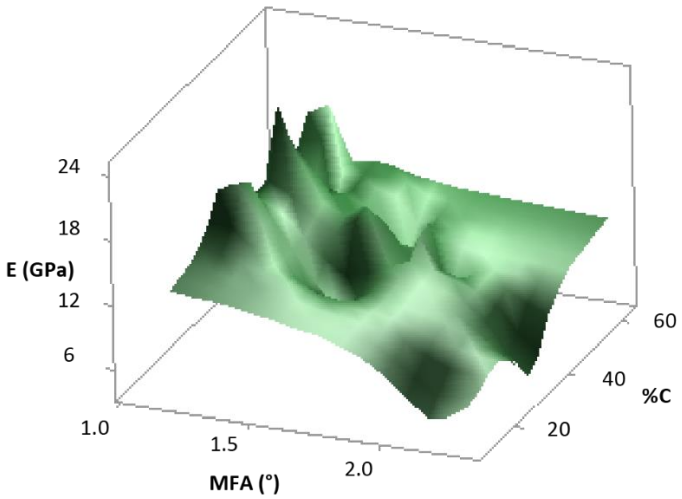

Figure 28. Comparison of modulus, MFA, and degree of crystallinity. A small trend between MFA and modulus can be observed in which higher MFA values correlate with a lower modulus.

Table 4: R^2 values for Structural Parameters

Parameter	MFA	%C	Density
R^2	24.6	6.8	2.2

Though no significant correlations could be drawn from any of these parameters alone, the apparent relationship seen in figure 28 indicates that the mechanical properties of cactus spines may be a function of the combination of crystallinity and MFA.

4.0 CONCLUSIONS

1. Cactus spines had resiliency comparable to low alloy steel and GFRP, and higher than carbon steel
2. Resiliency was higher for smaller spines
3. No correlation was found between density, %C, and modulus
4. A weak correlation was found between MFA and modulus

5.0 RECOMMENDATIONS

1. Testing of radial vs. central spines for differences in structural/mechanical properties as well as testing of fresh vs. dry spines for larger sample size
2. Use of a more accurate method of measuring density in order to better understand the effects of density on the crystallinity and mechanical properties
3. Further statistical analysis on the combined effects of multifibrillar angle and crystallinity

REFERENCES

1. Gourmelon, Gaelle. "Global Plastic Production Rises, Recycling Lags." *Worldwatch Institute Vision for a Sustainable World.* (http://www.worldwatch.org/global-plastic-production-rises-recycling-lags-0) Web. Dec. 9, 2016.
2. Vignon M.R., Heux L., Malainine M.E., Mahrouz M. "Arabinan-Cellulose Composite in *Opuntia Ficus-indica* prickly pear spines." *Carbohydrate Research*, vol. 339 (2004), pp. 123-131.
3. Malainine M.E., Dufresne A., Dupeyre D., Mahrouz M., Vuong R., Vignon M., "Structure and Morphology of Cladodes and Spines of *Opuntia Ficus-indica.* Cellulose extraction and characterization." *Carbohydrate Polymers*, vol. 51 (2003), pp. 77-83.
4. Gindl-Altmutter, W., & Keckes, J. "The Structure and Mechanical Properties of Spines From The Cactus *Opuntia Ficus-Indica*." *BioResources*, vol. 7, no. 1, 2012, pp. 1232-1237.
5. "Thorns, spines, and prickles" *Wikipedia.* (https://en.wikipedia.org/wiki/Thorns,_spines,_and_prickles) Web. Dec. 2, 2016.
6. Lucas P.W., Turner I.M., Dominy N.J, & Yamashita N. "Mechanical Defences to Herbivory." *Annals of Botany,* vol. 86, issue 5 (2000), pp. 913-920.
7. Halpern M., Raats D., & Lev-Yadun S. "Plant biological warfare: thorns inject pathogenic bacteria into herbivores." *Environmental Microbiology,* vol. 9, issue 3 (2007), pp. 584-592.
8. Shaffer R. "How do cacti survive in that environment?" *ScienceIQ.* (http://www.scienceiq.com/facts/cactisurvive.cfm)Web. Dec. 12, 2016.
9. Huang, F., Qiu, H., & Guo, W. "Microstructures and mechanical properties of fiber cells from *Echinocactus grusonii* cactus spine." *Science China Technological Sciences*, vol. 57, no. 4, April 2014, pp. 706-712.
10. Huang, F., & Guo, W. "Structural and mechanical properties of the spines from *Echinocactus grusonii* cactus." *Journal of Materials Chemistry*, vol. 48, March 2013, pp. 5420-5428.
11. Mauseth, J.D. "Cytokinin- and Gibberellic Acid-Induced Effects on the Determination and Morphogenesis of Leaf Primordia in Opuntia polyacantha (Cactaceae)." *American Journal of Botany,* vol. 64, no. 3, Mar. 1977, pp. 337-346.
12. Cactus spines clipart. *Florida Center for Instructional Technology.* (http://etc.usf.edu/clipart/83700/83786/83786_cactus_spine.htm) Web. Jan. 10, 2016.
13. Barcenas-Arguello M.L., Terrazas T., Arias S., "Trichomes with Crystals in the *Cephalocereus* Pfeiff. Areoles." *Botanical Sciences,* vol. 92, no. 3 (2014), pp. 335-342.
14. "Cellulose." *Wikipedia.* (https://en.wikipedia.org/wiki/Cellulose) Web. Dec. 10, 2016.
15. "Hemicellulose." *Wikipedia.* (https://en.wikipedia.org/wiki/Hemicellulose) Web. Dec. 10, 2016.
16. Clifford C.B., "Hemicellulose" *Alternative Fuels from Biomass Sources,* Chapter 6.2.3 (2015). Web. Dec. 10, 2016.
17. Laine C. "Structures of Hemicelluloses and Pectins in Wood and Pulp." *KCL Communications* (2010).
18. "Arabinan (Sugar Beet)." *Megazyme.* (https://secure.megazyme.com/files/Booklet/P-ARAB_DATA.pdf) Web. Dec. 10, 2016.
19. "Lignin." *Wikipedia*. (https://en.wikipedia.org/wiki/Lignin) Web. Dec. 10, 2016.
20. "Pectin." *Wikipedia.* (https://en.wikipedia.org/wiki/Pectin) Web. Dec. 2, 2016.
21. ASTM Standard D790, 2010. "Standard Test Methods for Flexural Properties of Unreinforced and Reinforced Plastics and Electrical Insulating Materials," ASTM International, West Conshohocken, PA, 2010, DOI: 10.1520/D0790-10

Appendix A: List of All Species Tested

Astrophytum ornatum
Echinocactus grusonii
Echinocactus polycephalus
Echinocereus boyce-thompsonii
Echinocereus englemanii
Echinocereus triglochidiatus
Echinopsis spachiana
Echinopsis terschekii
Ferocactus chrysacanthus
Ferocactus cylindraceus
Ferocactus emoryi
Ferocactus pilosus
Ferocactus viridescens
Ferocactus wislizenianus
Grusonia emoryi
Myrtillocactus geometrizans
Oreocereus celcianus
Pachycereus pringlei
Sclerocactus parviflorus
Sclerocactus polyancistrus
Stenocactus crispatus
Stenocactus multicostatus
Stenocereus thurberi
Tephrocactus alexanderi

Appendix B: Fracture Images

Astrophytum ornatum

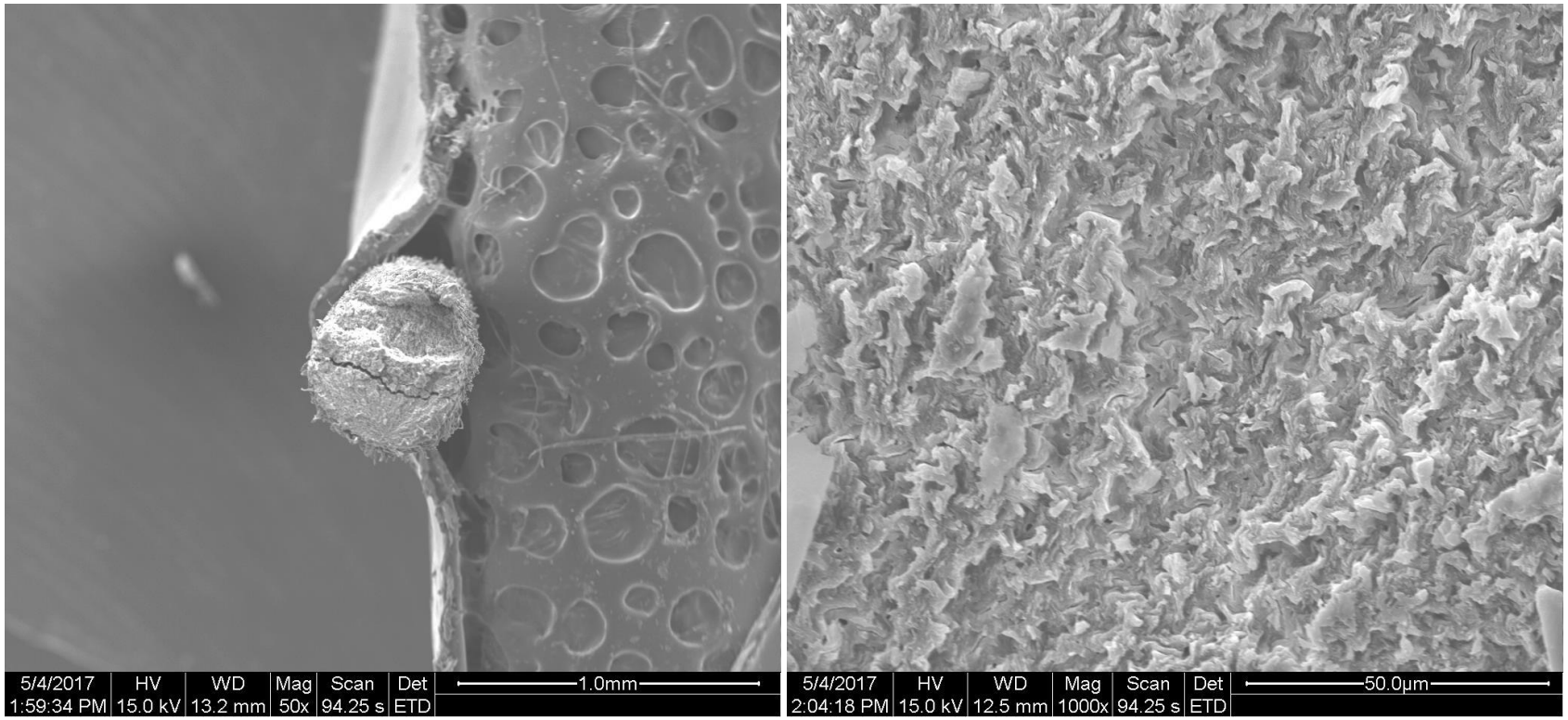

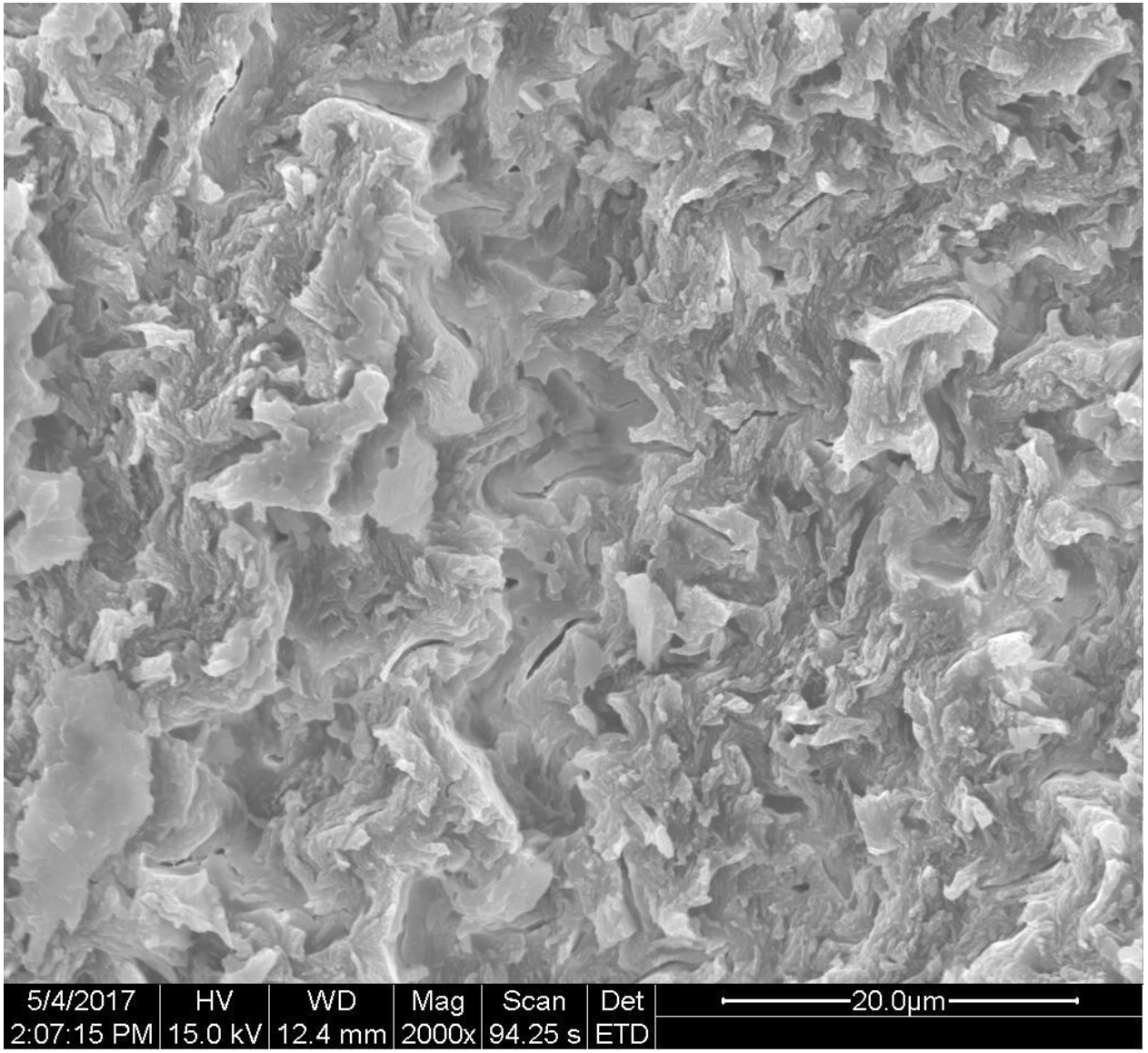
5/4/2017
2:07:15 PM
HV
15.0 kV
WD
12.4 mm
Mag
2000x
Scan
94.25 s
Det
ETD
20.0µm

Echinocactus grusonii

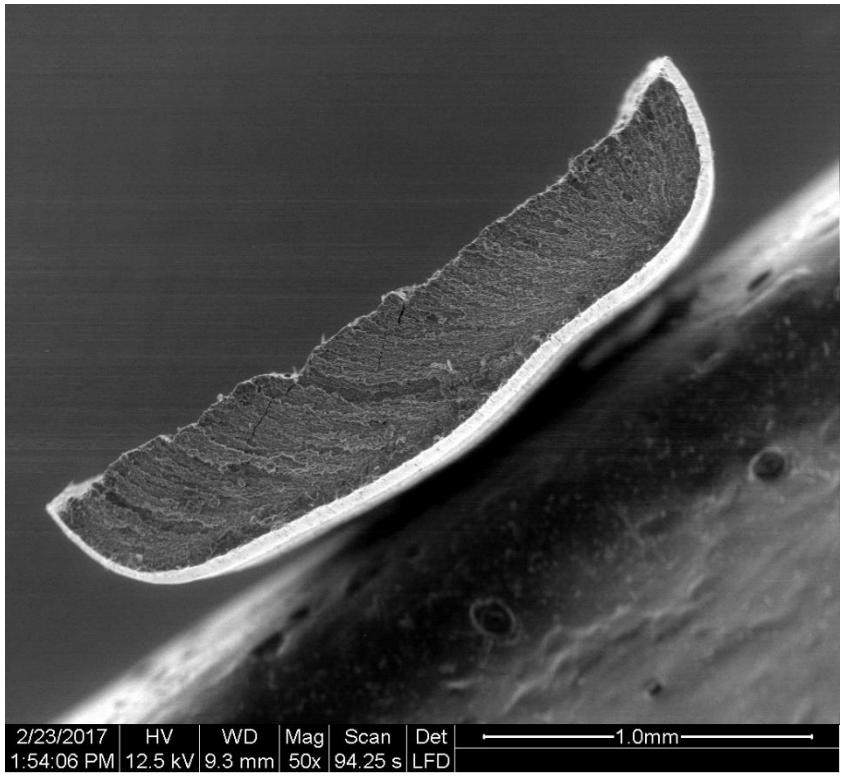

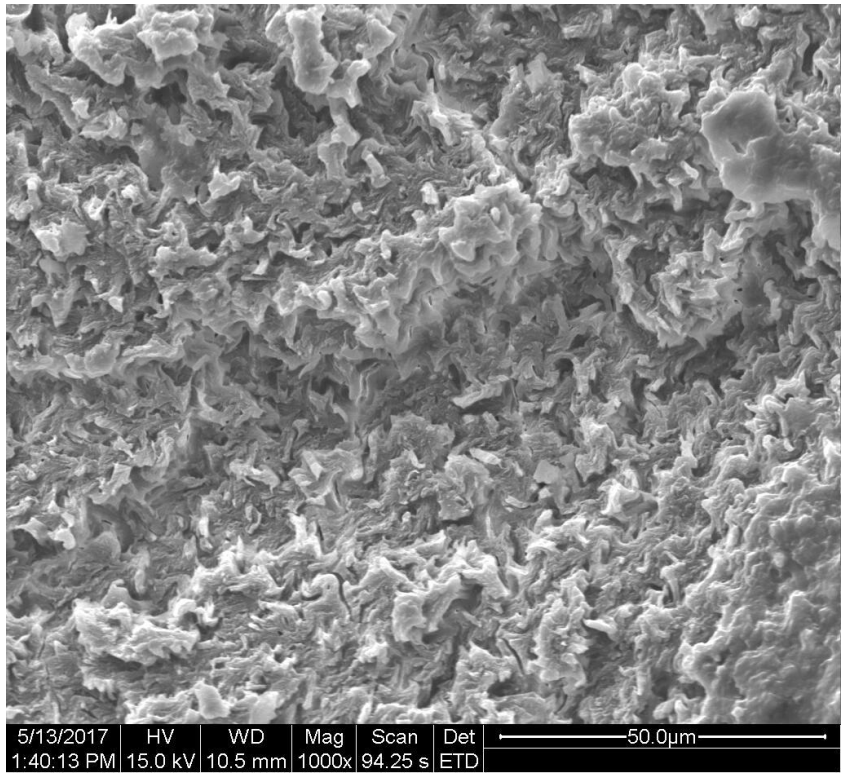

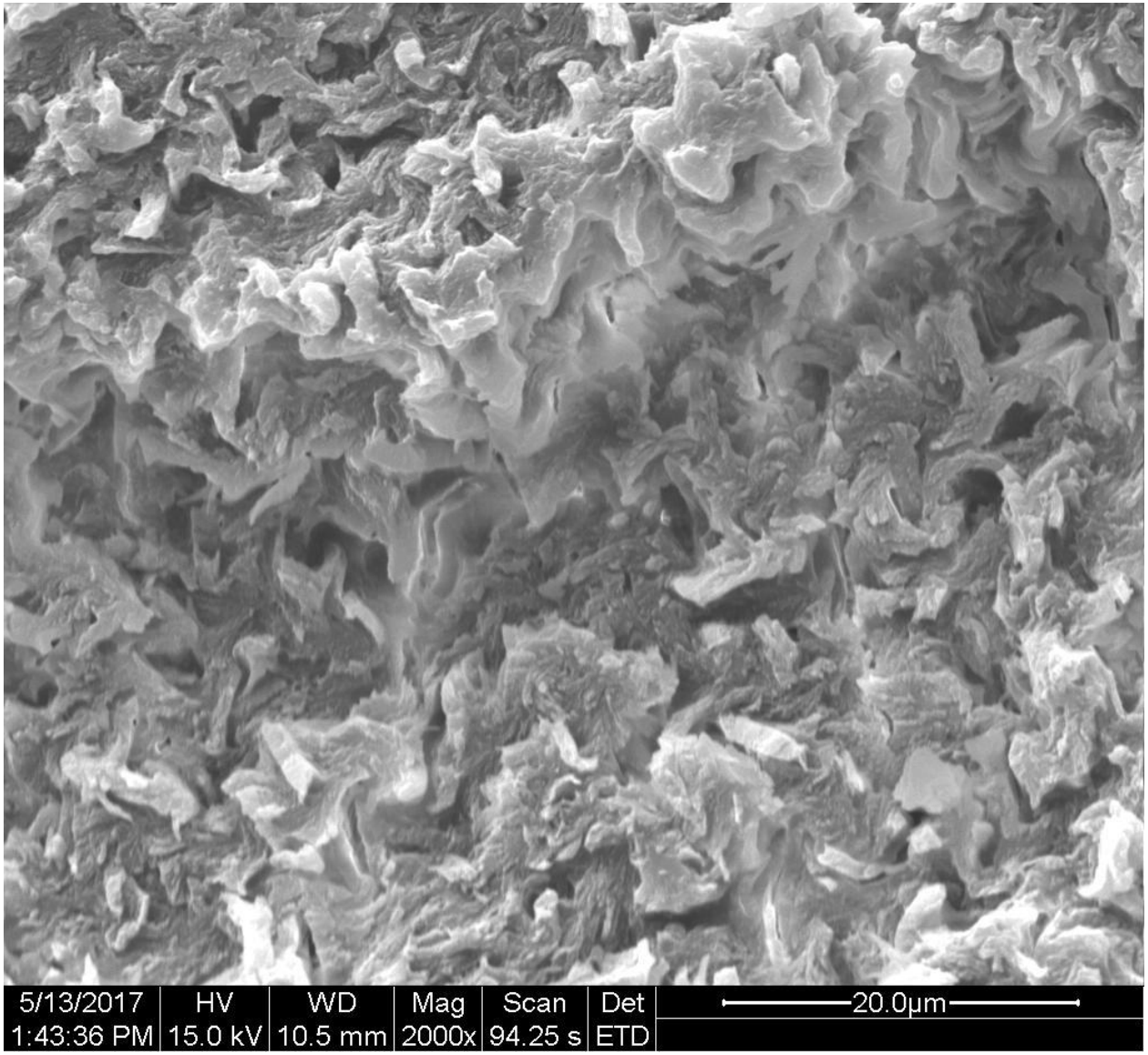
5/13/2017
1:43:36 PM
HV
15.0 kV
WD
10.5 mm
Mag
2000x
Scan
94.25 s
Det
ETD
20.0µm

Echinocactus polycephalus

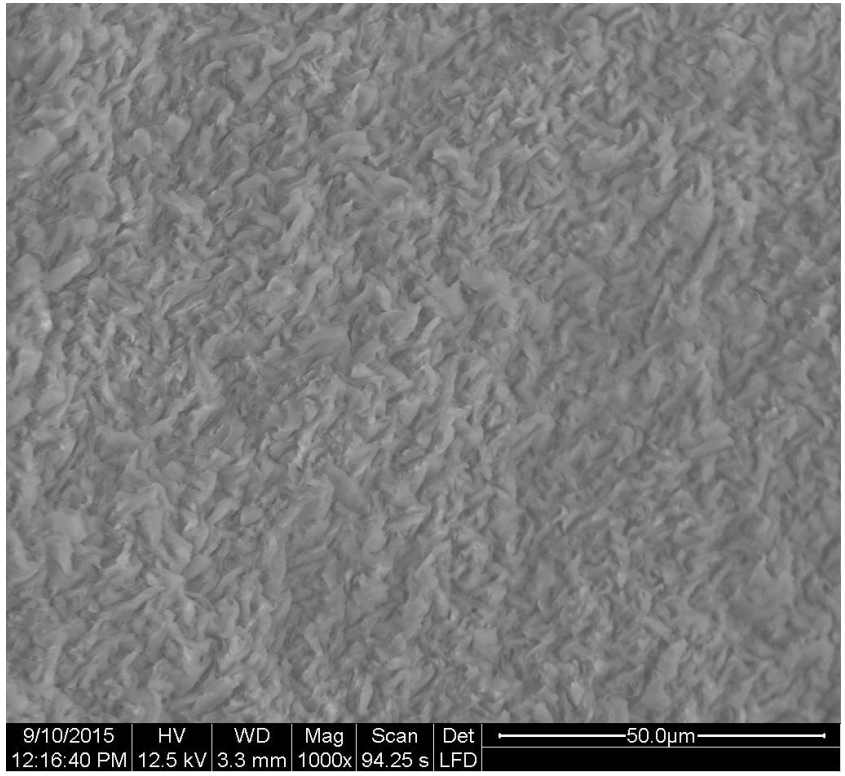

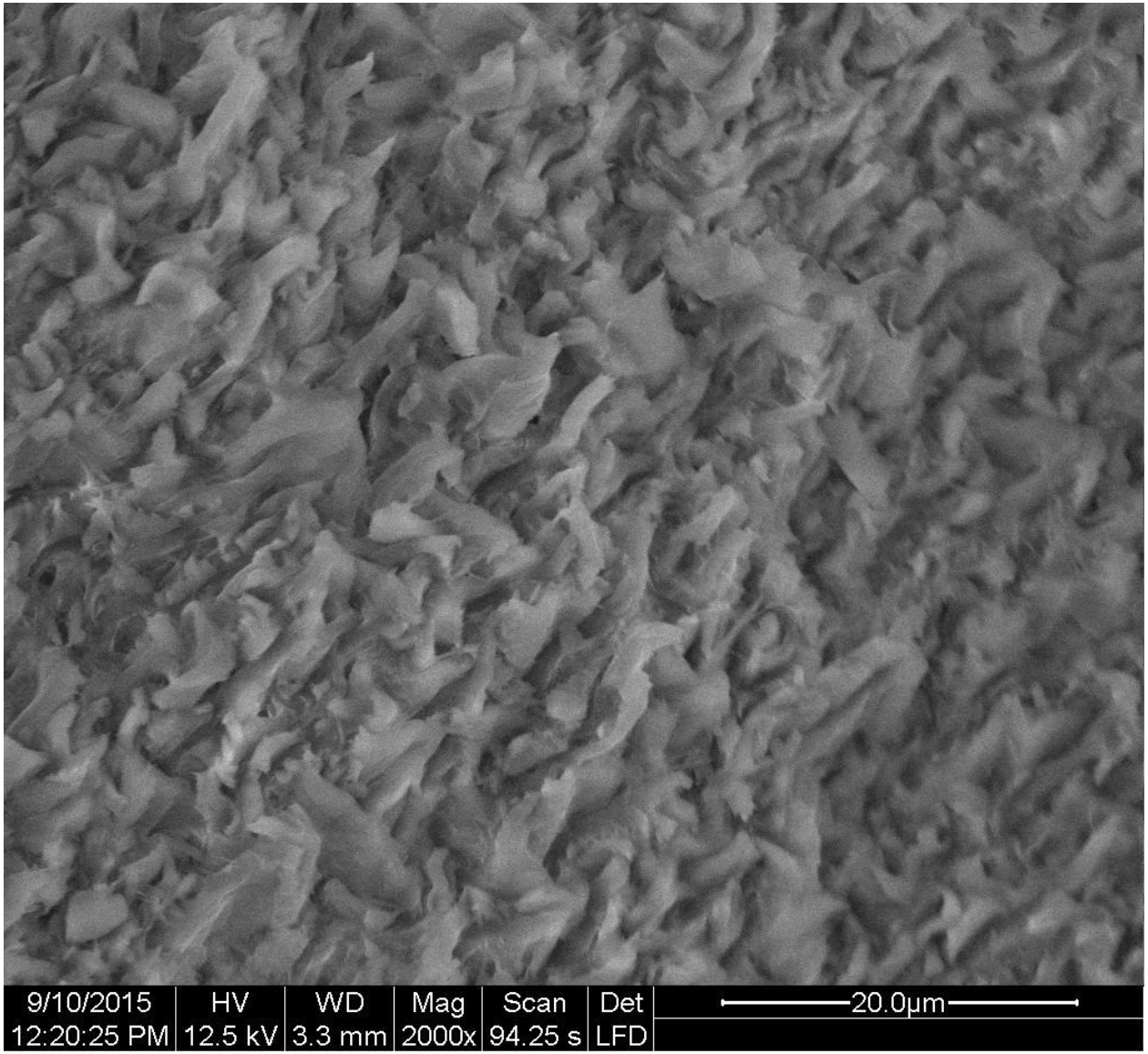
9/10/2015
12:20:25 PM
HV
12.5 kV
WD
3.3 mm
Mag
2000x
Scan
94.25 s
Det
LFD
20.0µm

Echinocereus boyce-thompsonii

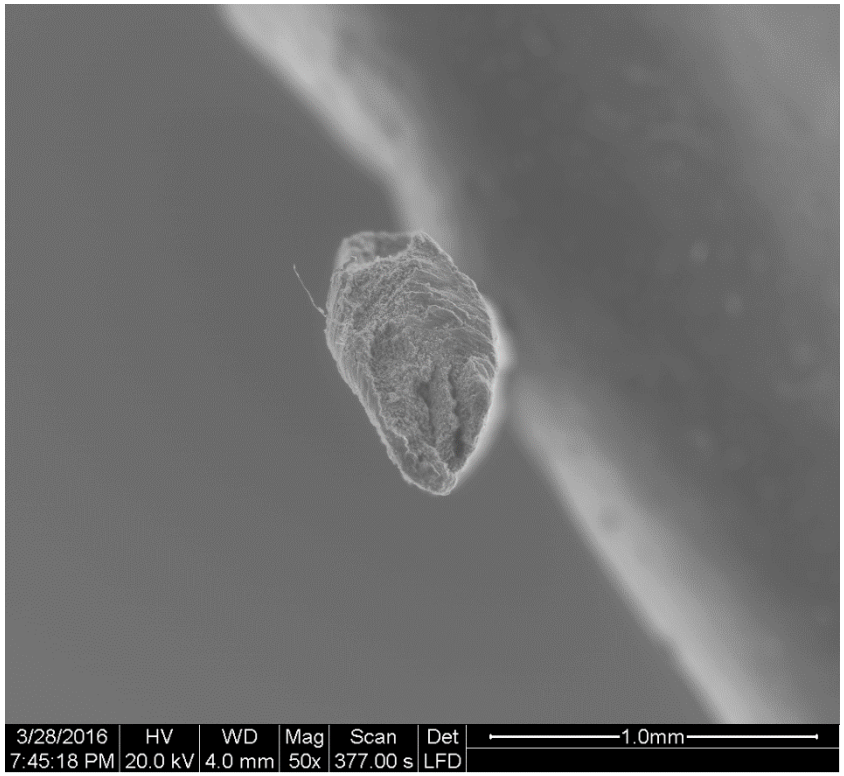

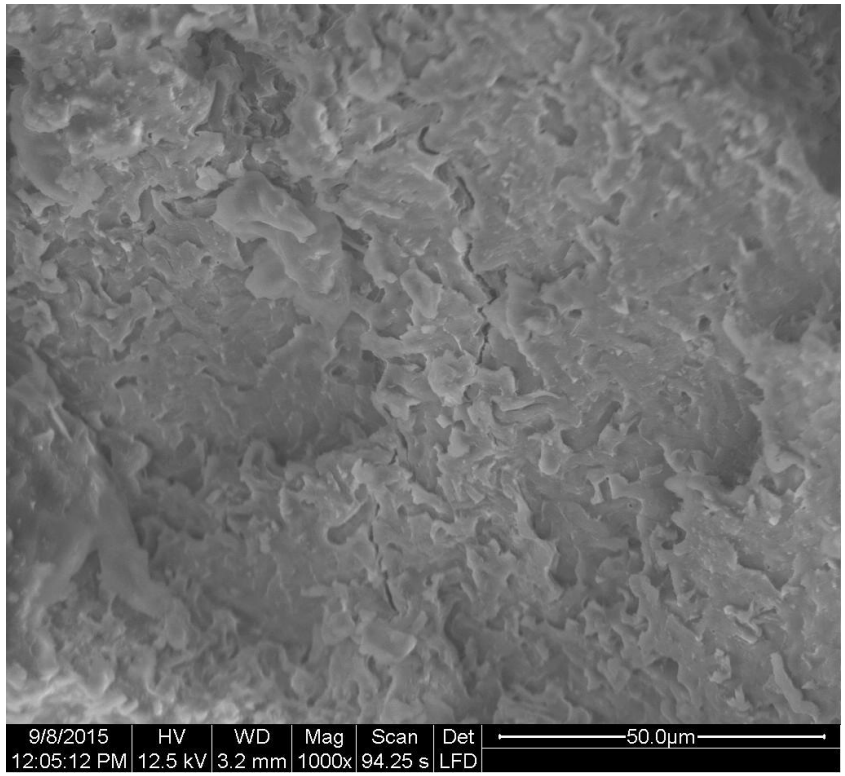

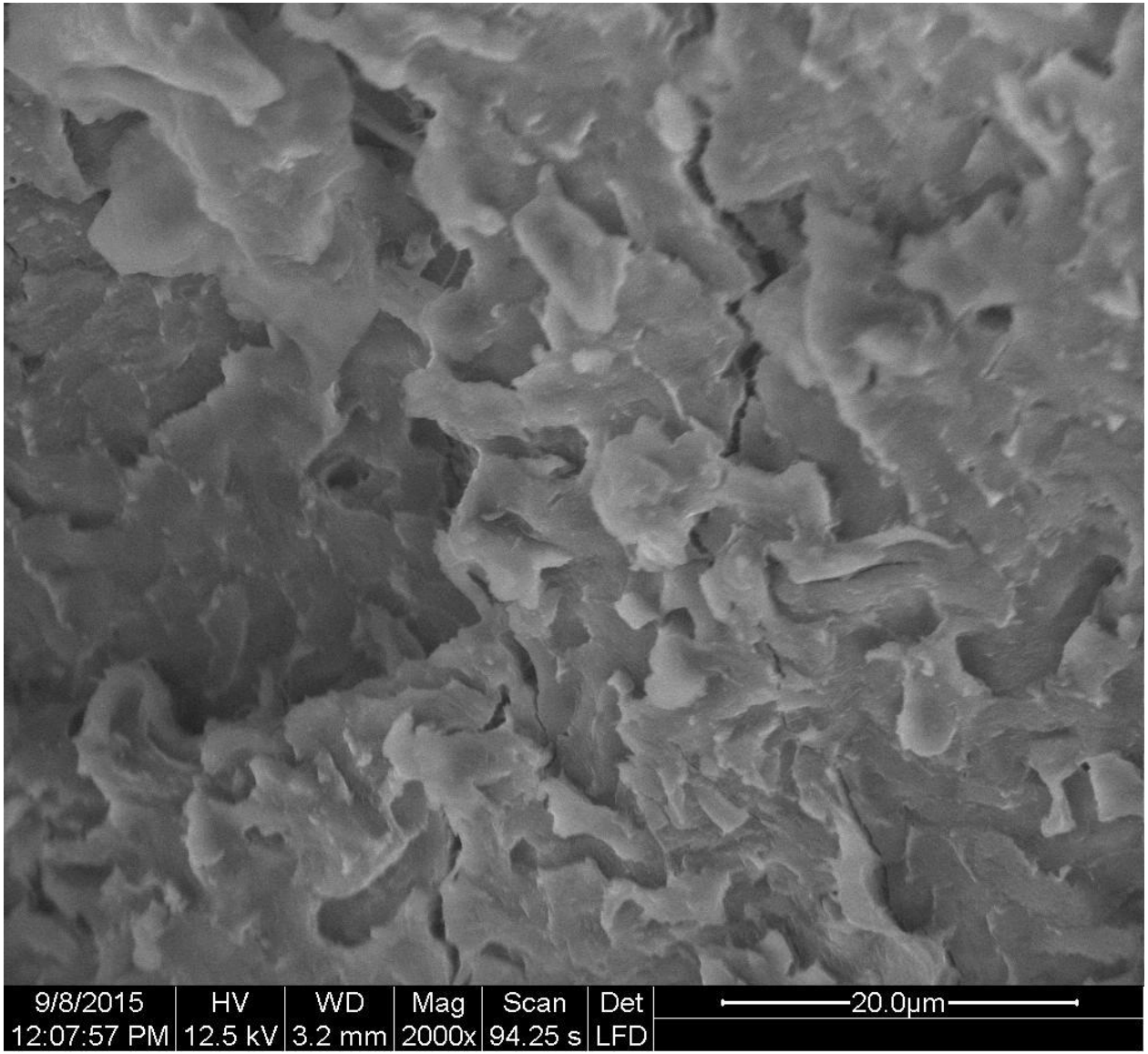
9/8/2015
12:07:57 PM
HV
12.5 kV
WD
3.2 mm
Mag
2000x
Scan
94.25 s
Det
LFD
20.0µm

Echinocereus englemanii

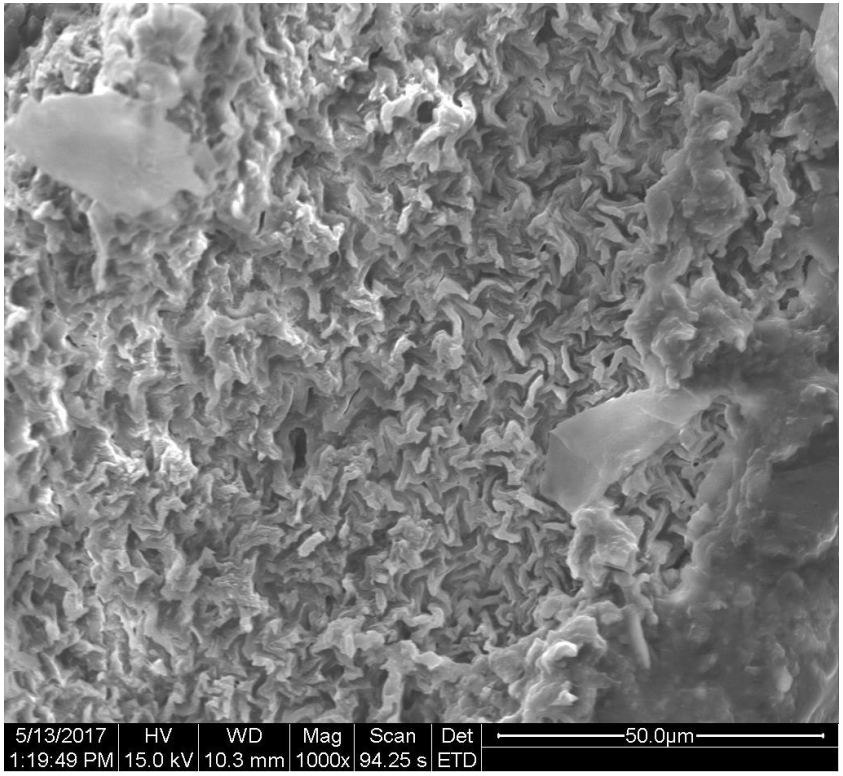

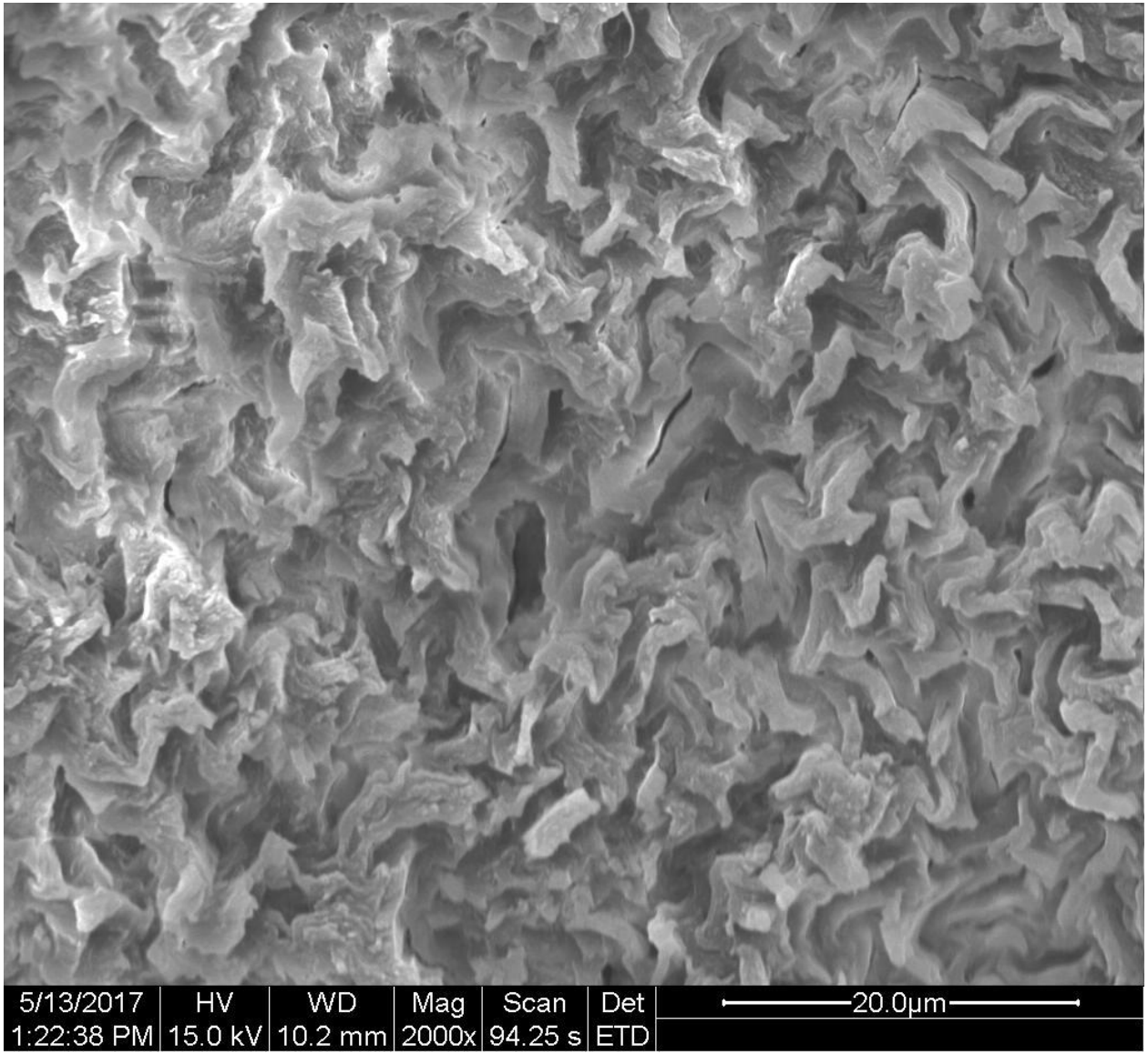
5/13/2017
1:22:38 PM
HV
15.0 kV
WD
10.2 mm
Mag
2000x
Scan
94.25 s
Det
ETD
20.0µm

Echinocereus triglochidiatus

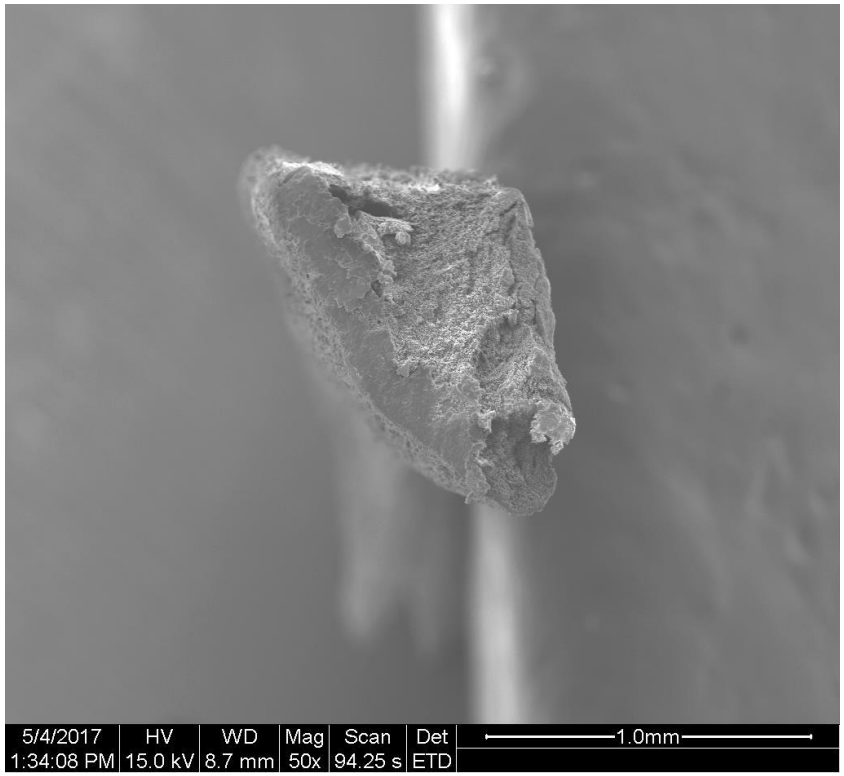

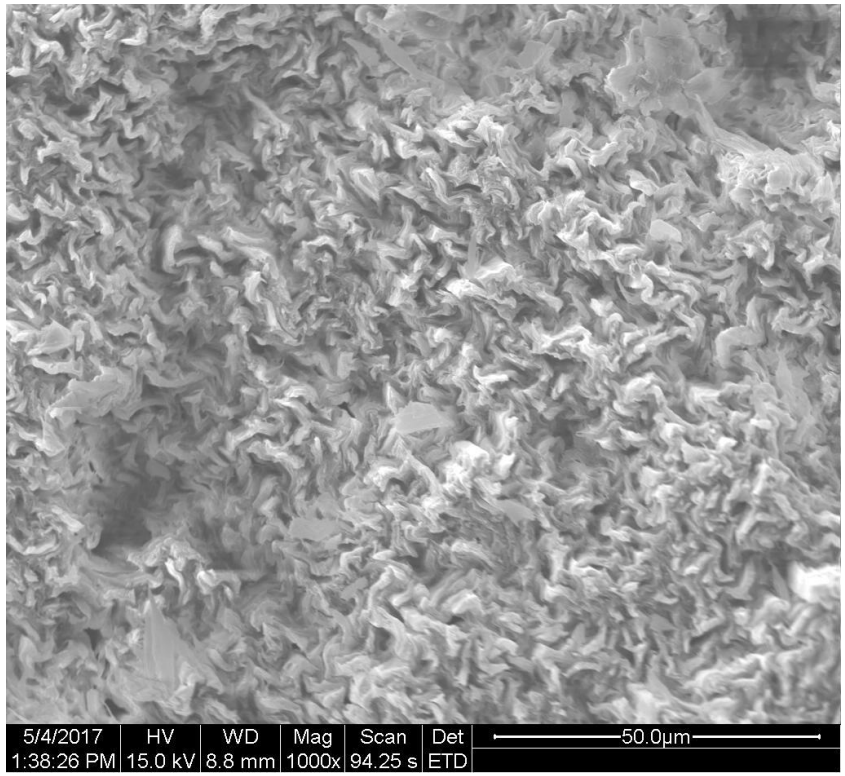

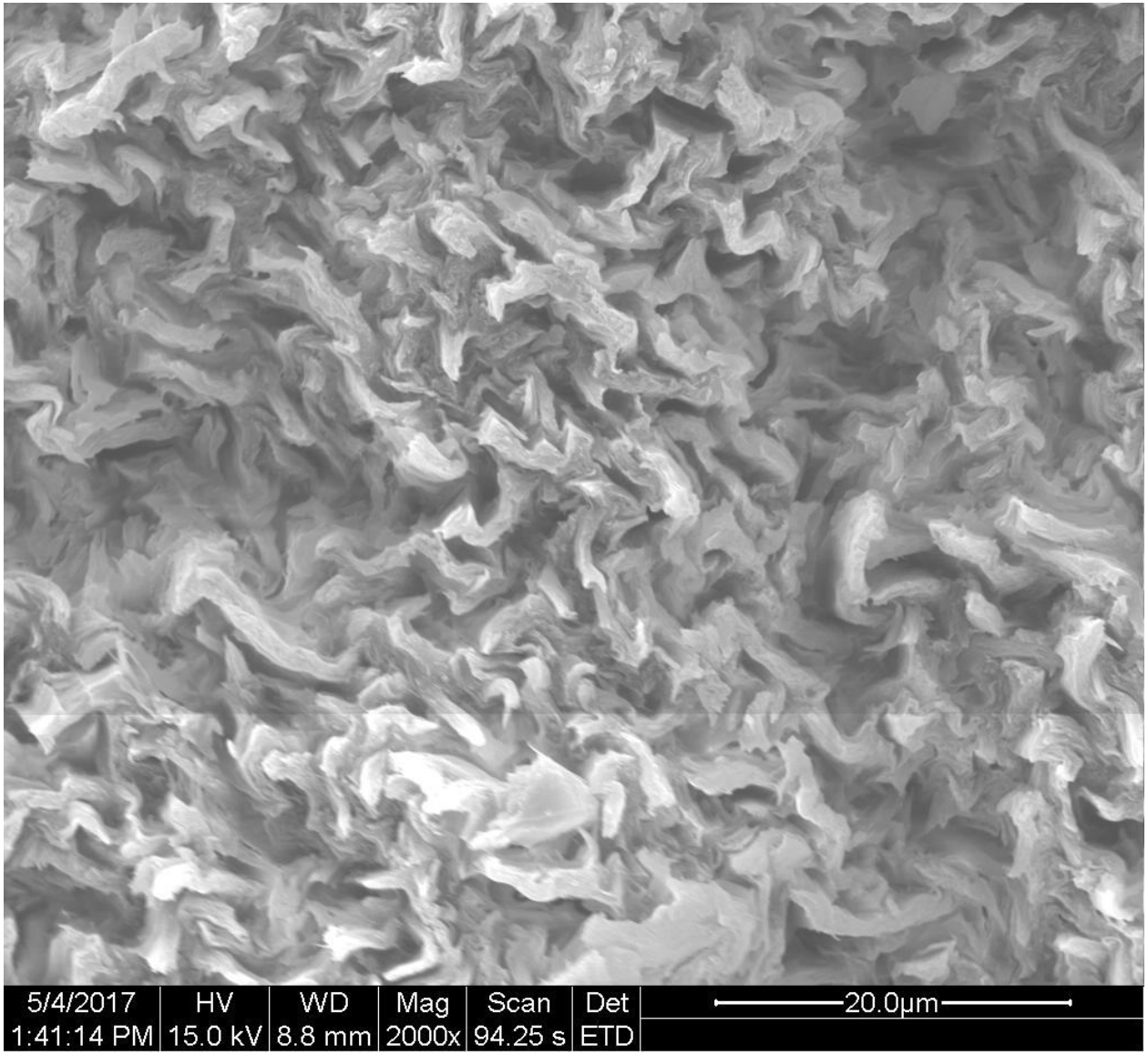
5/4/2017
1:41:14 PM
HV
15.0 kV
WD
8.8 mm
Mag
2000x
Scan
94.25 s
Det
ETD
20.0µm

Echinopsis spachiana

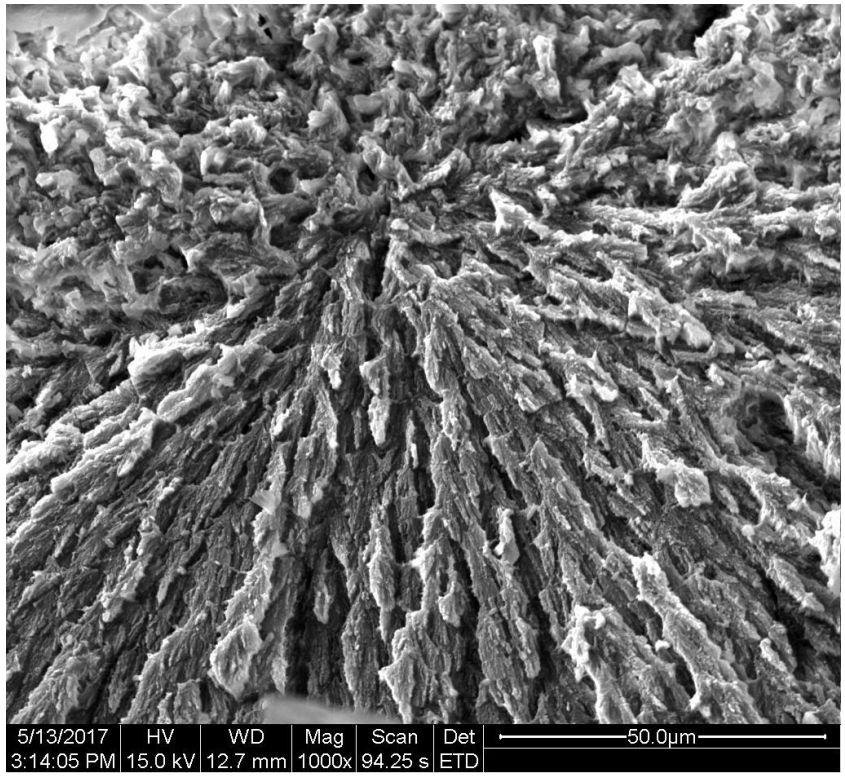

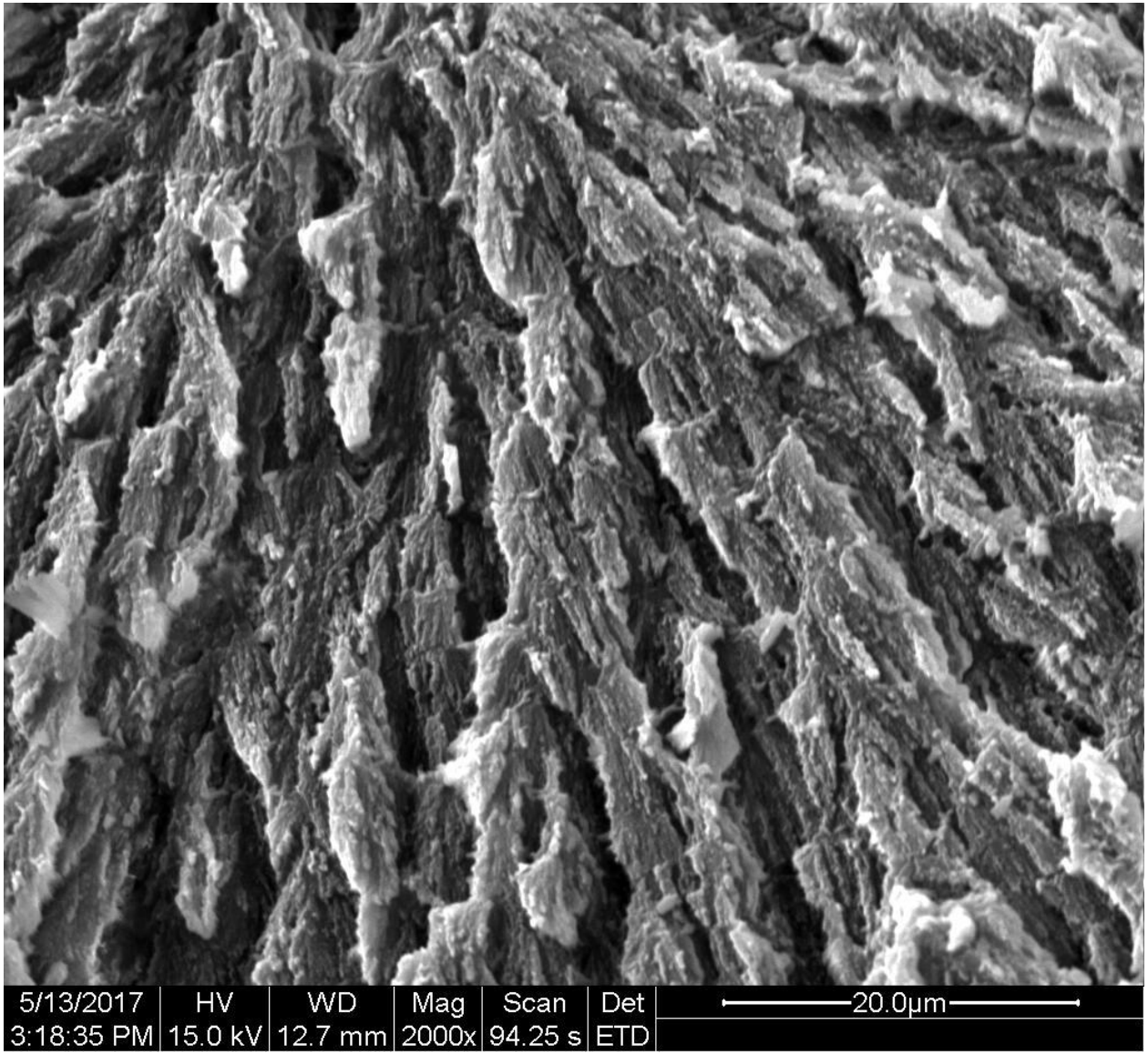
5/13/2017
3:18:35 PM
HV
15.0 kV
WD
12.7 mm
Mag
2000x
Scan
94.25 s
Det
ETD
20.0µm

Echinopsis terschekii

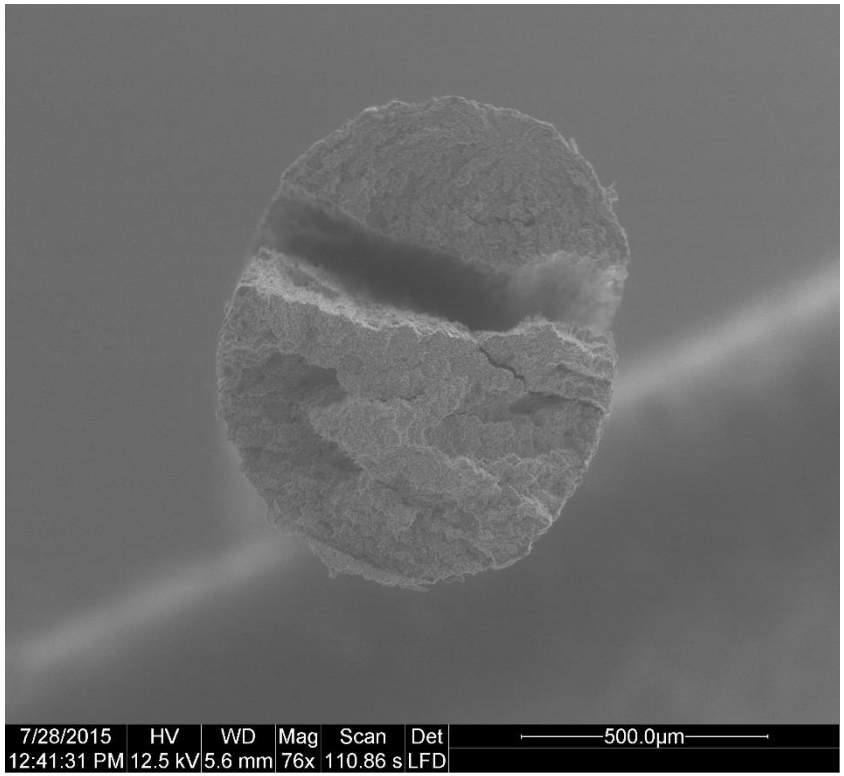

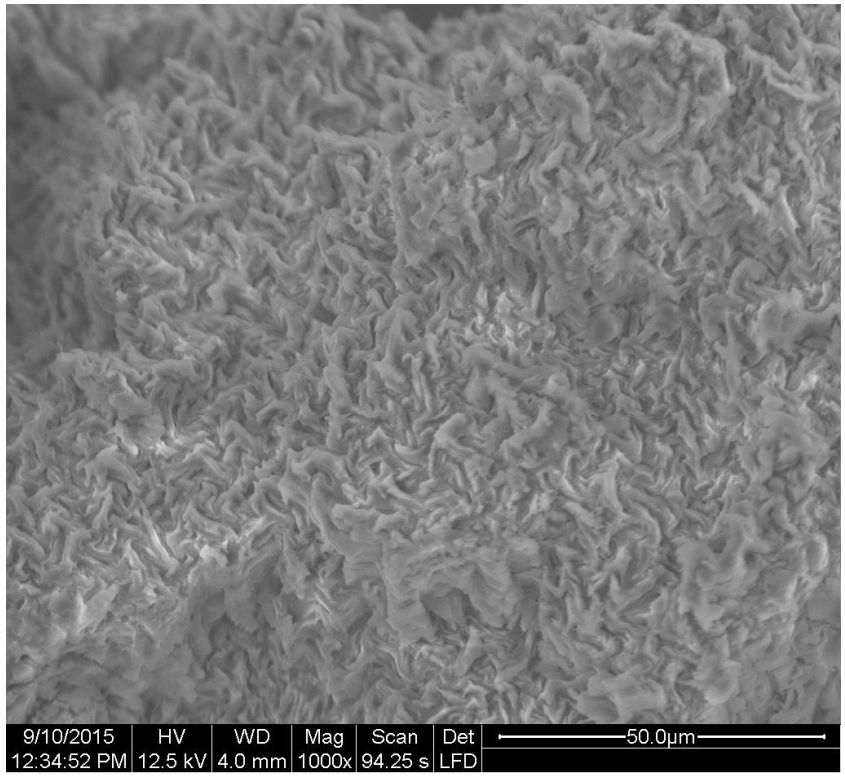

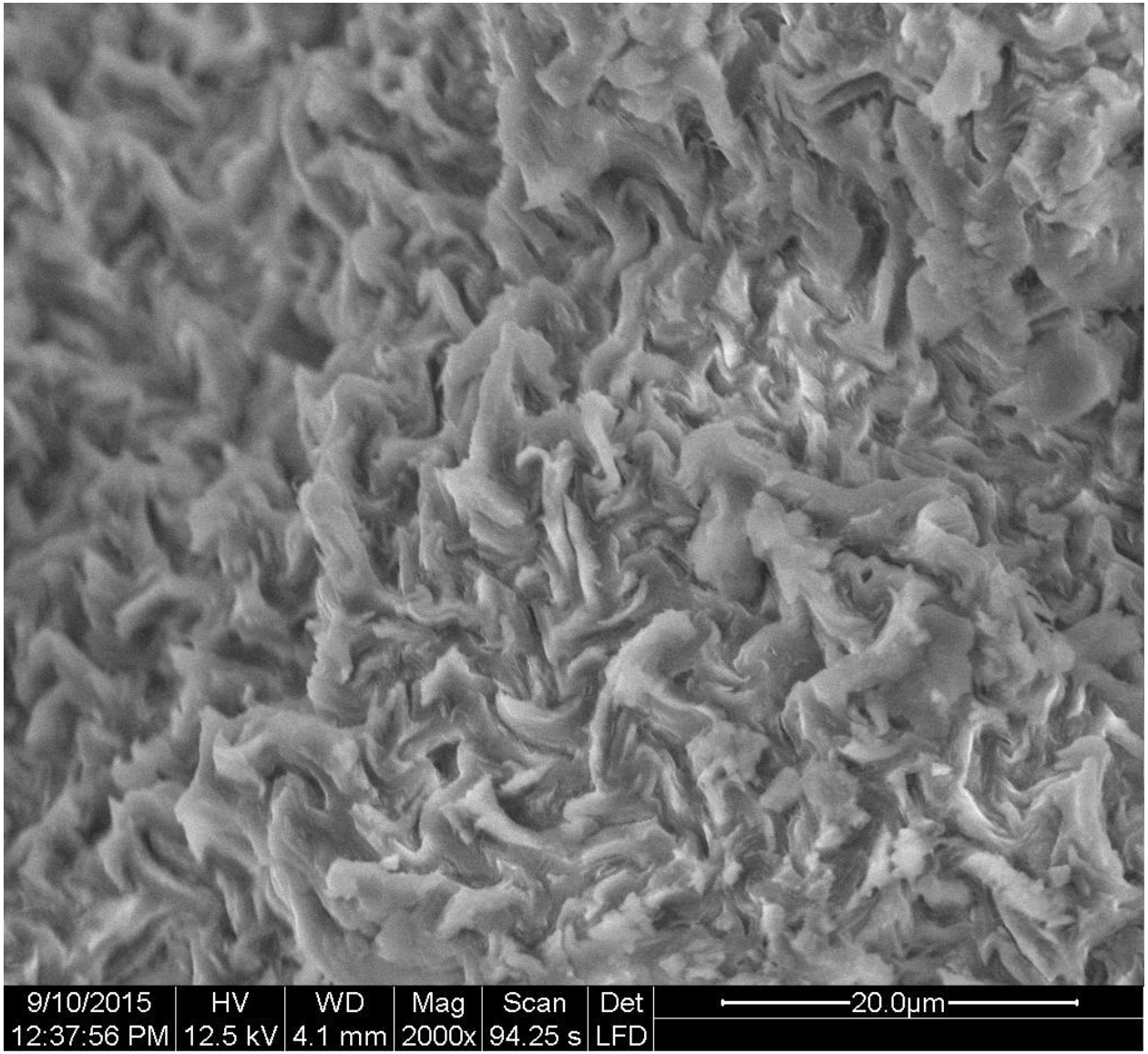
9/10/2015
12:37:56 PM
HV
12.5 kV
WD
4.1 mm
Mag
2000x
Scan
94.25 s
Det
LFD
20.0µm

Ferocactus chrysacanthus

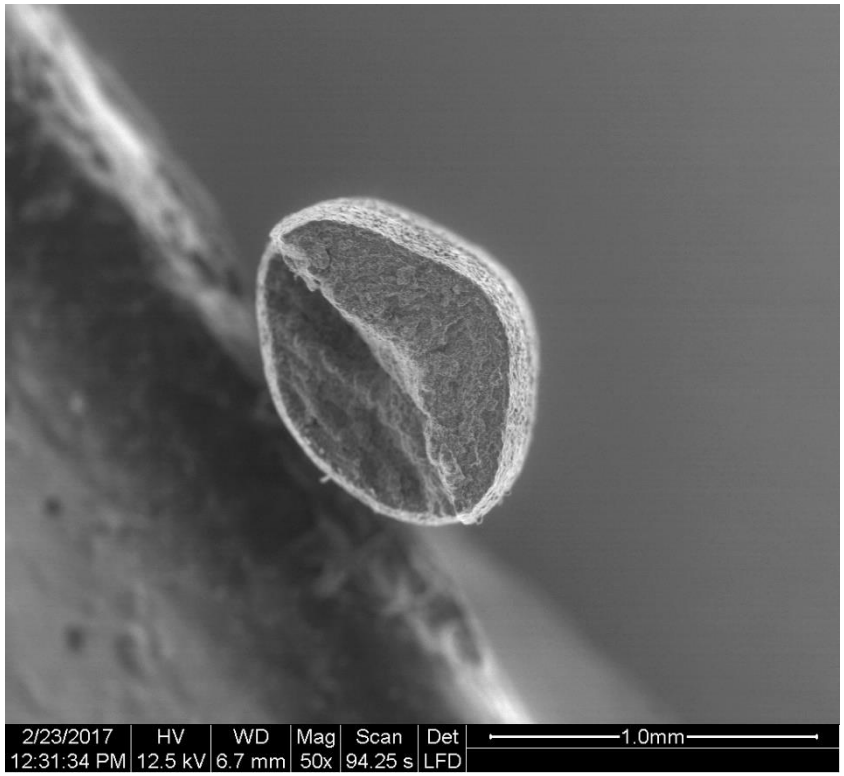

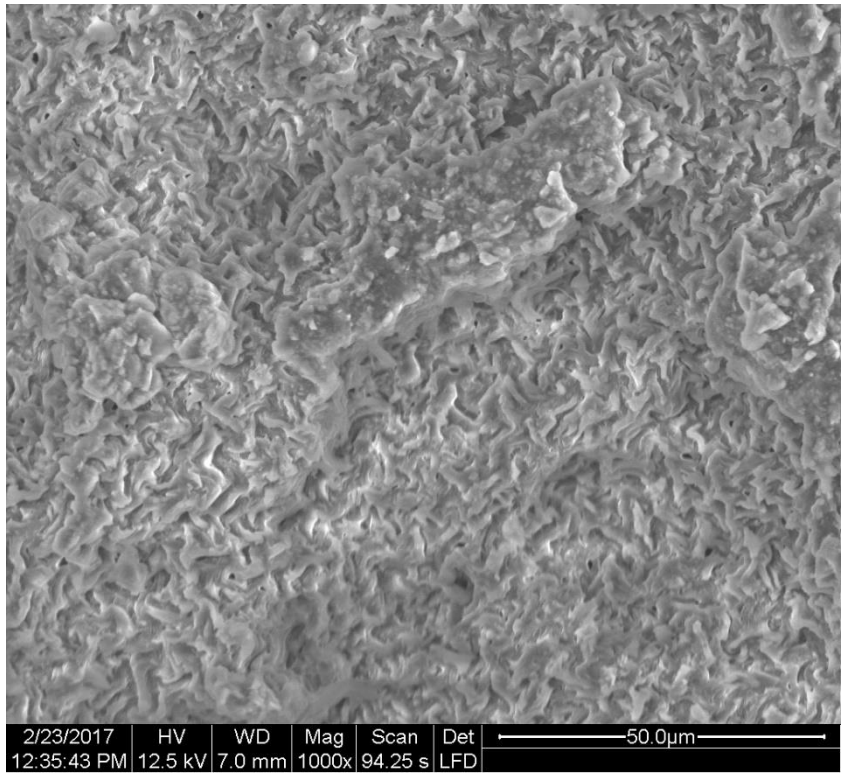

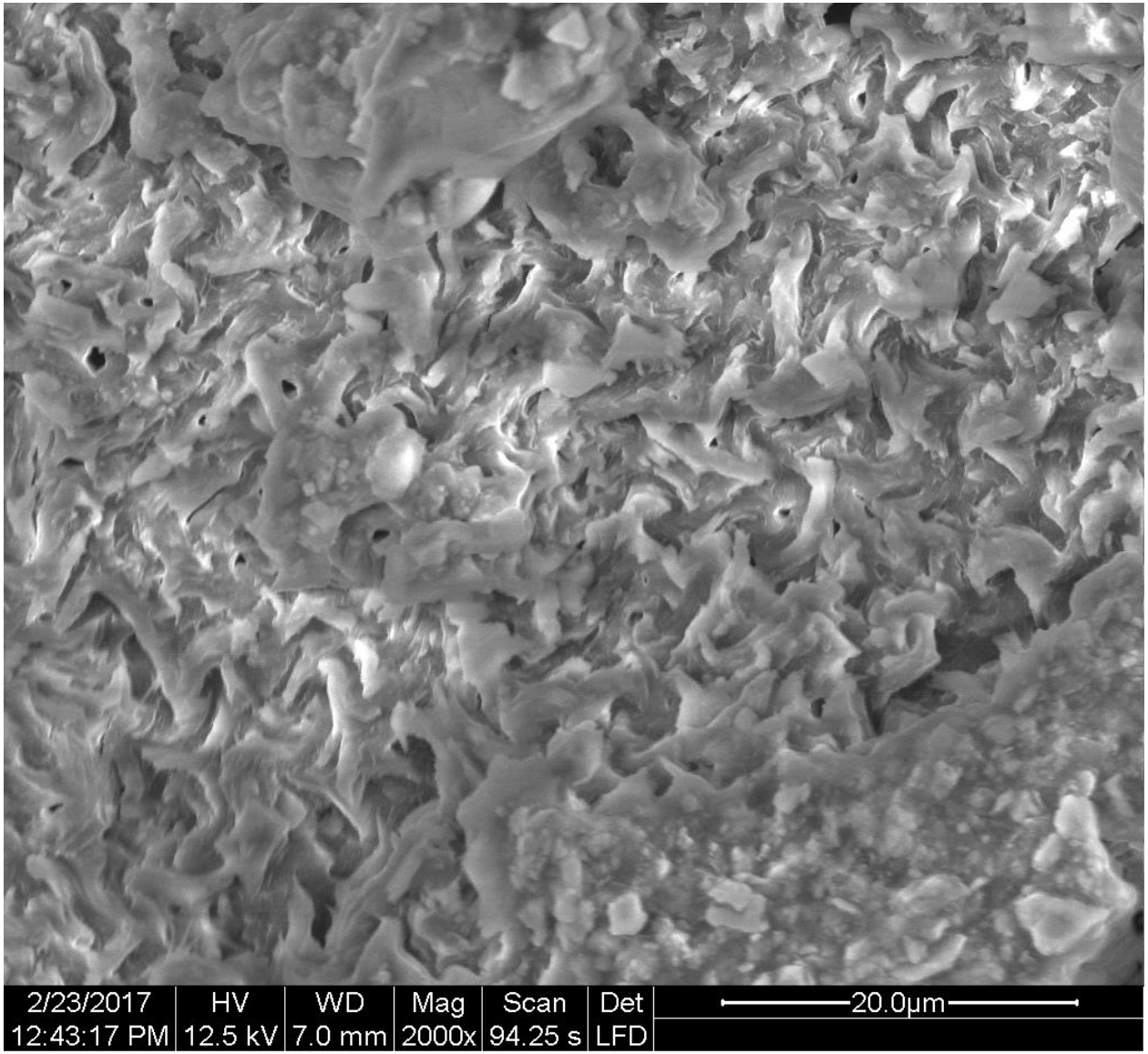
2/23/2017
12:43:17 PM
HV
12.5 kV
WD
7.0 mm
Mag
2000x
Scan
94.25 s
Det
LFD
20.0µm

Ferocactus cylindraceus

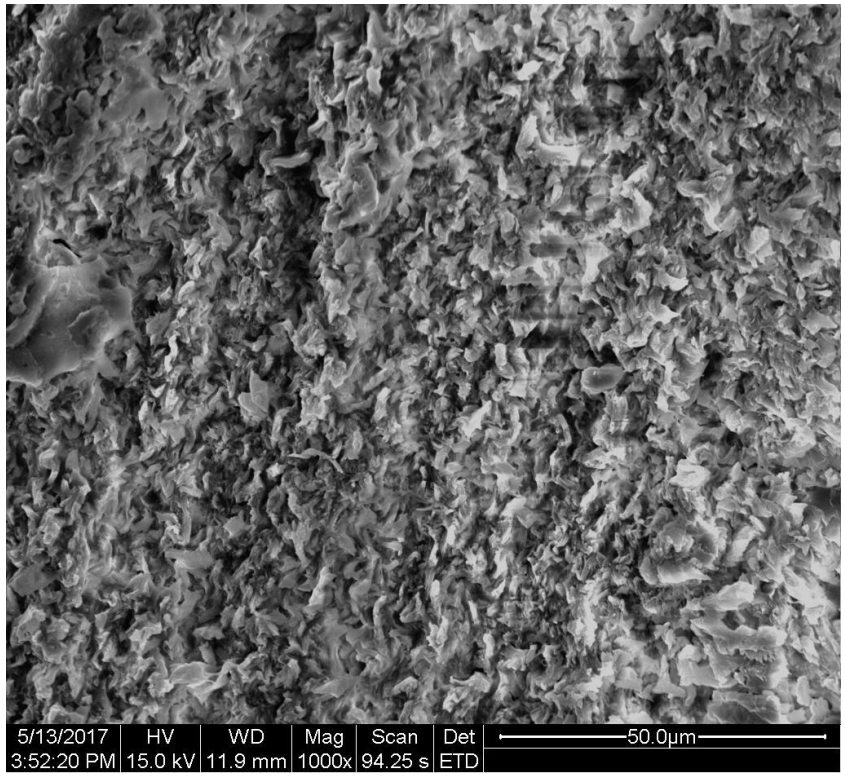

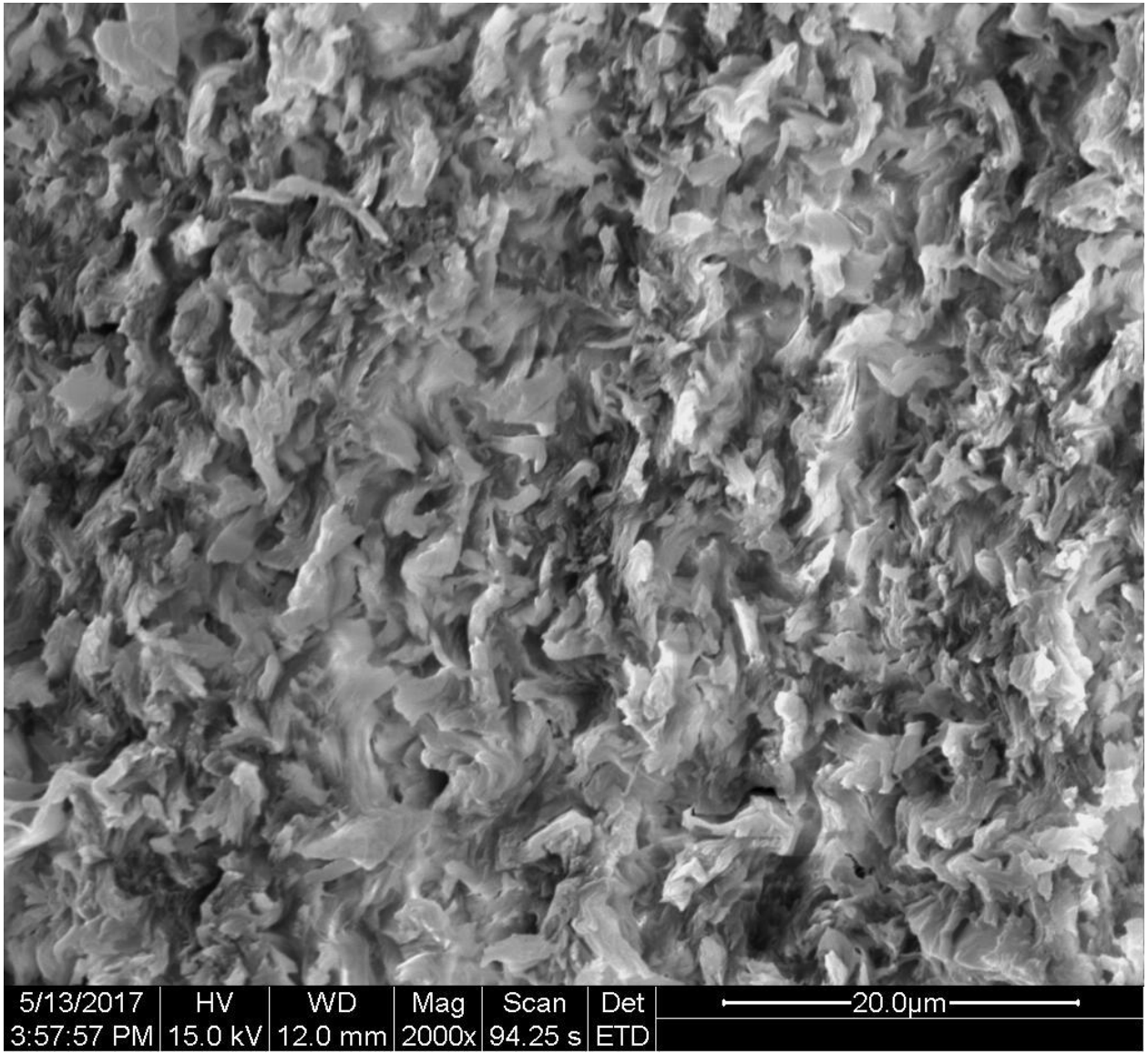
5/13/2017
3:57:57 PM
HV
15.0 kV
WD
12.0 mm
Mag
2000x
Scan
94.25 s
Det
ETD
20.0µm

Ferocactus emoryi

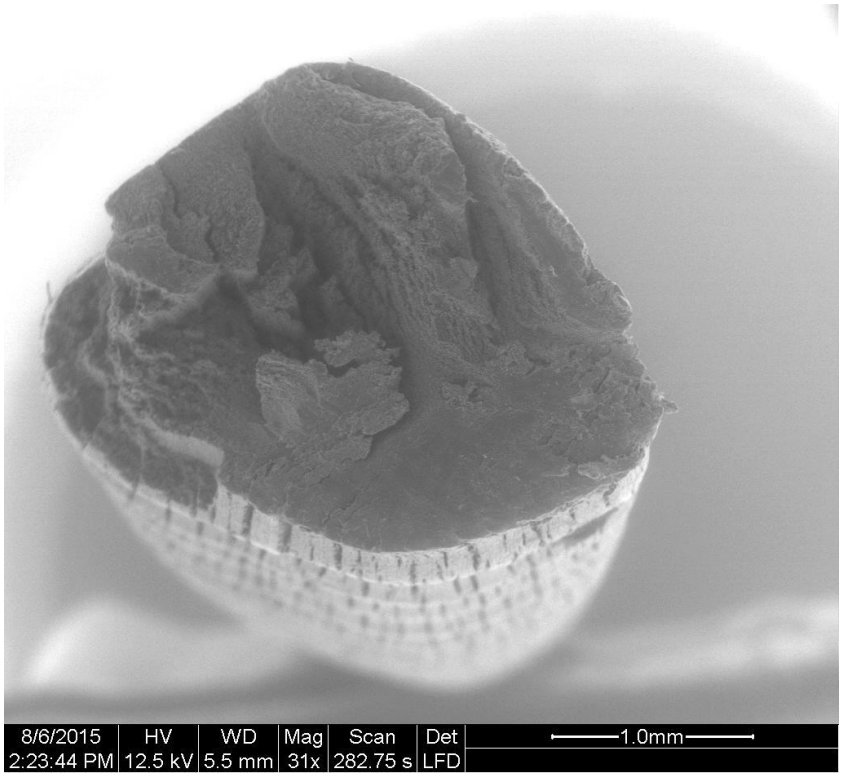

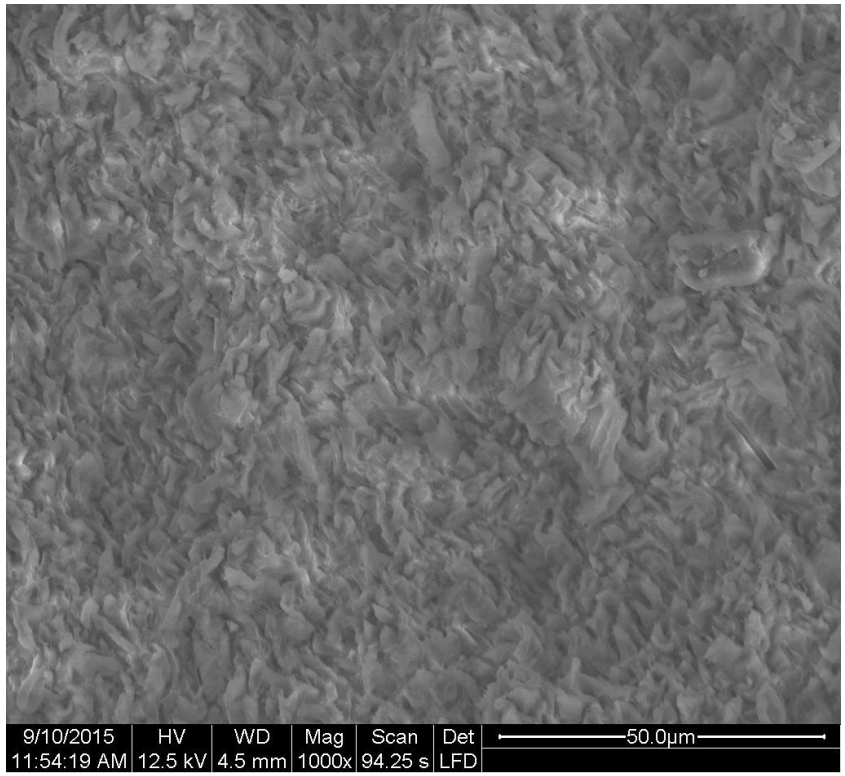

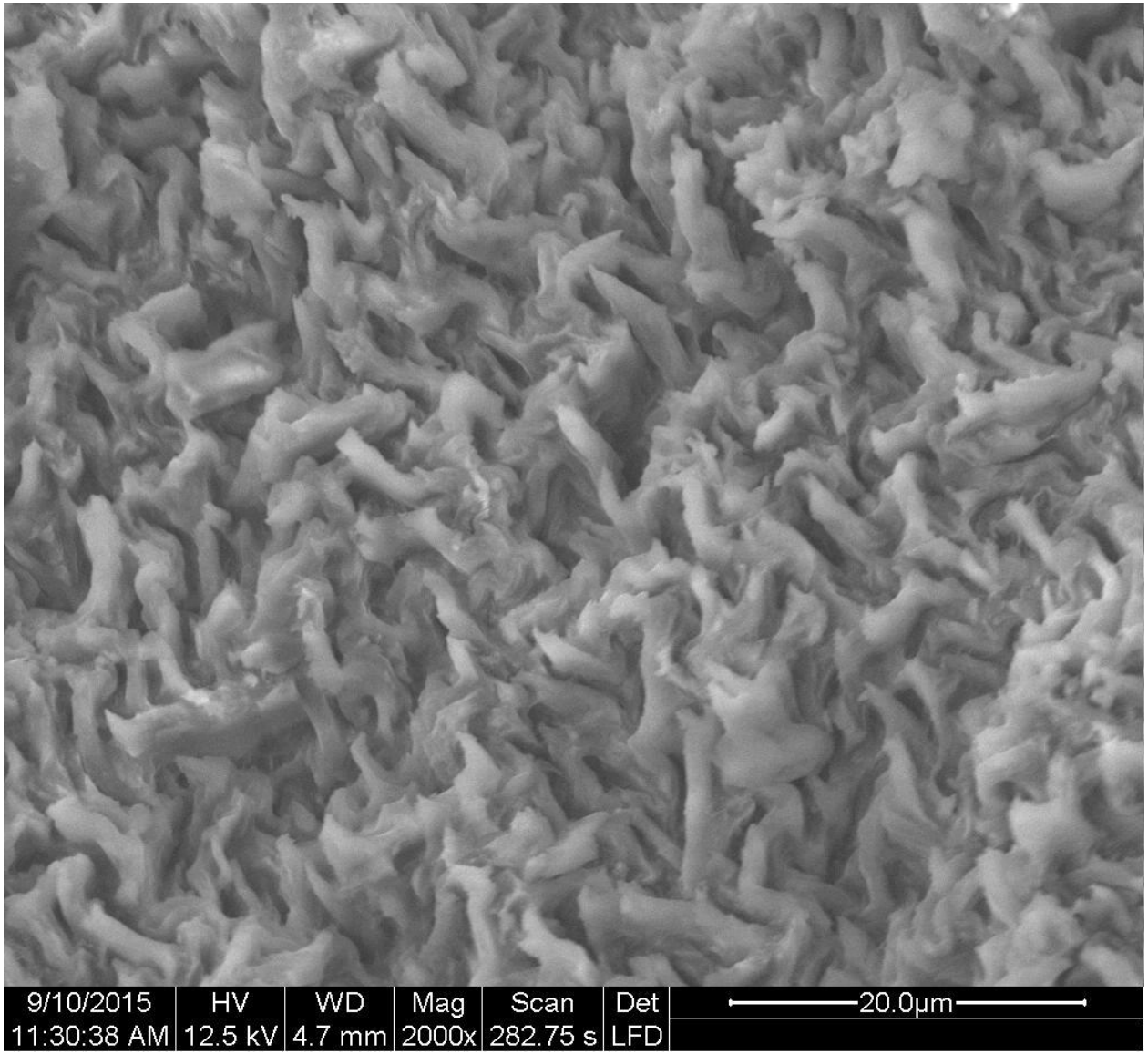
9/10/2015
11:30:38 AM
HV
12.5 kV
WD
4.7 mm
Mag
2000x
Scan
282.75 s
Det
LFD
20.0µm

Ferocactus pilosus

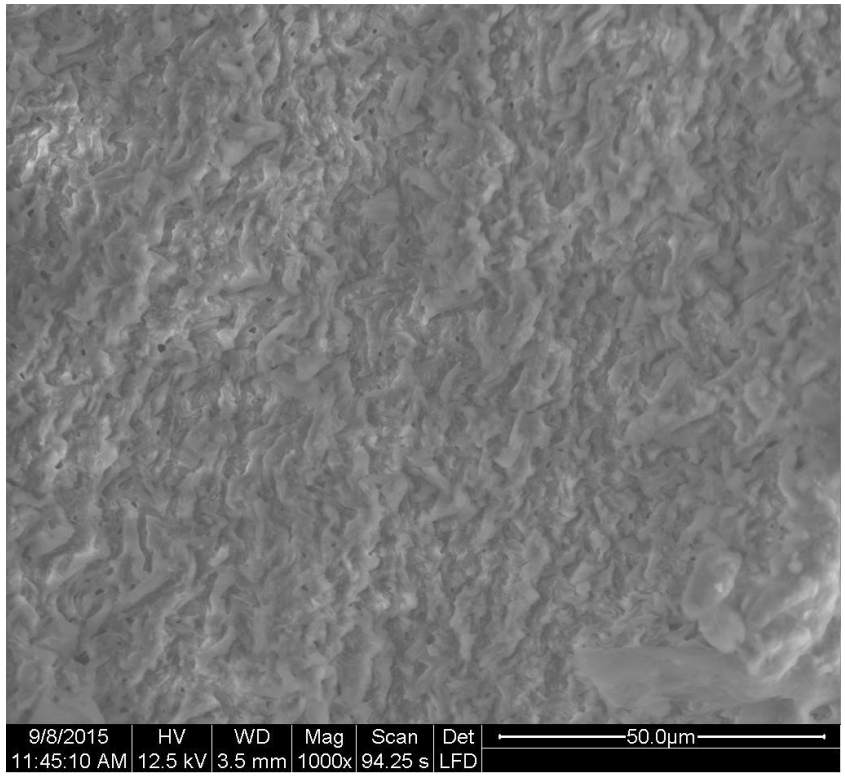

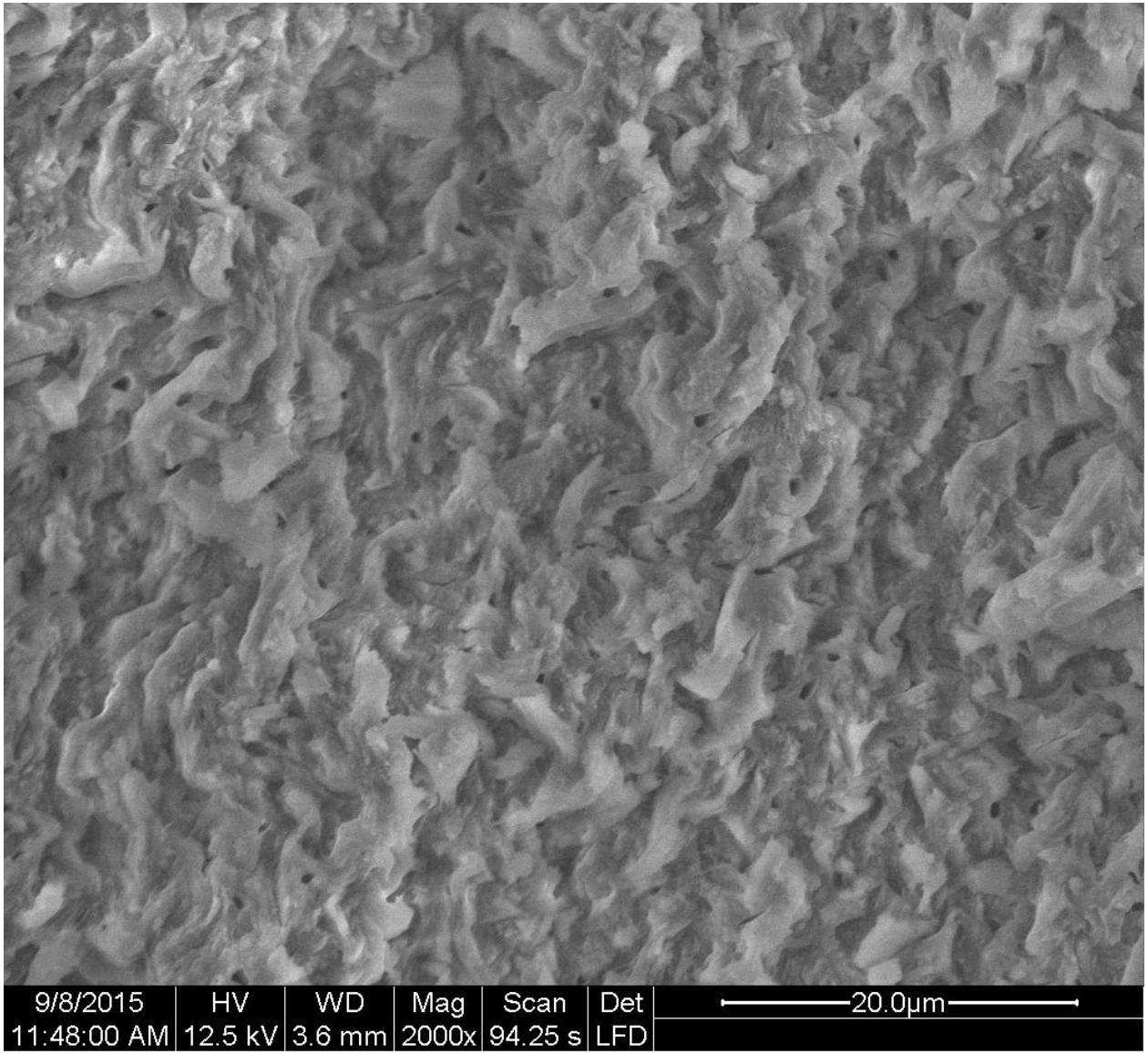
9/8/2015
11:48:00 AM
HV
12.5 kV
WD
3.6 mm
Mag
2000x
Scan
94.25 s
Det
LFD
20.0µm

Ferocactus viridescens

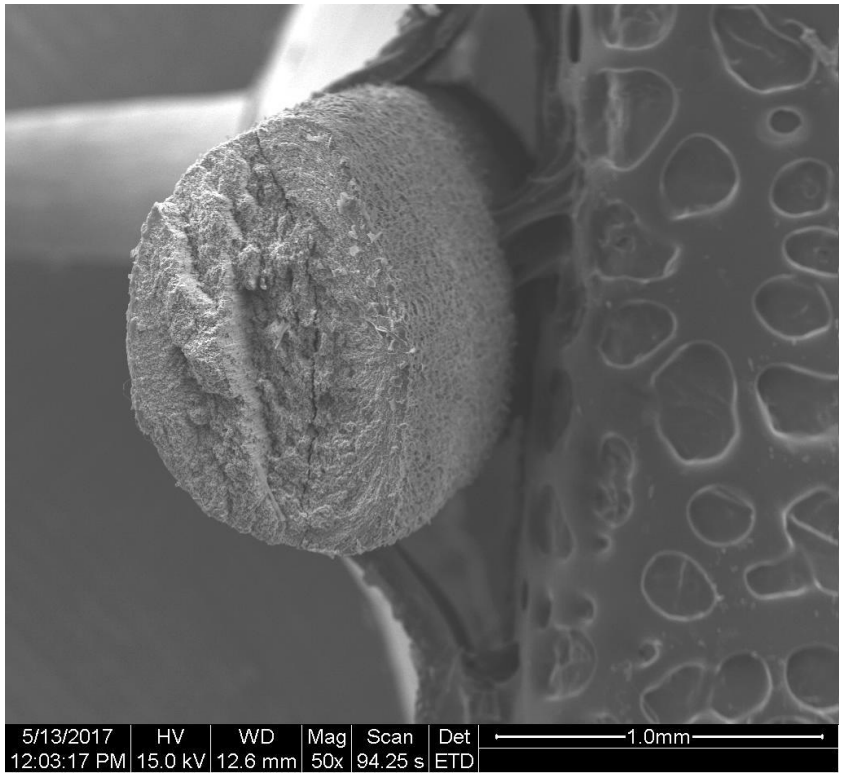

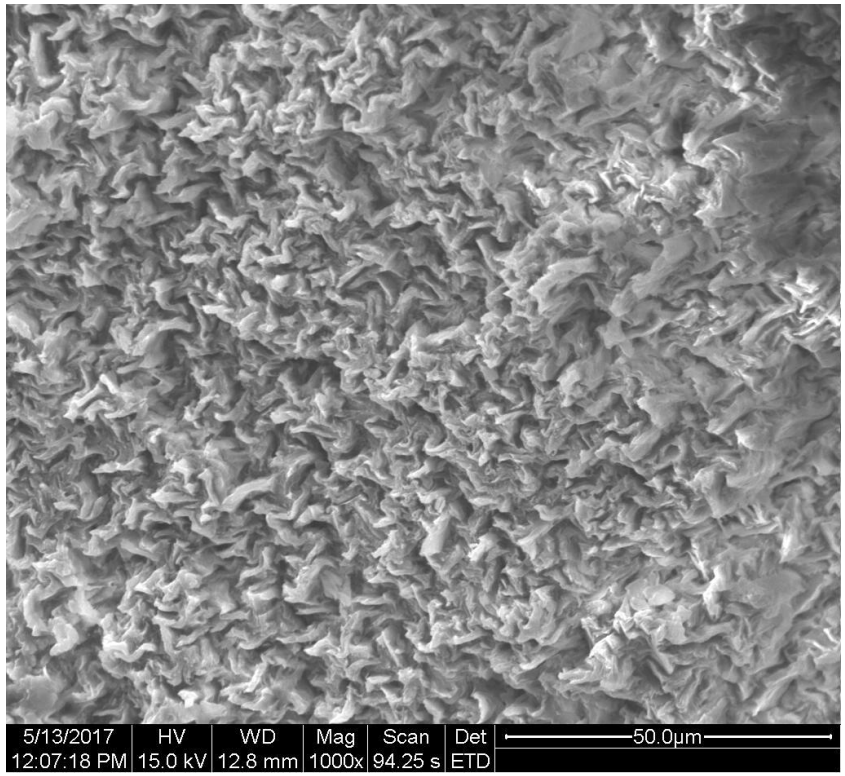

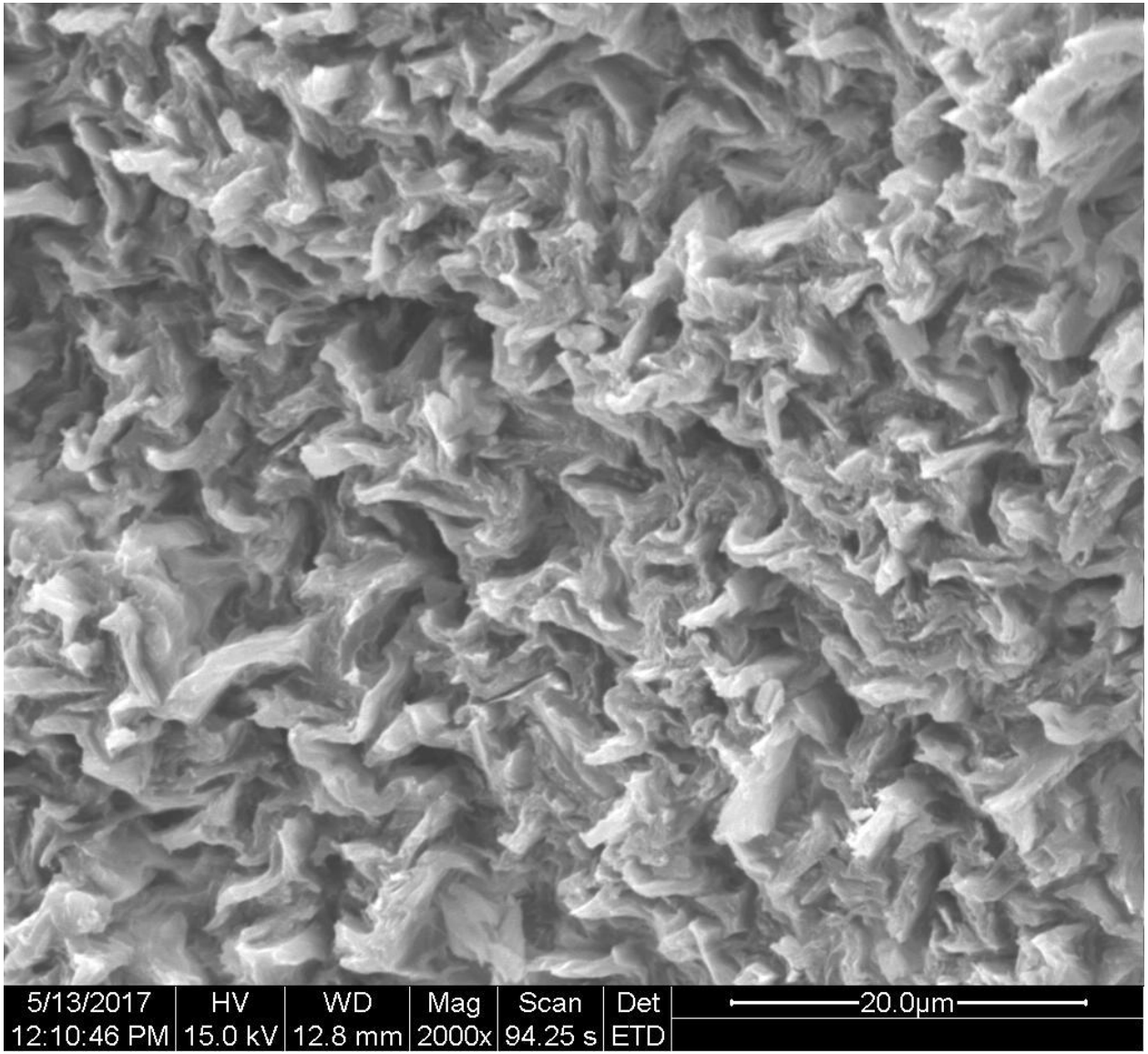
5/13/2017
12:10:46 PM
HV
15.0 kV
WD
12.8 mm
Mag
2000x
Scan
94.25 s
Det
ETD
20.0µm

Ferocactus wislizenianus

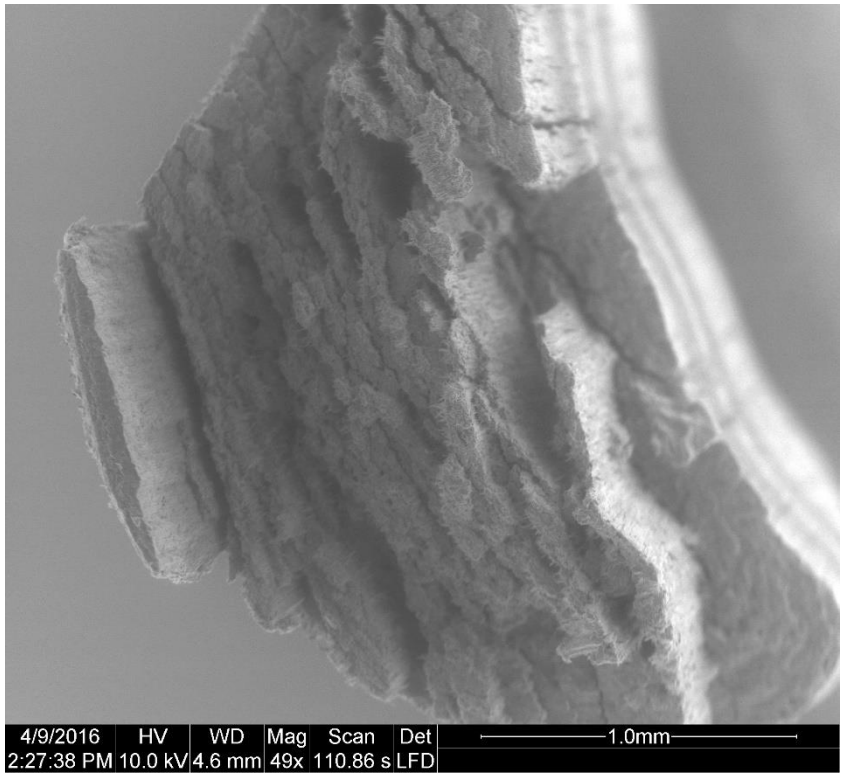

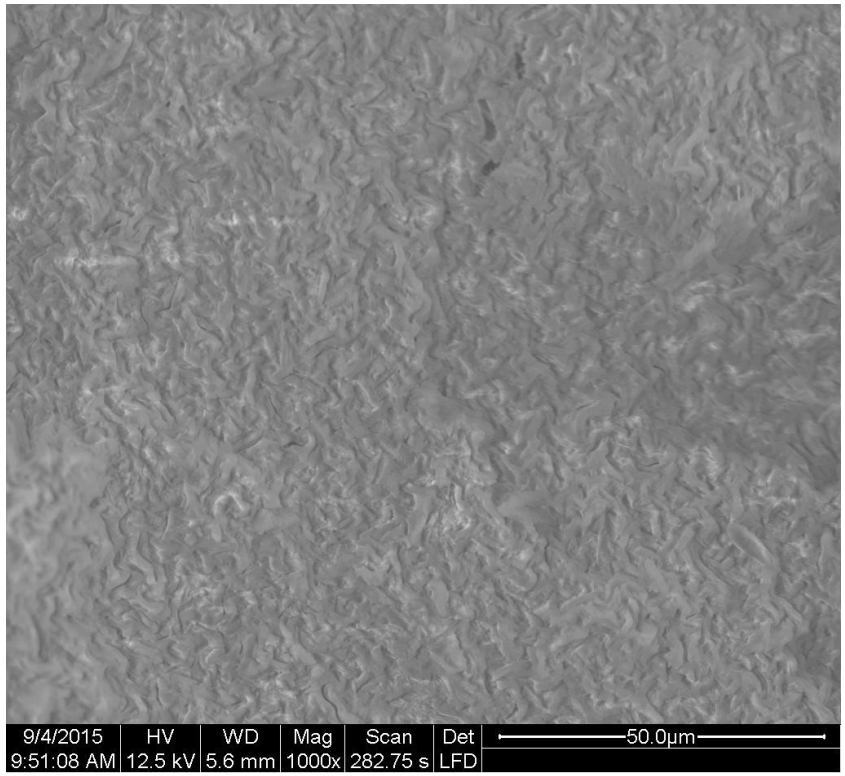

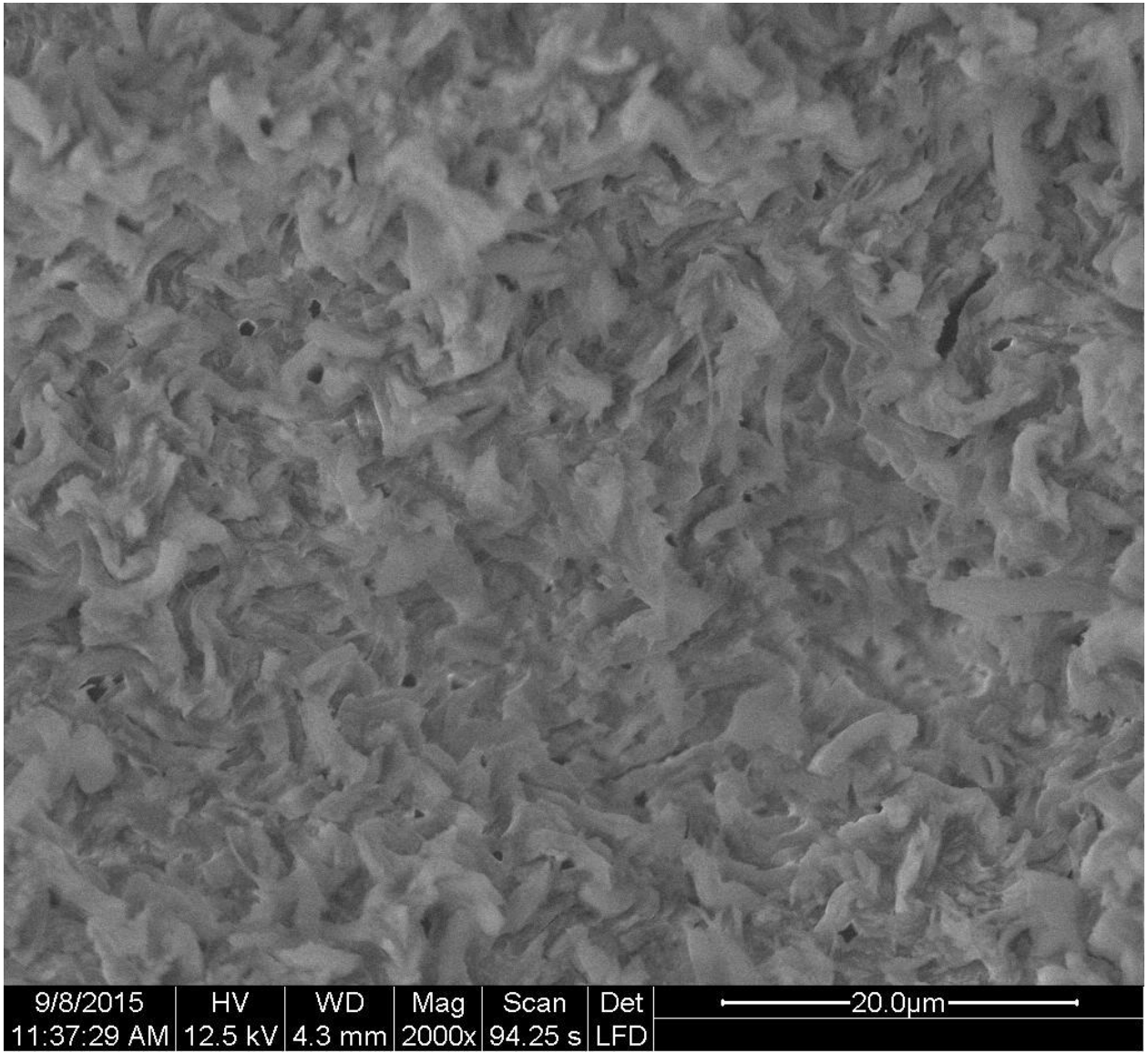
9/8/2015
11:37:29 AM
HV
12.5 kV
WD
4.3 mm
Mag
2000x
Scan
94.25 s
Det
LFD
20.0µm

Gruosnia emoryi

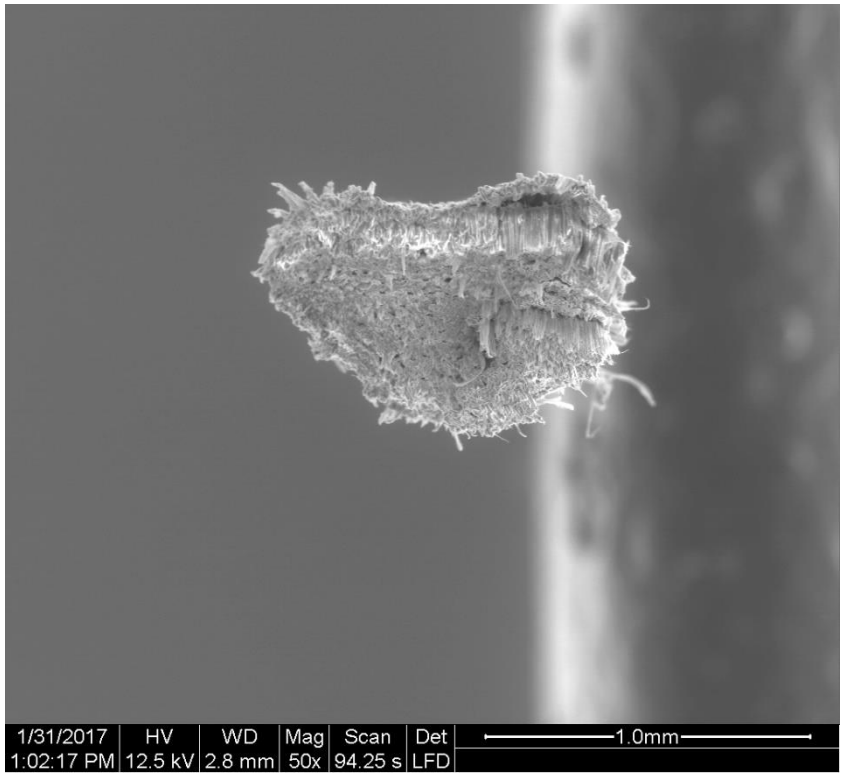

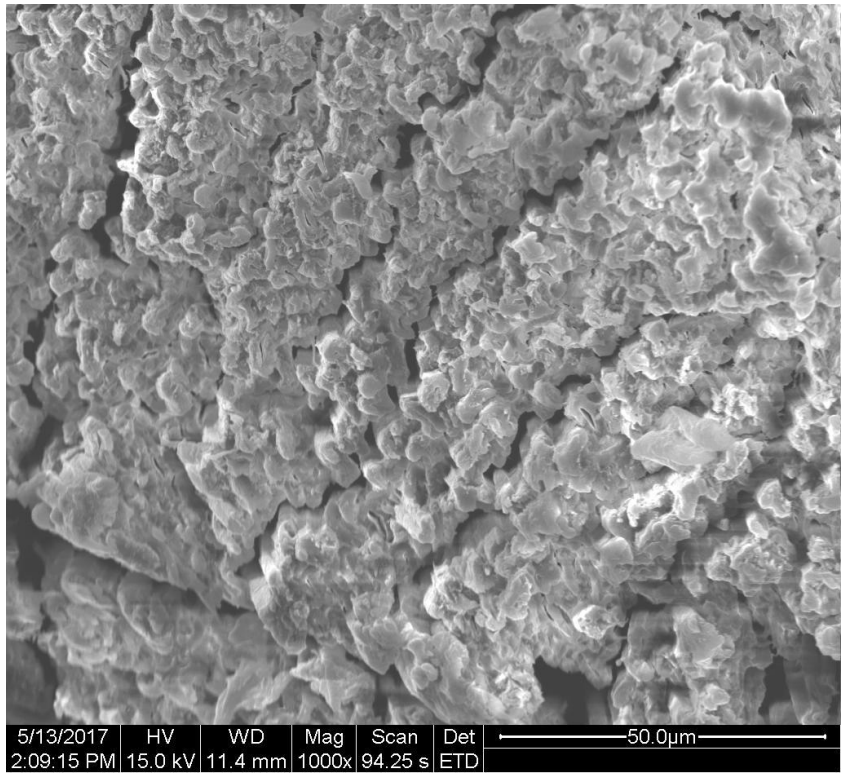

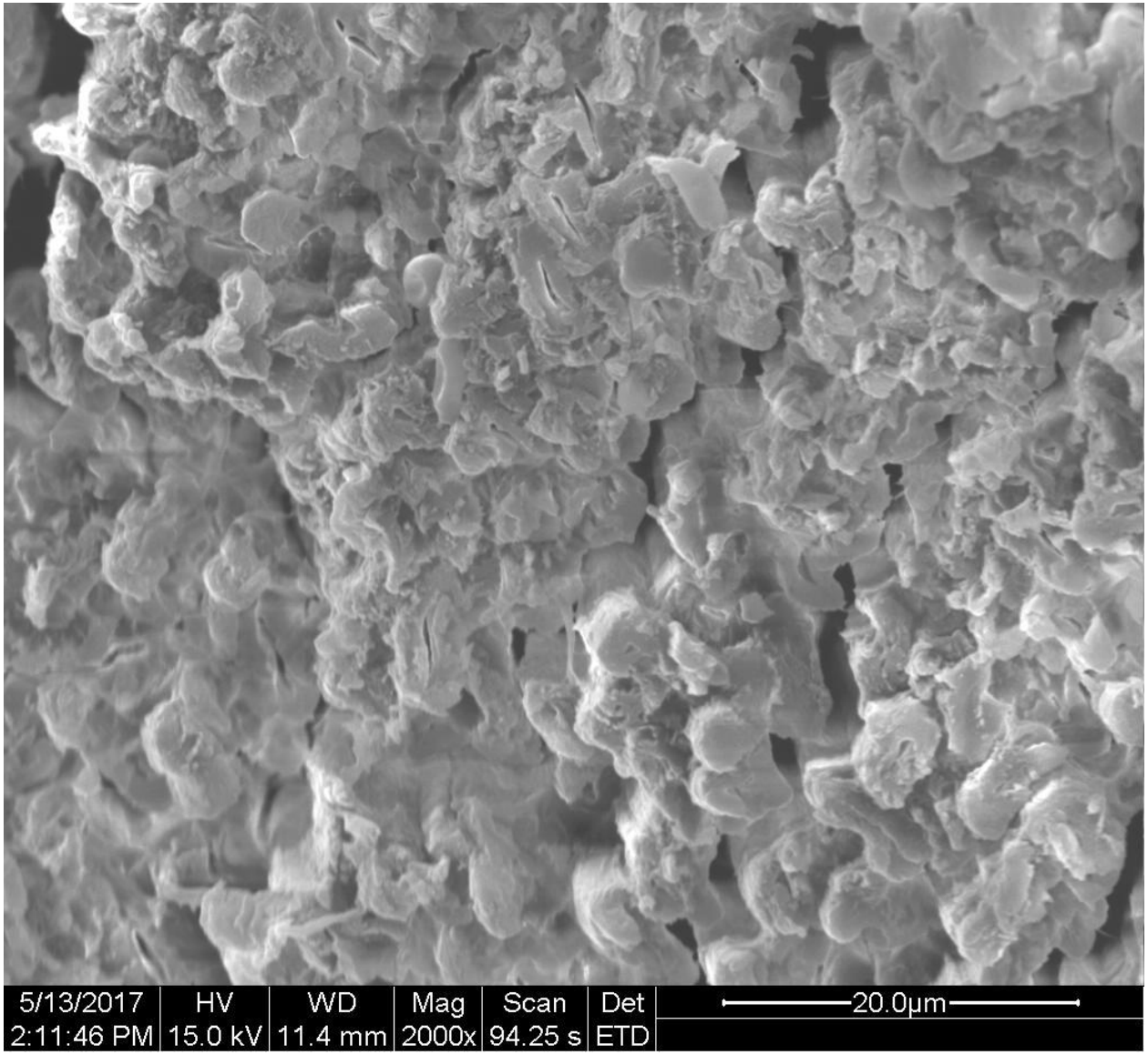
5/13/2017
2:11:46 PM
HV
15.0 kV
WD
11.4 mm
Mag
2000x
Scan
94.25 s
Det
ETD
20.0µm

Myrtillocactus geometrizans

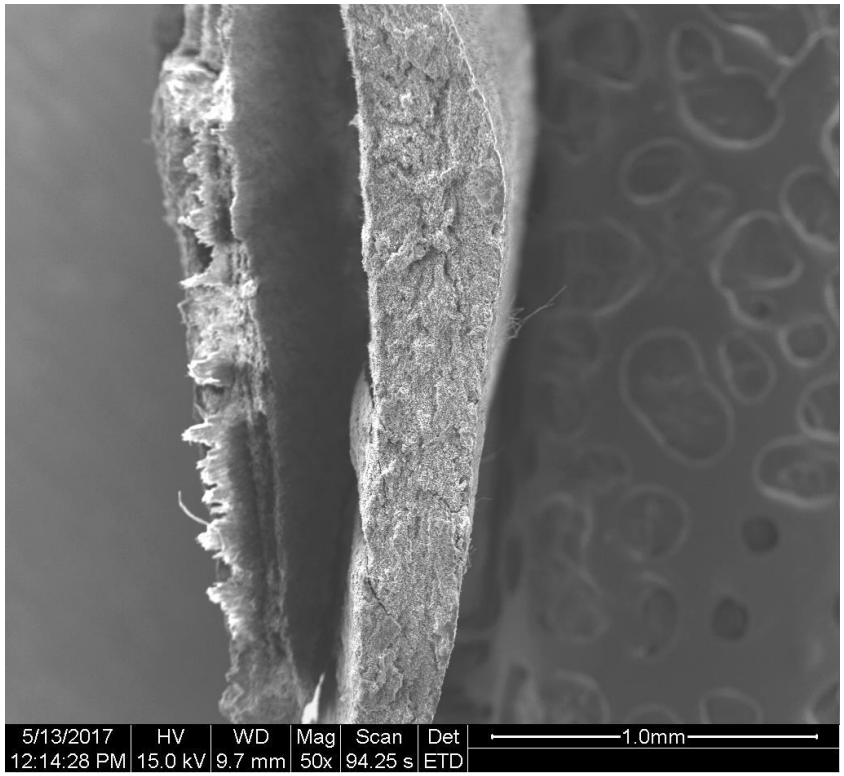

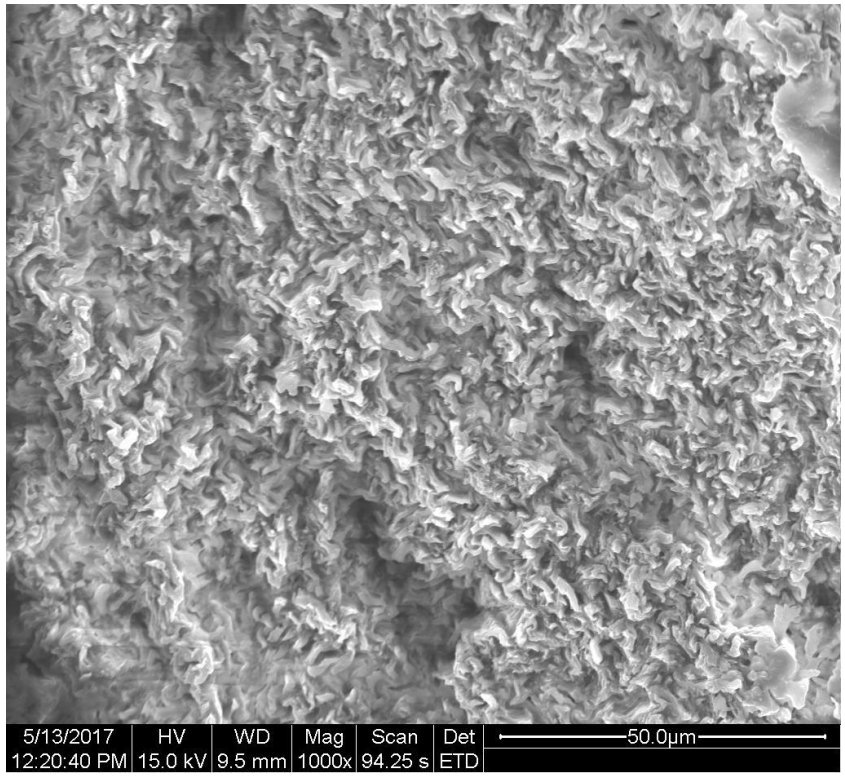

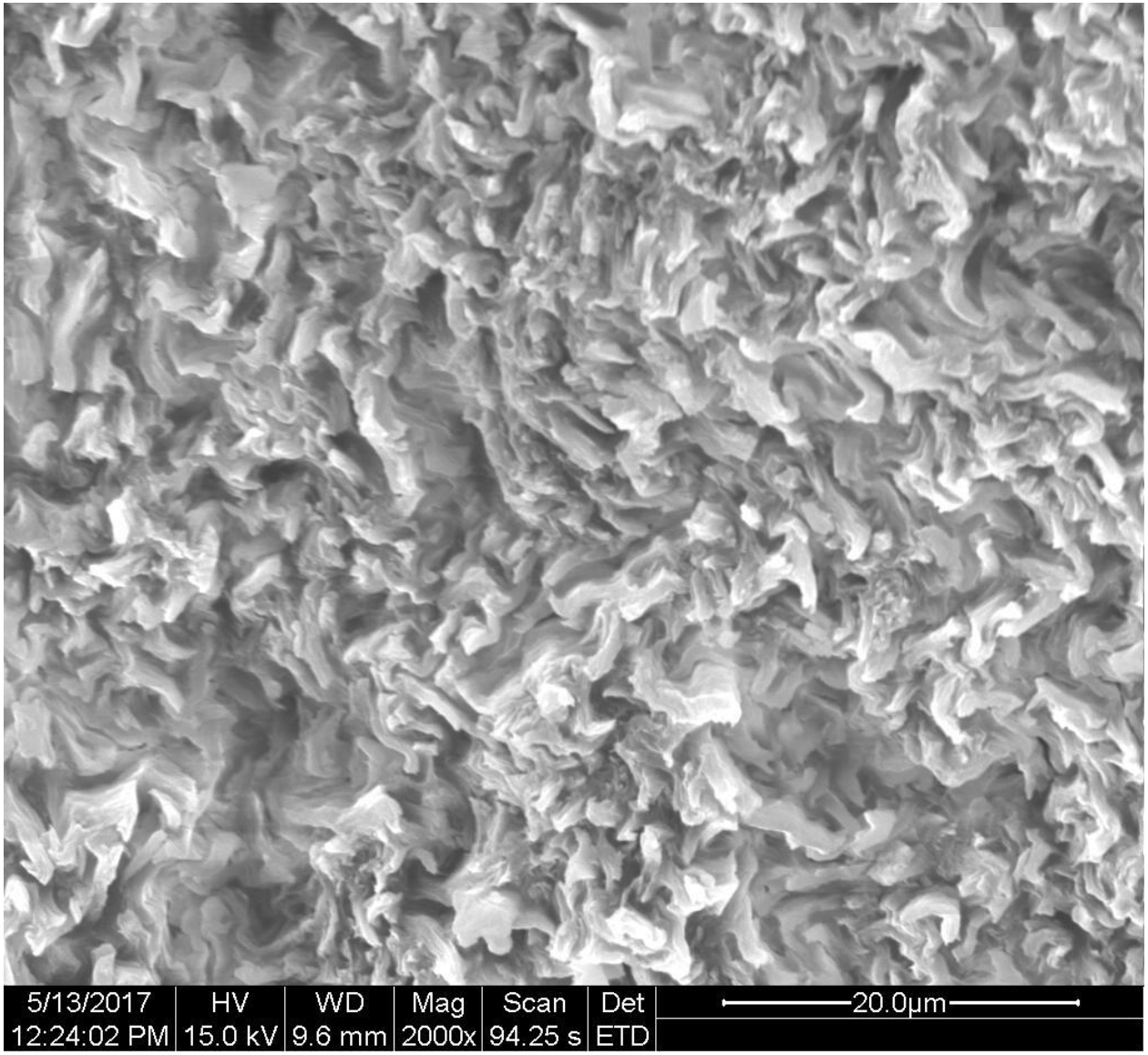
5/13/2017
12:24:02 PM
HV
15.0 kV
WD
9.6 mm
Mag
2000x
Scan
94.25 s
Det
ETD
20.0µm

Oreocereus celsianus

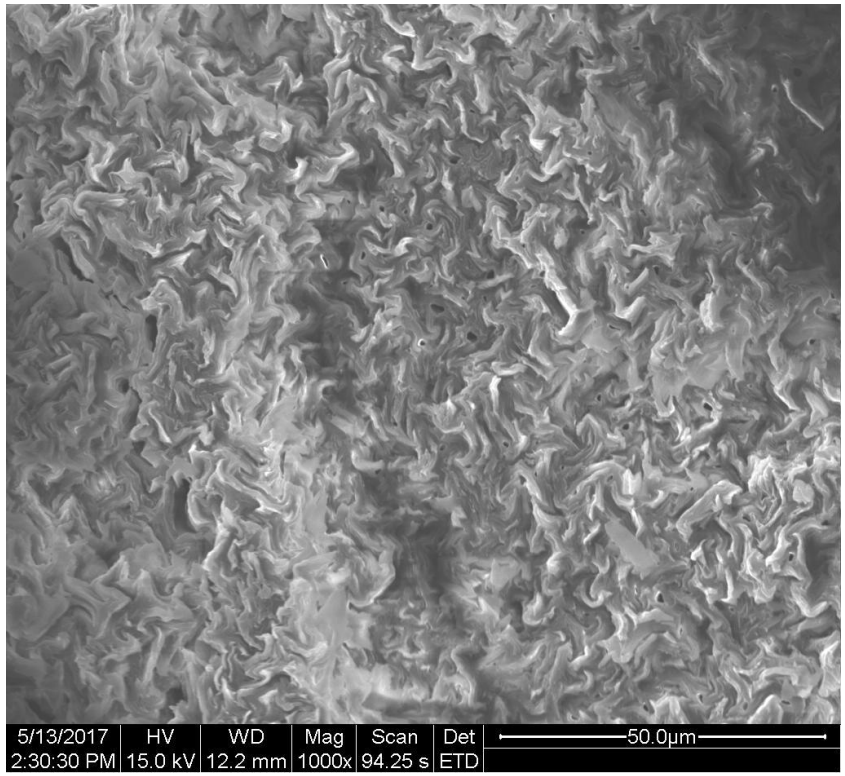

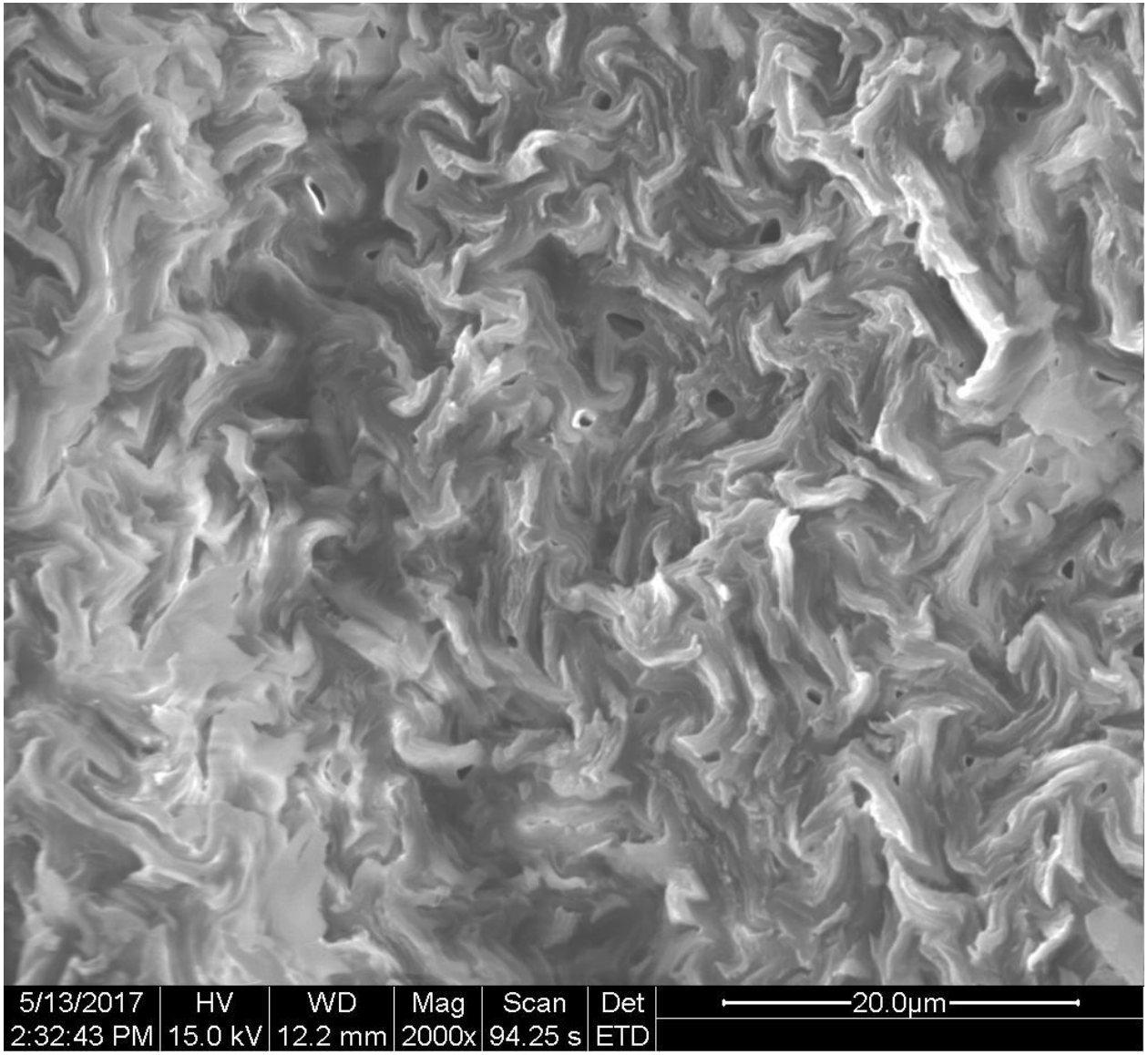
5/13/2017
2:32:43 PM
HV
15.0 kV
WD
12.2 mm
Mag
2000x
Scan
94.25 s
Det
ETD
20.0µm

Pachycereus pringlei

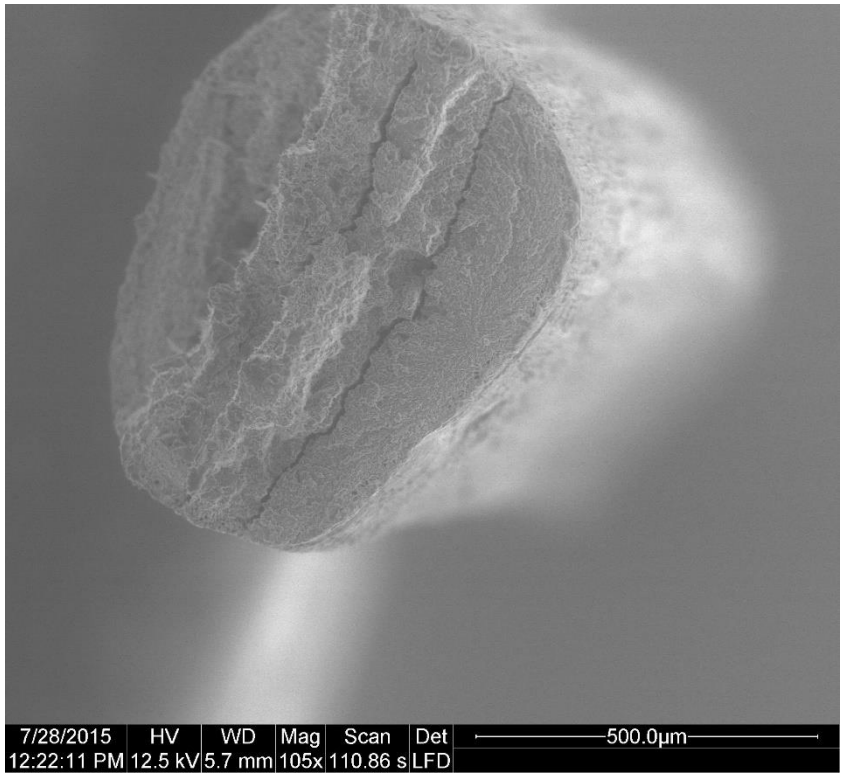

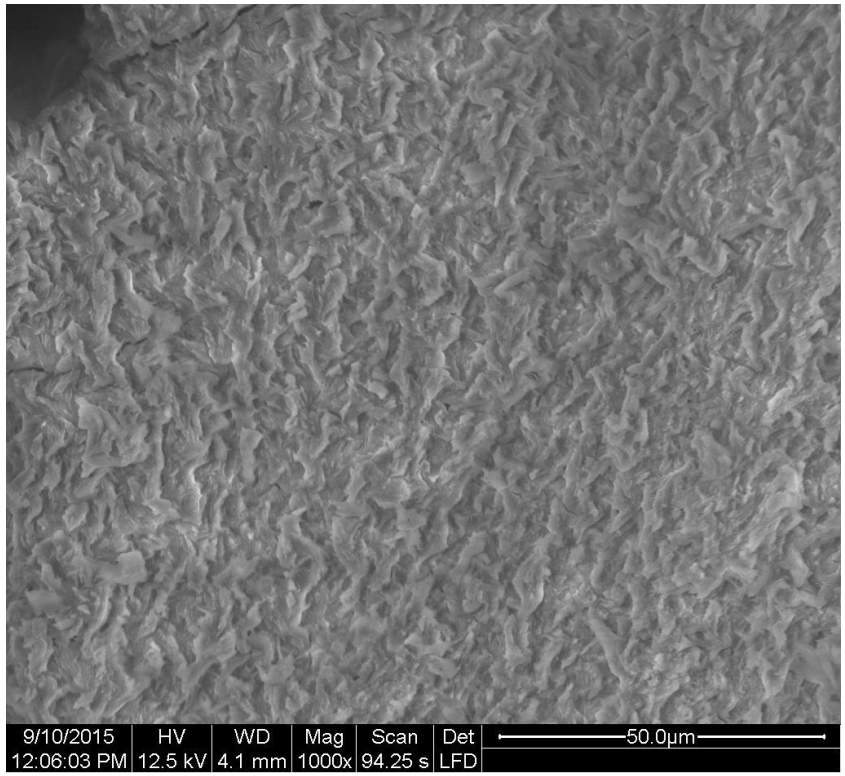

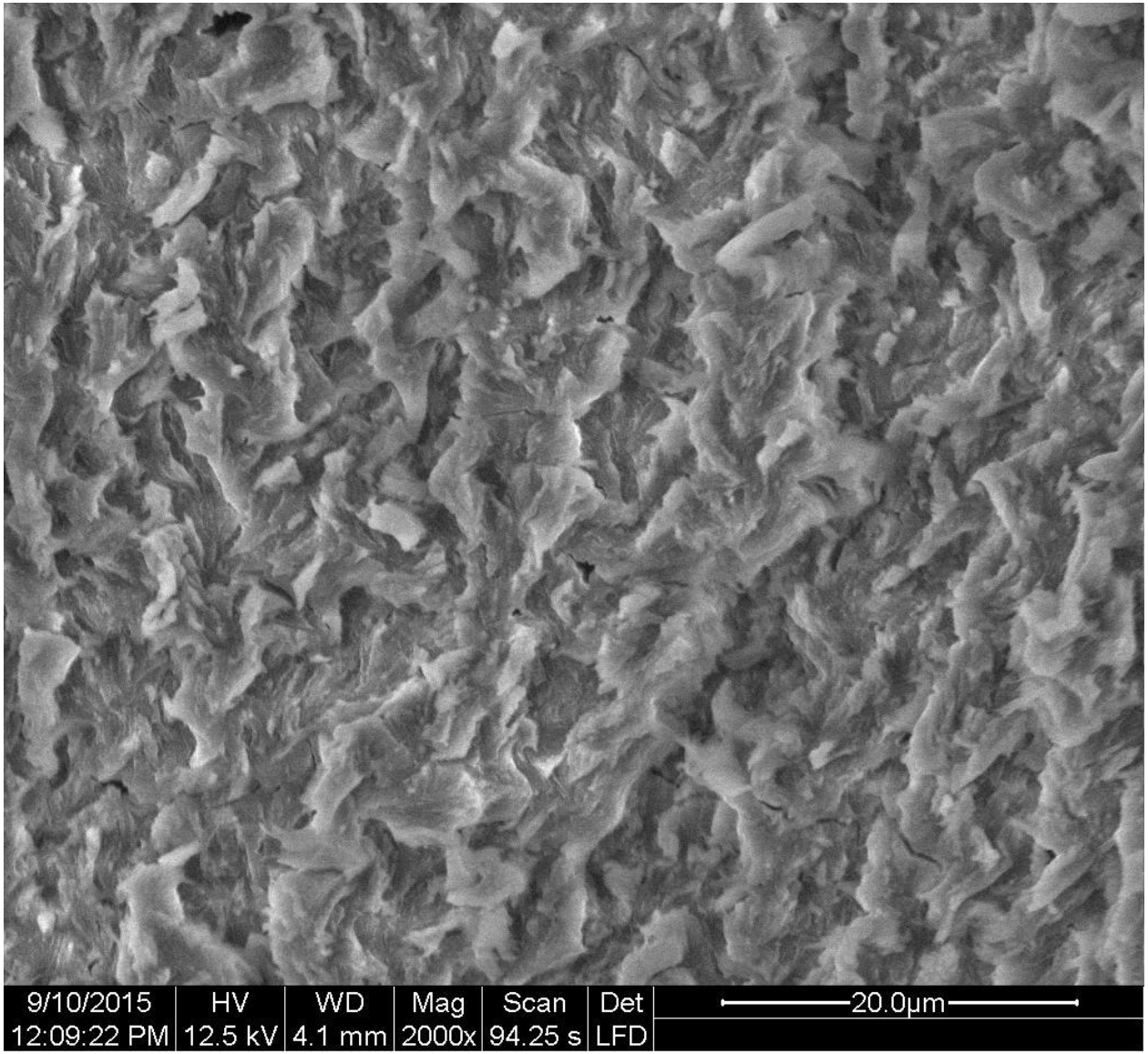
9/10/2015
12:09:22 PM
HV
12.5 kV
WD
4.1 mm
Mag
2000x
Scan
94.25 s
Det
LFD
20.0µm

Sclerocactus parviflorus

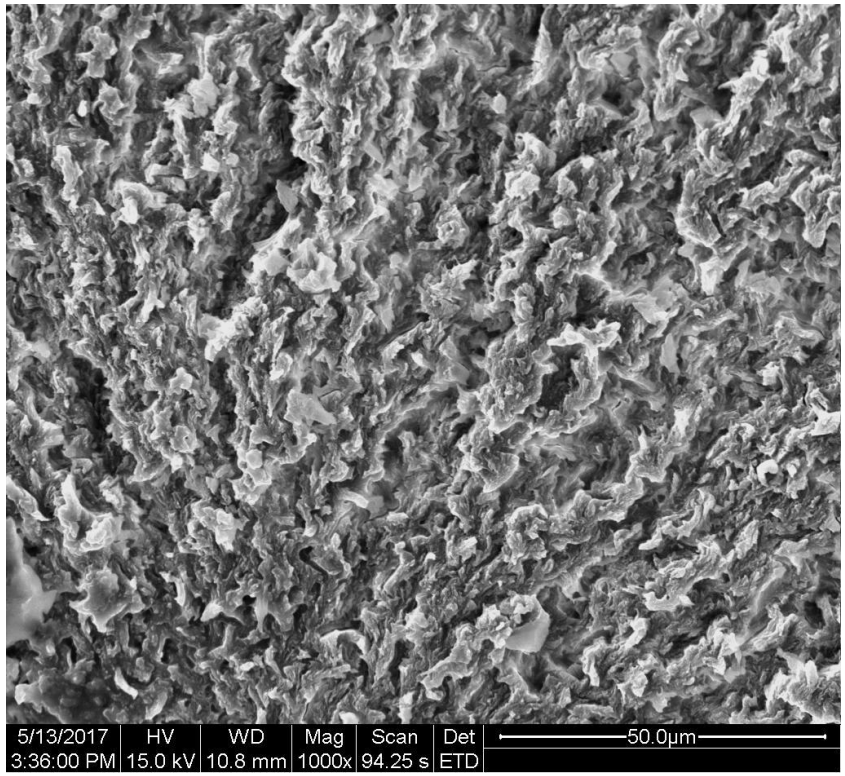

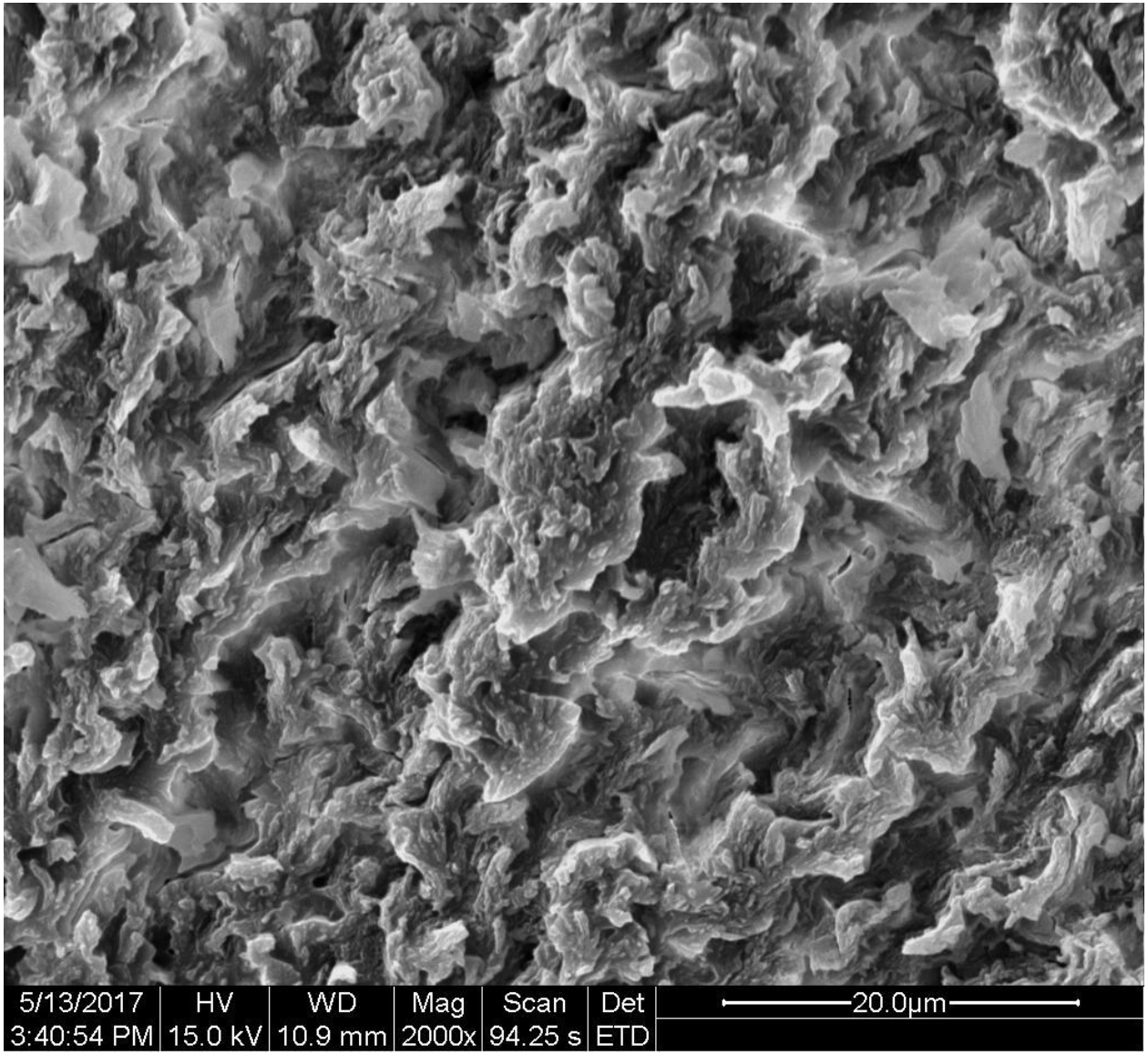
5/13/2017
3:40:54 PM
HV
15.0 kV
WD
10.9 mm
Mag
2000x
Scan
94.25 s
Det
ETD
20.0µm

Sclerocactus polyancistrus

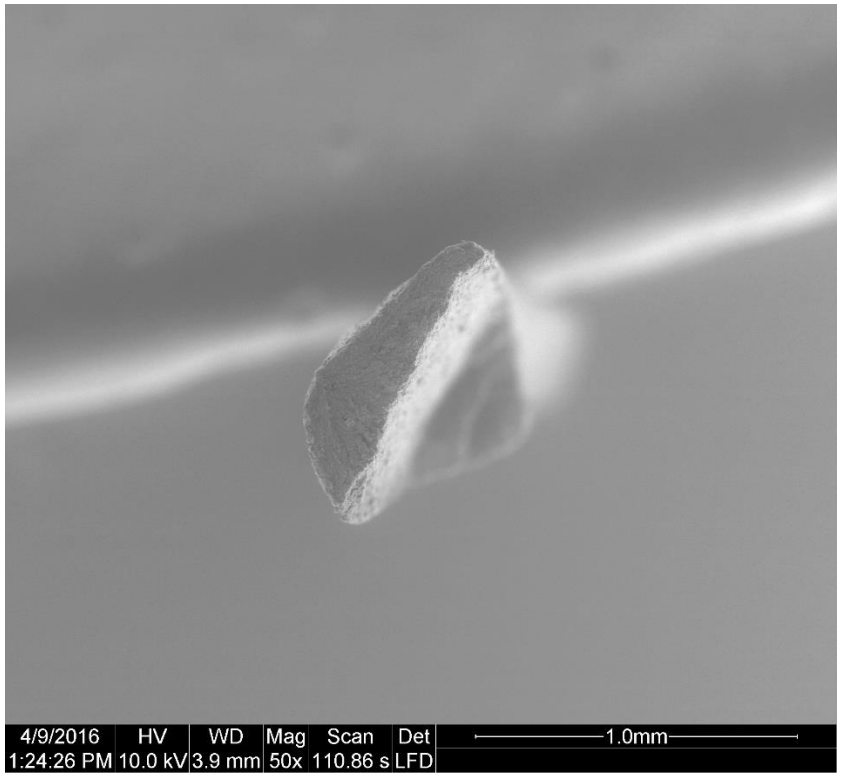

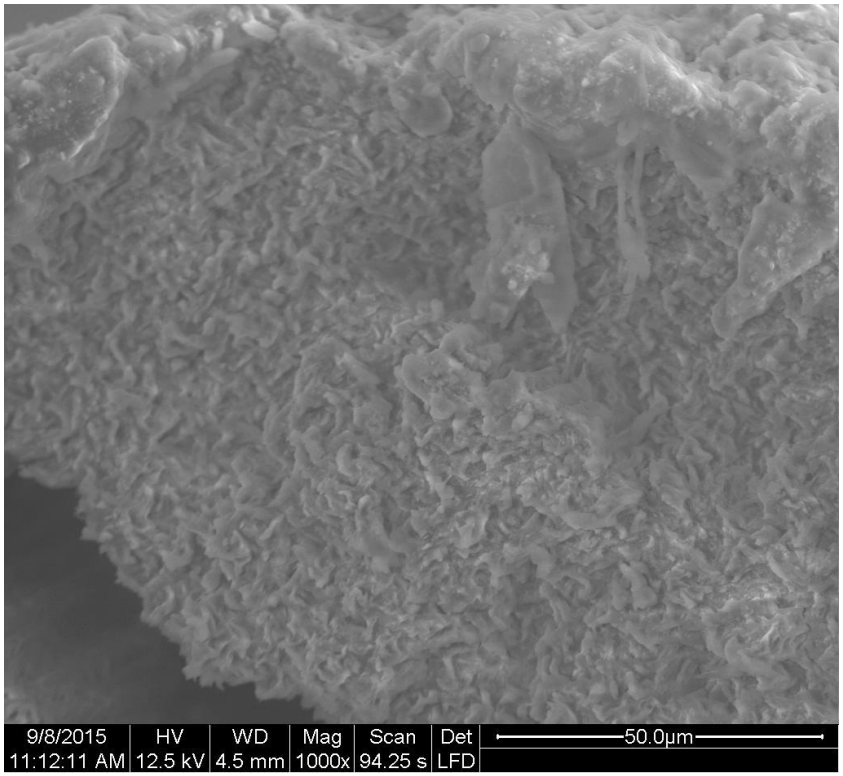

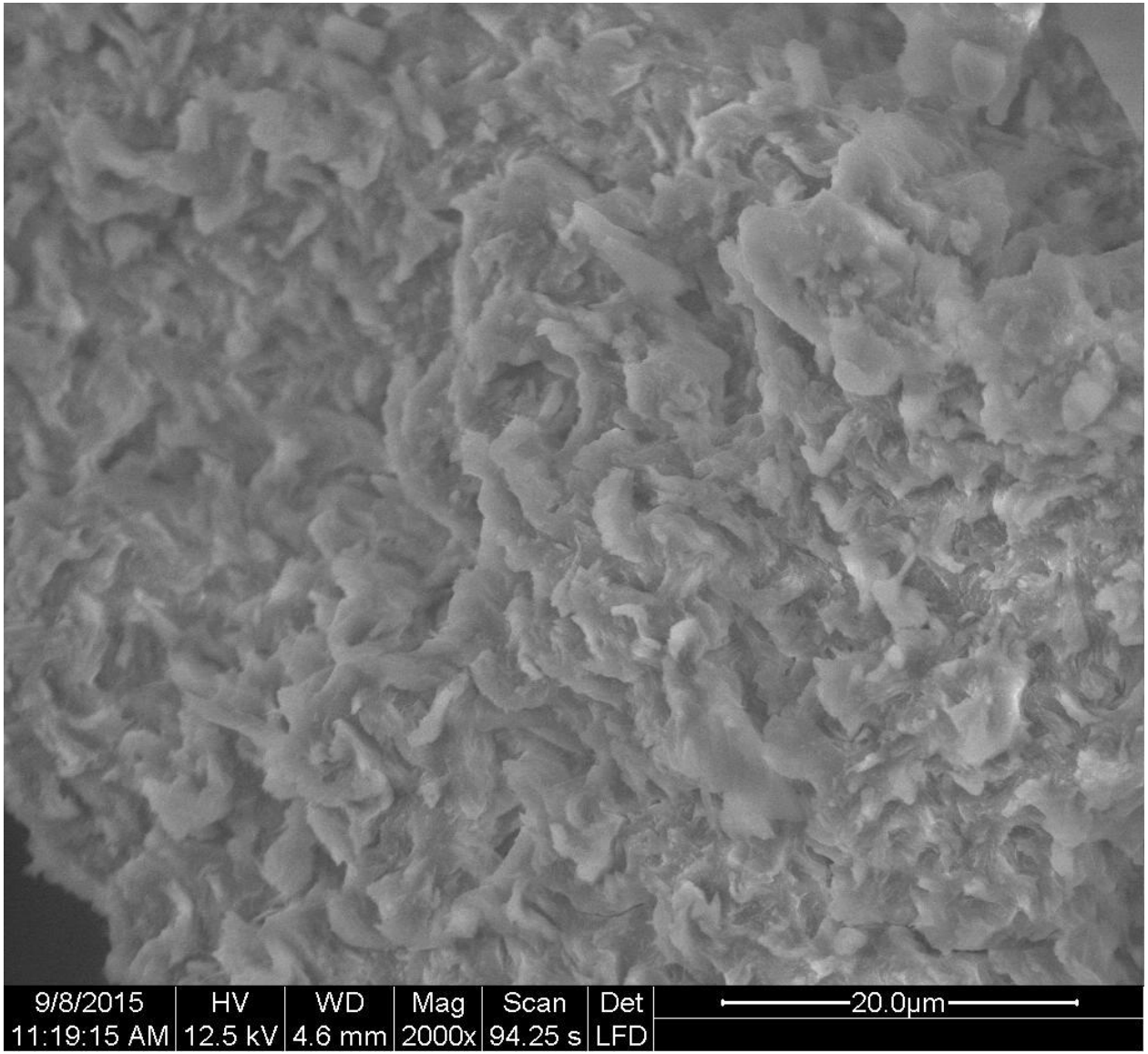
9/8/2015
11:19:15 AM
HV
12.5 kV
WD
4.6 mm
Mag
2000x
Scan
94.25 s
Det
LFD
20.0µm

Stenocactus crispatus

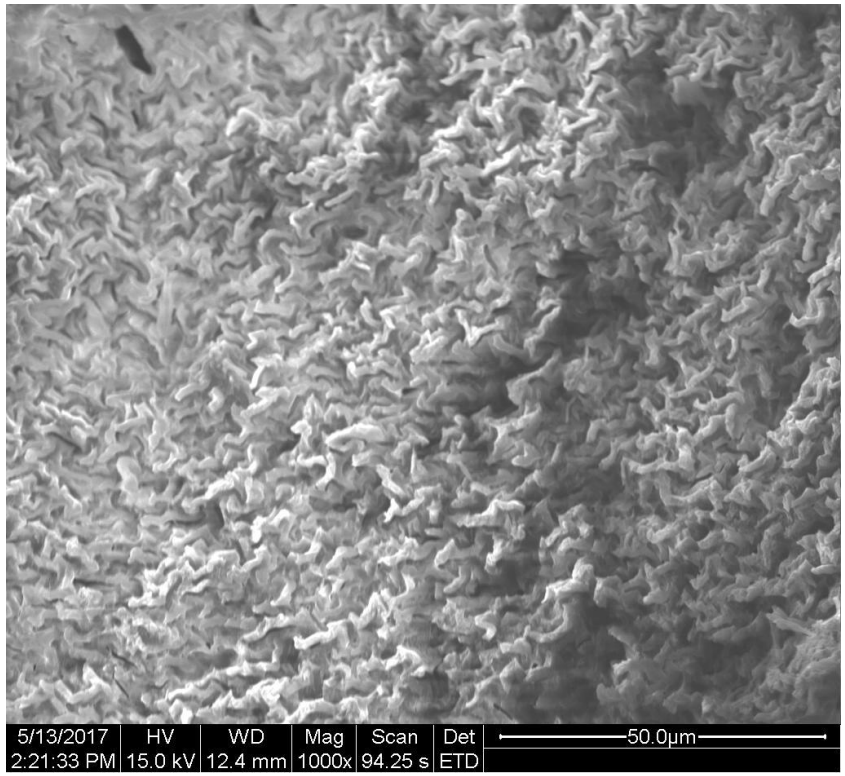

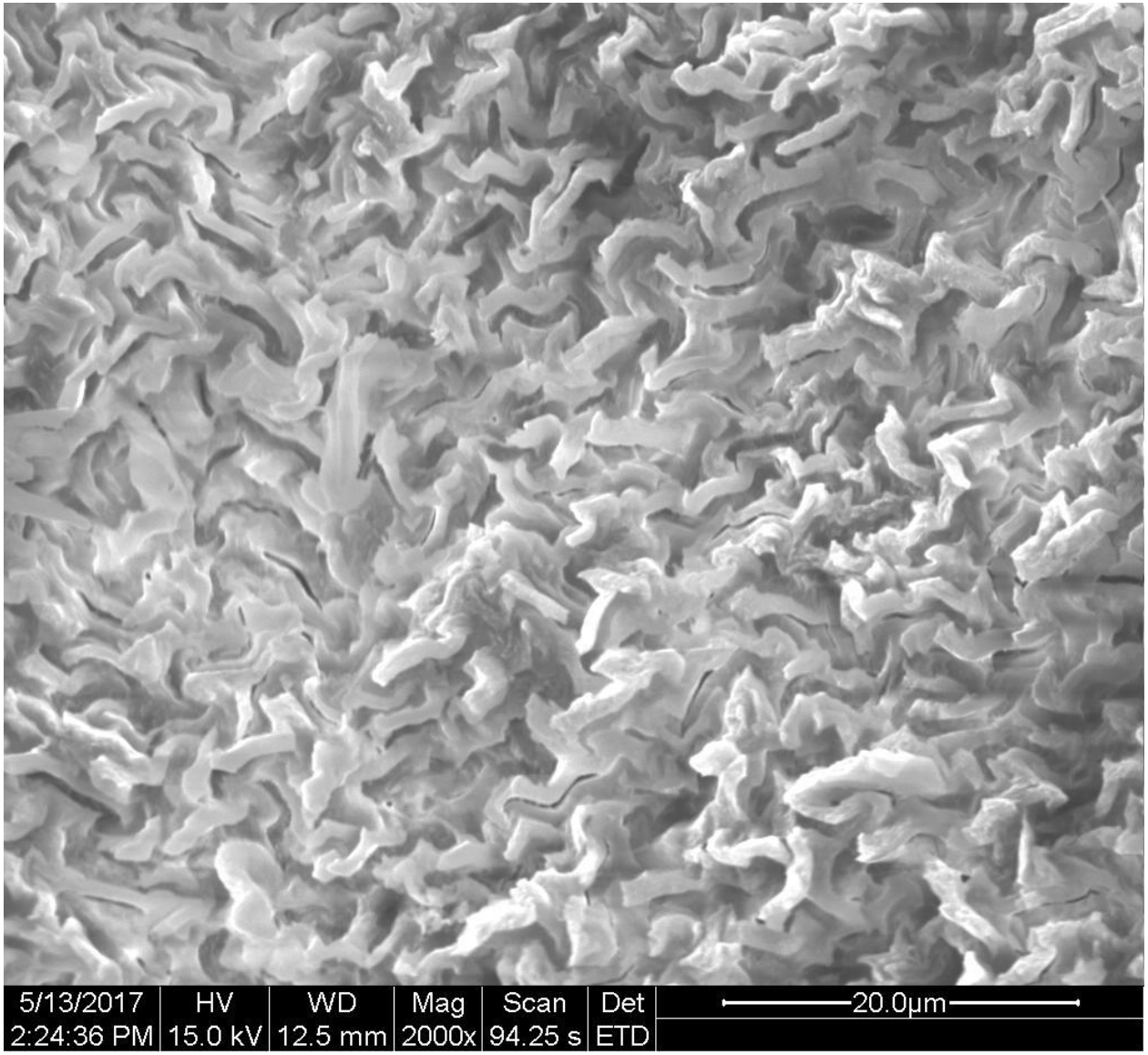
5/13/2017
2:24:36 PM
HV
15.0 kV
WD
12.5 mm
Mag
2000x
Scan
94.25 s
Det
ETD
20.0µm

Stenocactus multicostatus

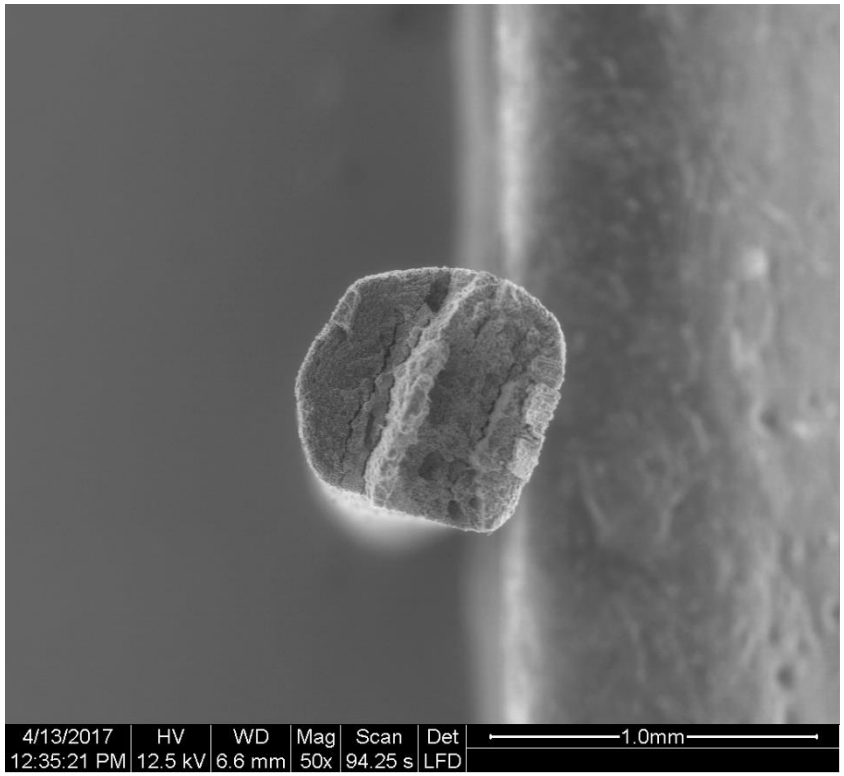

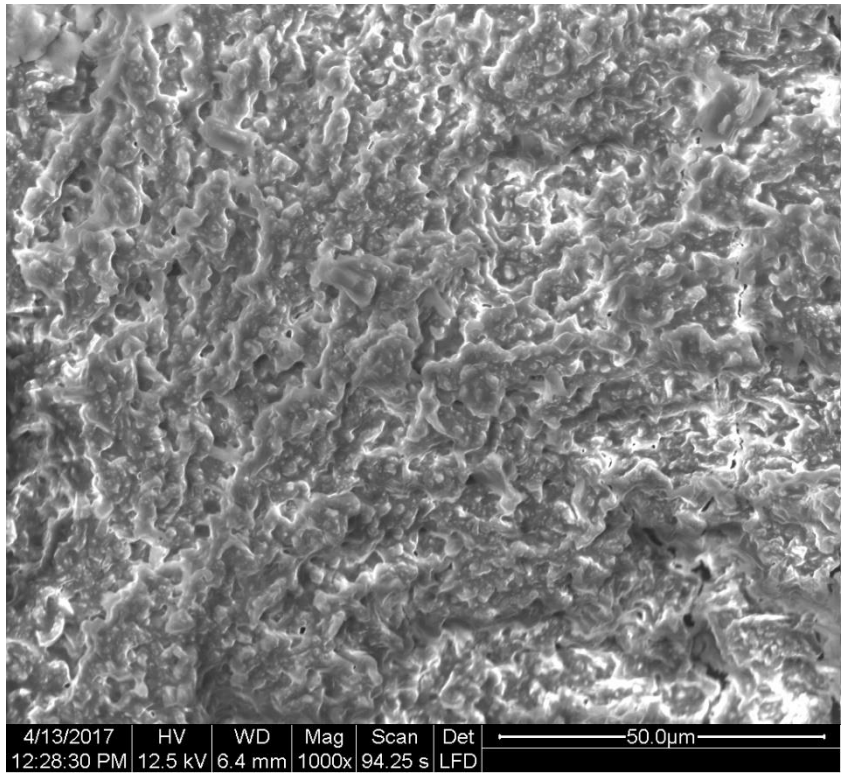

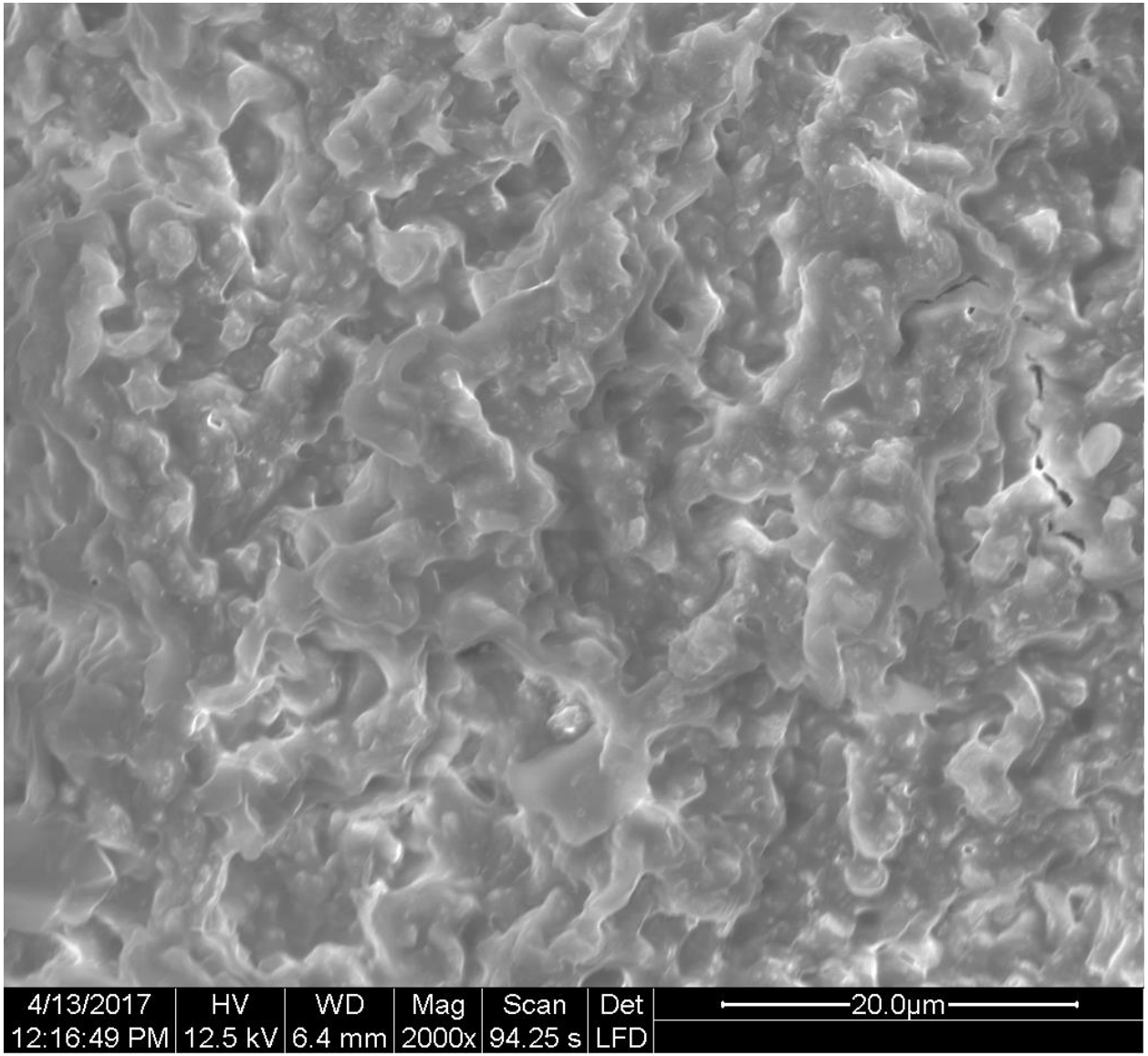
4/13/2017
12:16:49 PM
HV
12.5 kV
WD
6.4 mm
Mag
2000x
Scan
94.25 s
Det
LFD
20.0µm

Stenocereus thurberi

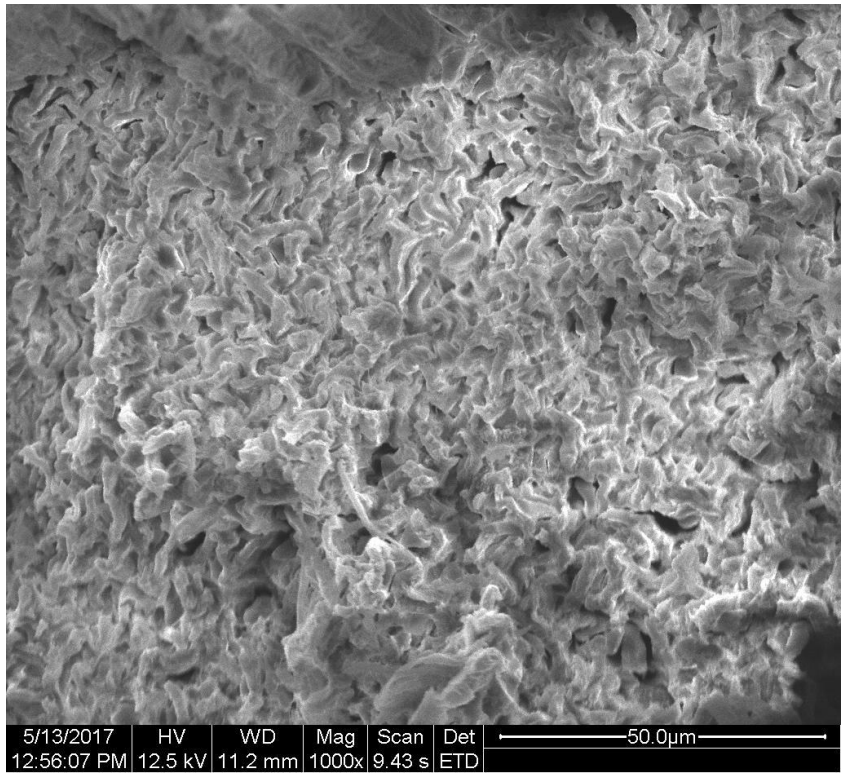

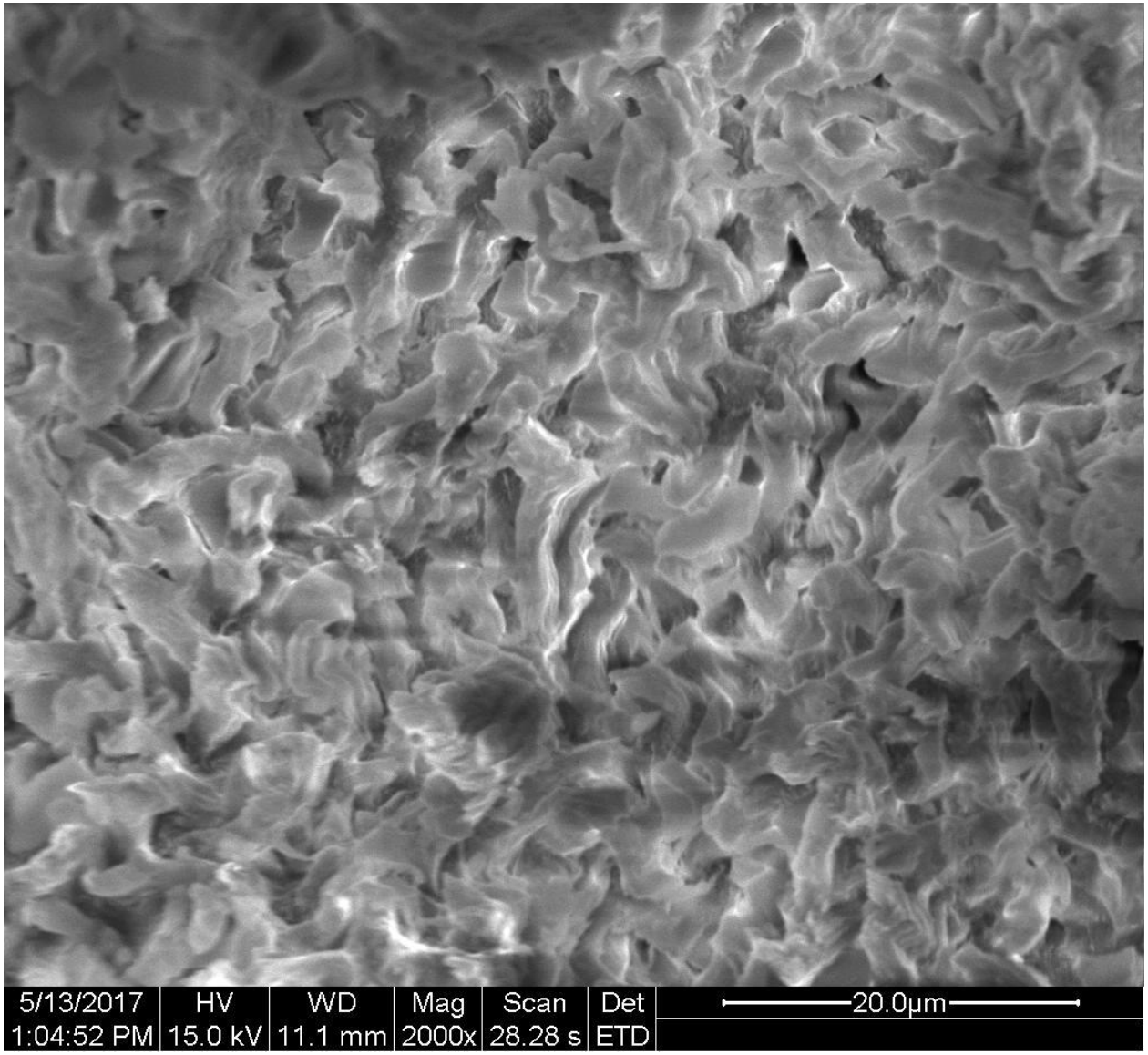
5/13/2017
1:04:52 PM
HV
15.0 kV
WD
11.1 mm
Mag
2000x
Scan
28.28 s
Det
ETD
20.0µm

Tephrocactus alexanderi

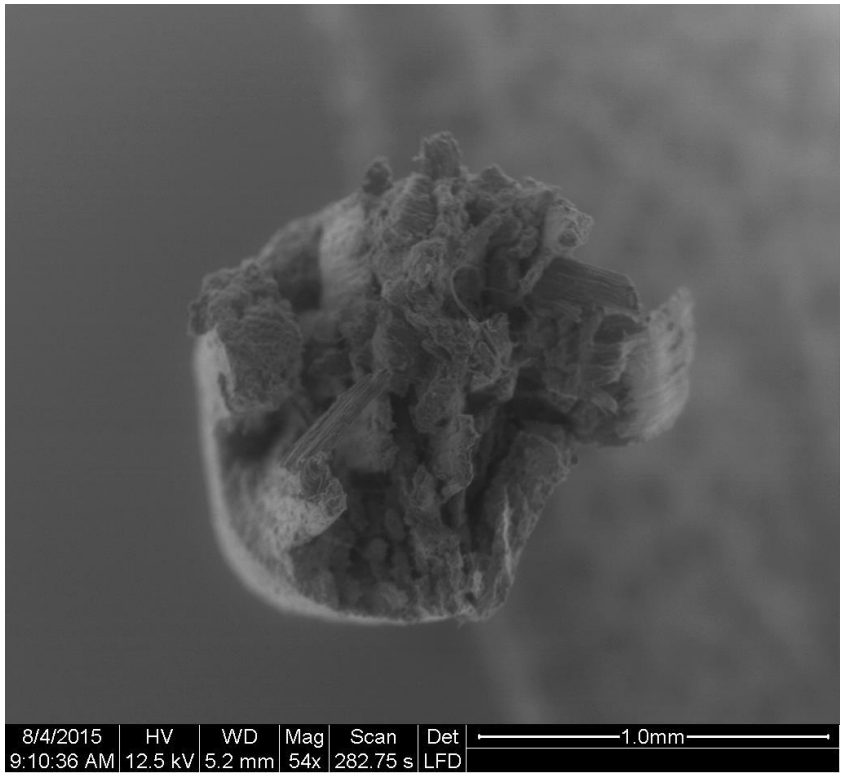

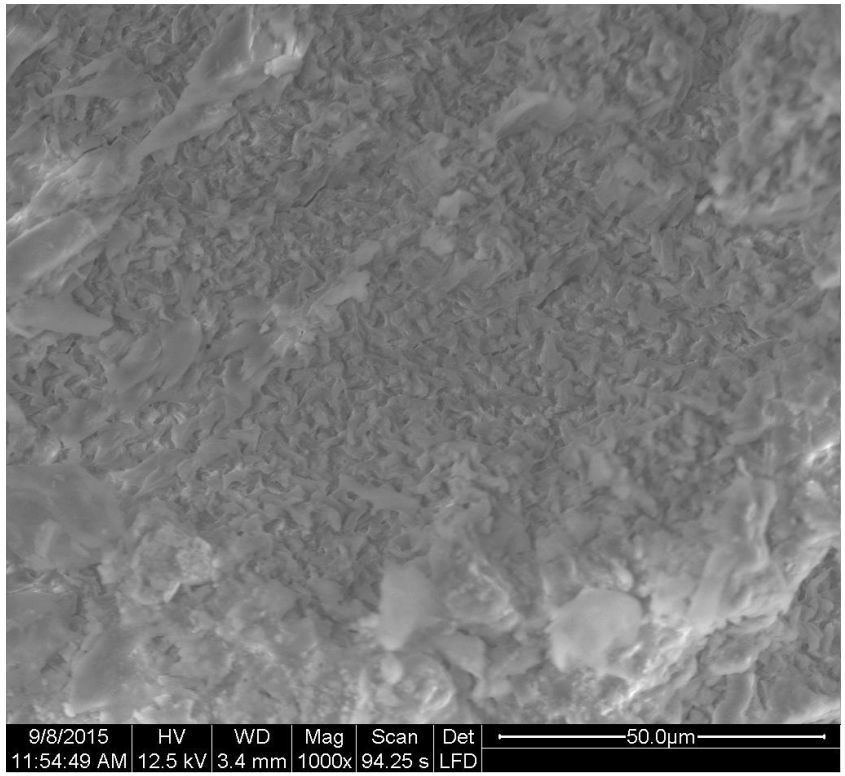

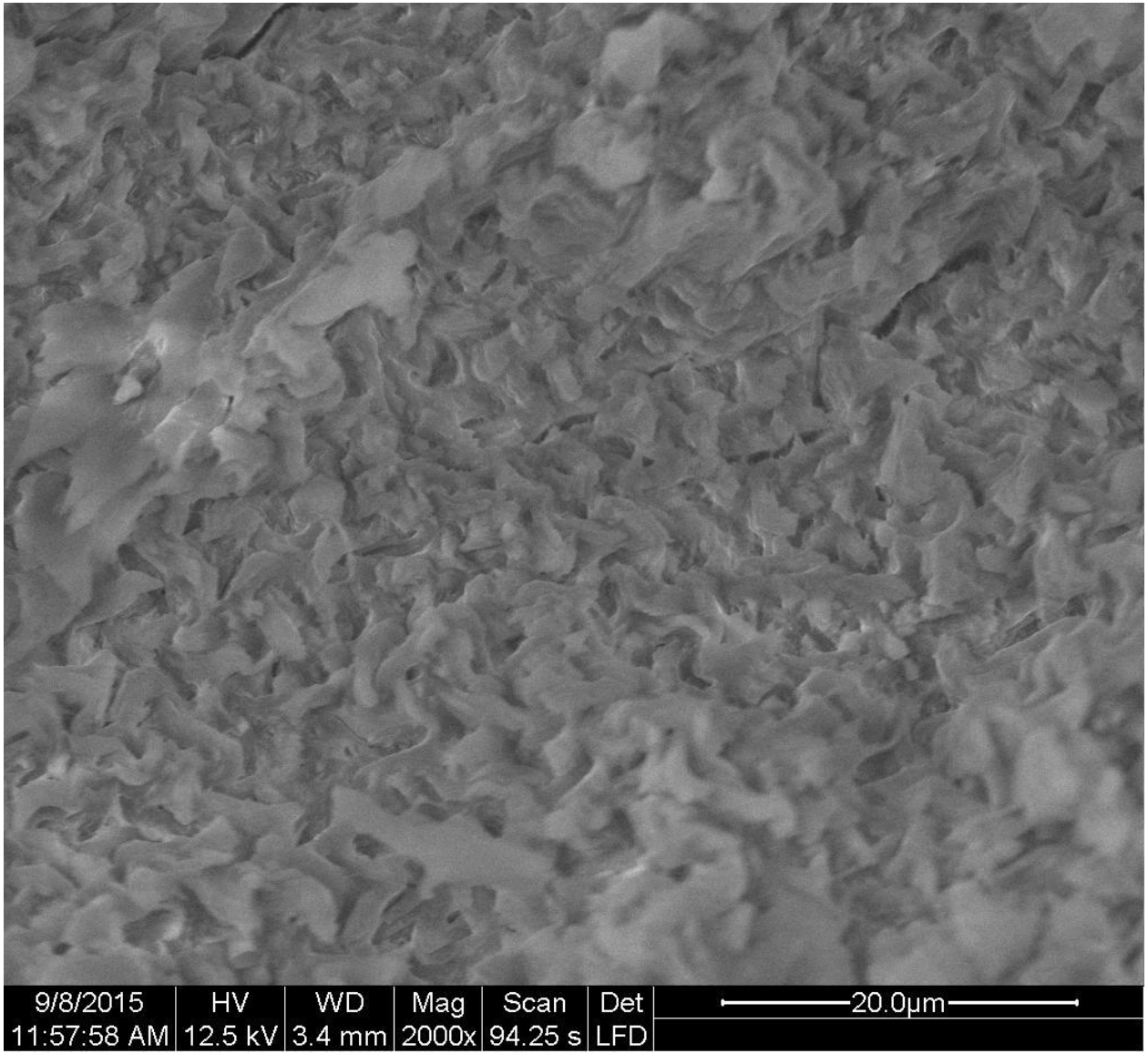
9/8/2015
11:57:58 AM
HV
12.5 kV
WD
3.4 mm
Mag
2000x
Scan
94.25 s
Det
LFD
20.0µm

Appendix C: X-Ray Diffraction Graphs

Astrophytum ornatum

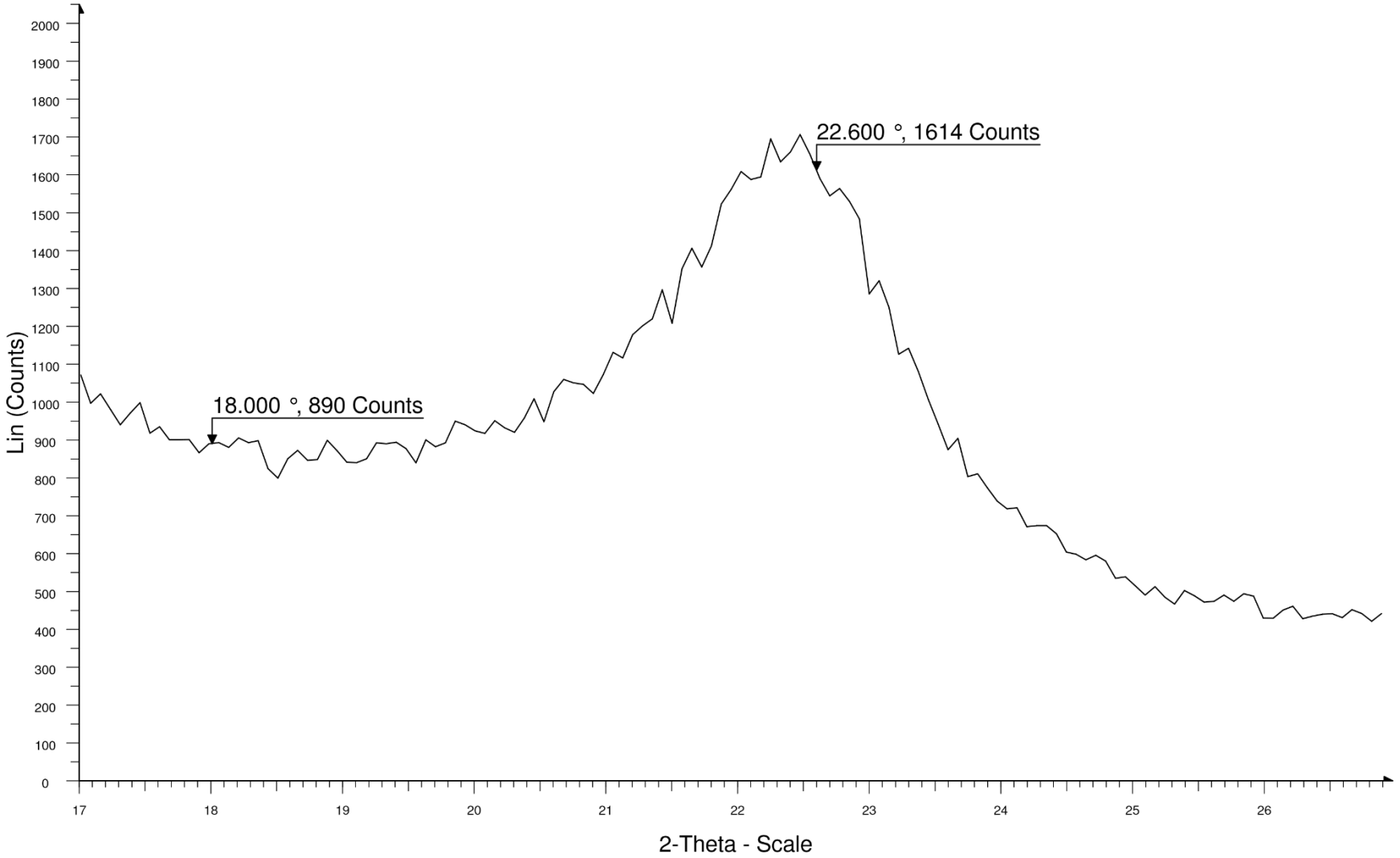

Density (g/cm³)	Crystallinity Index (%)	Multifibrillar angle (°)
1.291-1.391	39.90-49.52	1.575-2.100

Echinocactus grusonii

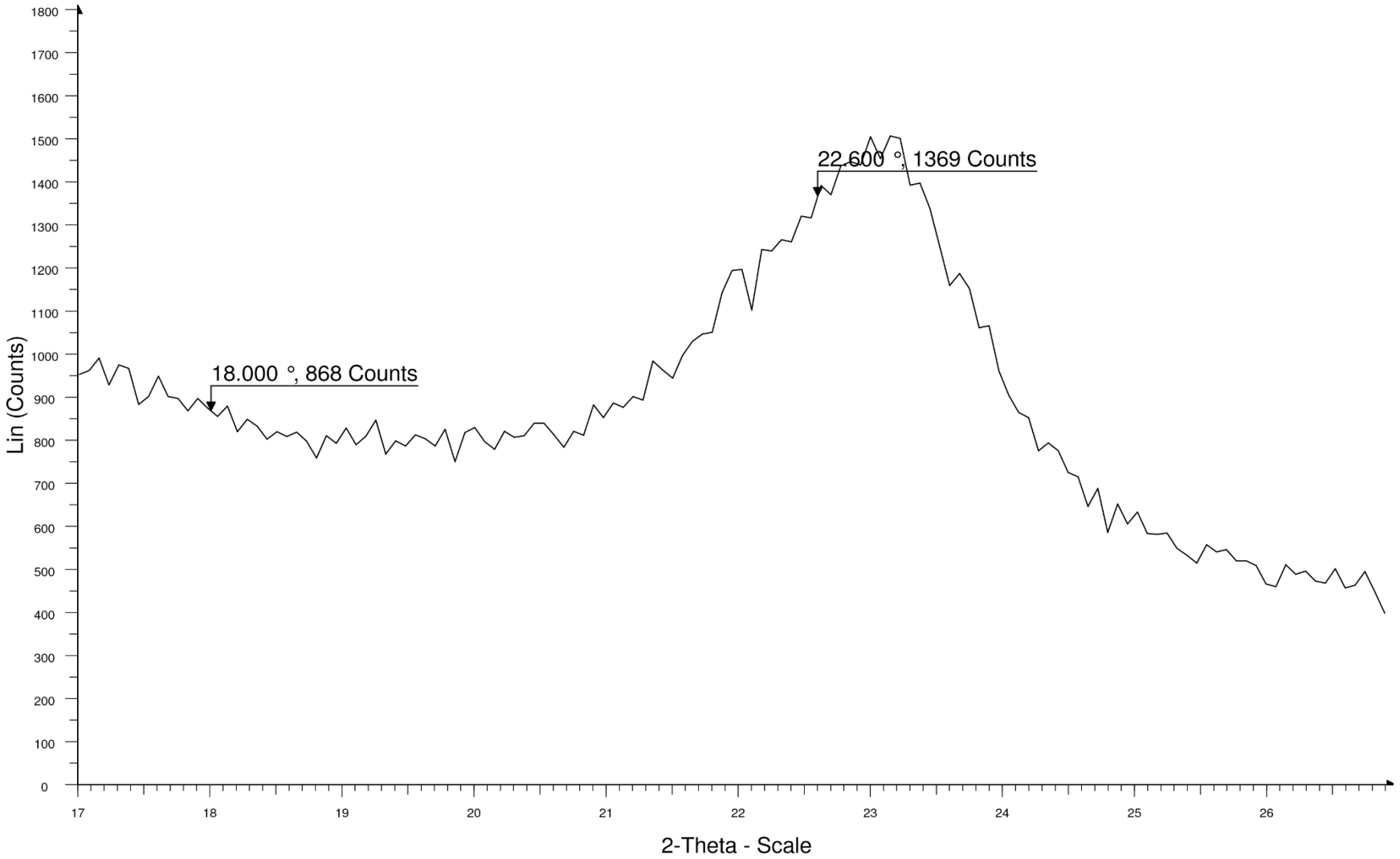

Density (g/cm3)	Crystallinity Index (%)	Multifibrillar angle (°)
1.265-1.365	30.40-42.35	1.680-2.085

Echinocactus polycephalus

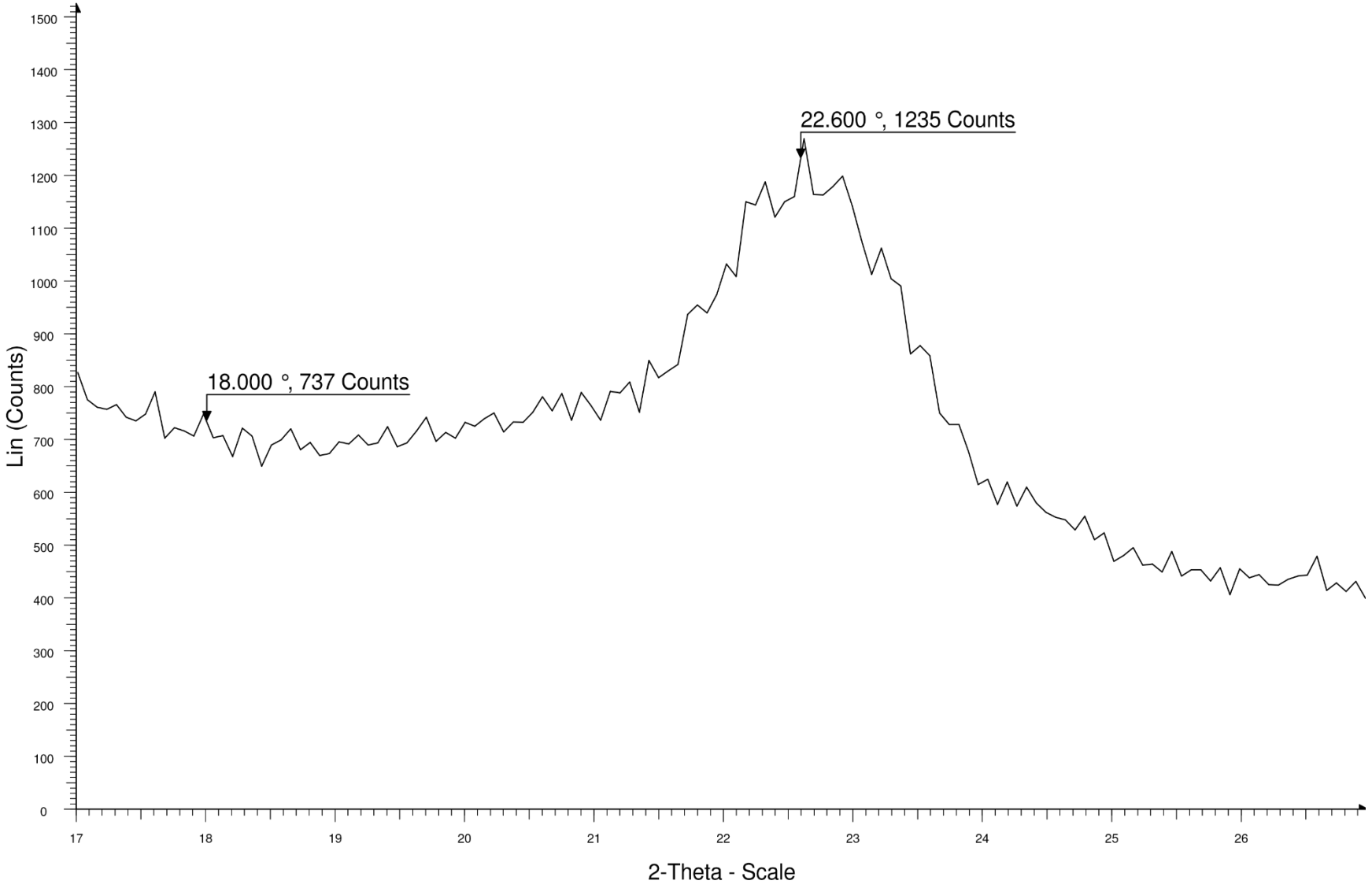

Density (g/cm³)	Crystallinity Index (%)	Multifibrillar angle (°)
1.339-1.439	39.02-41.61	1.725-1.905

Echinocereus boyce-thompsonii

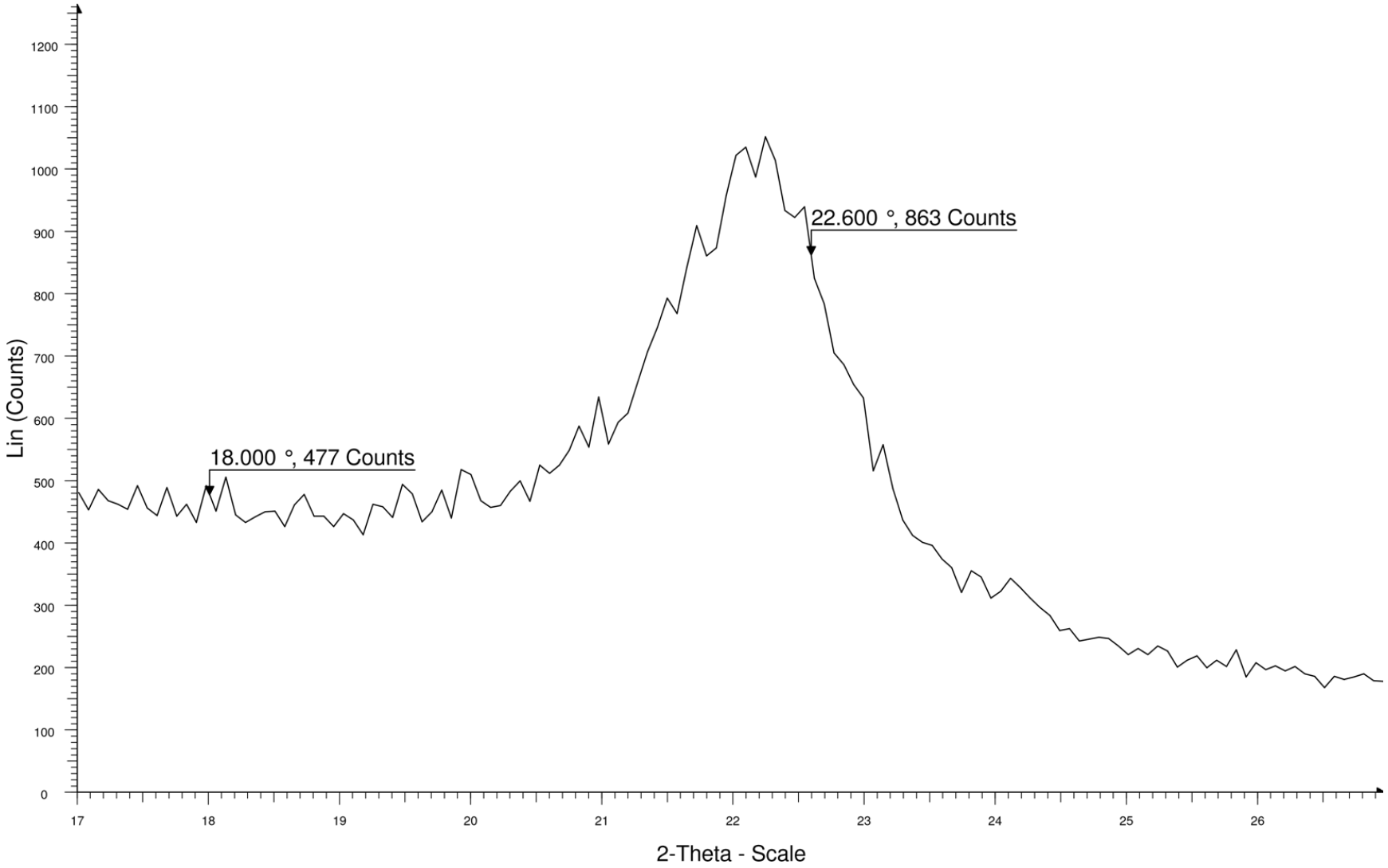

Density (g/cm3)	Crystallinity Index (%)	Multifibrillar angle (°)
1.313-1.413	42.91-46.51	1.155-1.545

Echinocereus englemanii

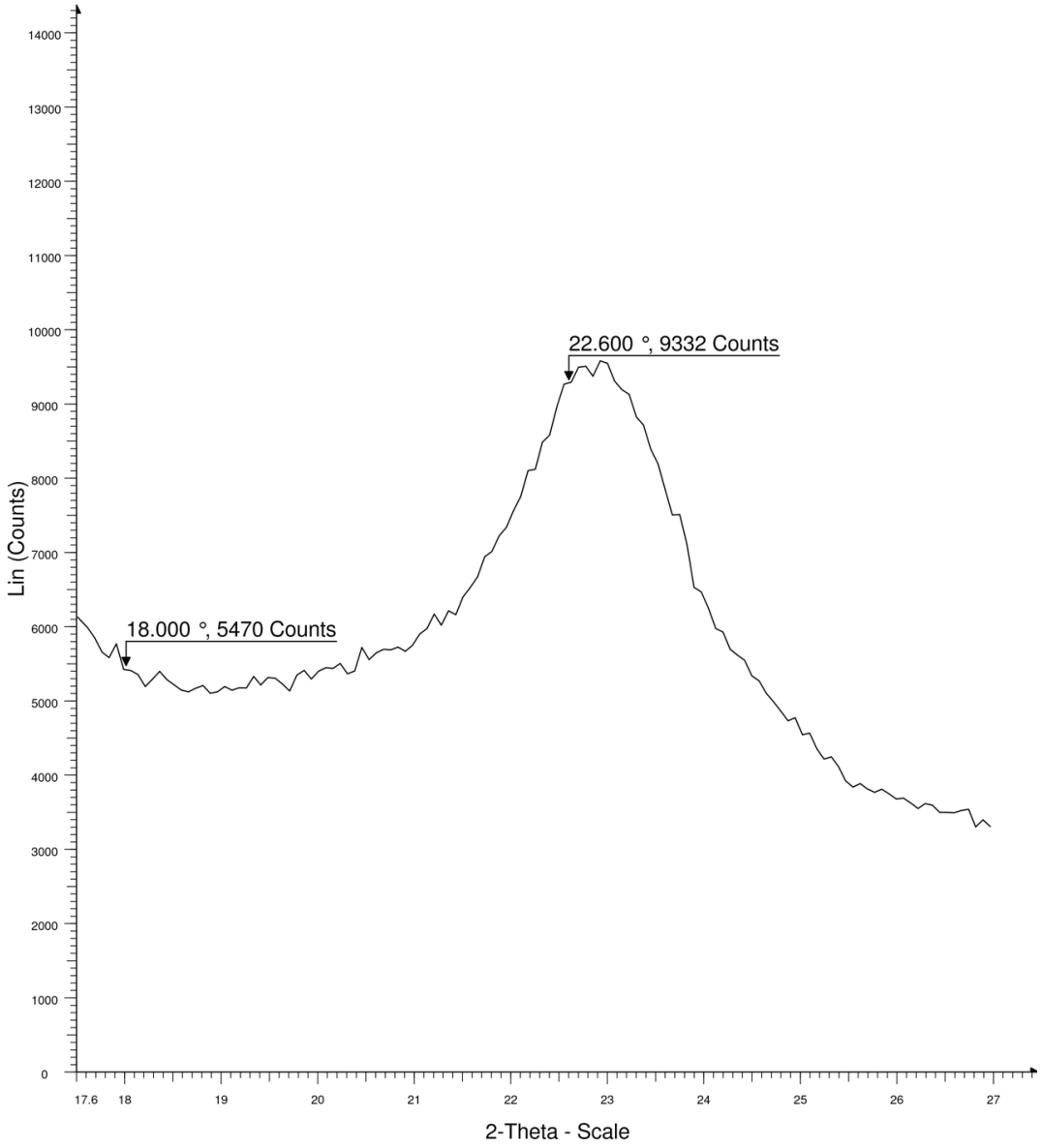

Density (g/cm^3)	Crystallinity Index (%)	Multifibrillar angle (°)
1.292-1.392	63.44-64.64	1.310-1.880

Echinocereus triglochidiatus

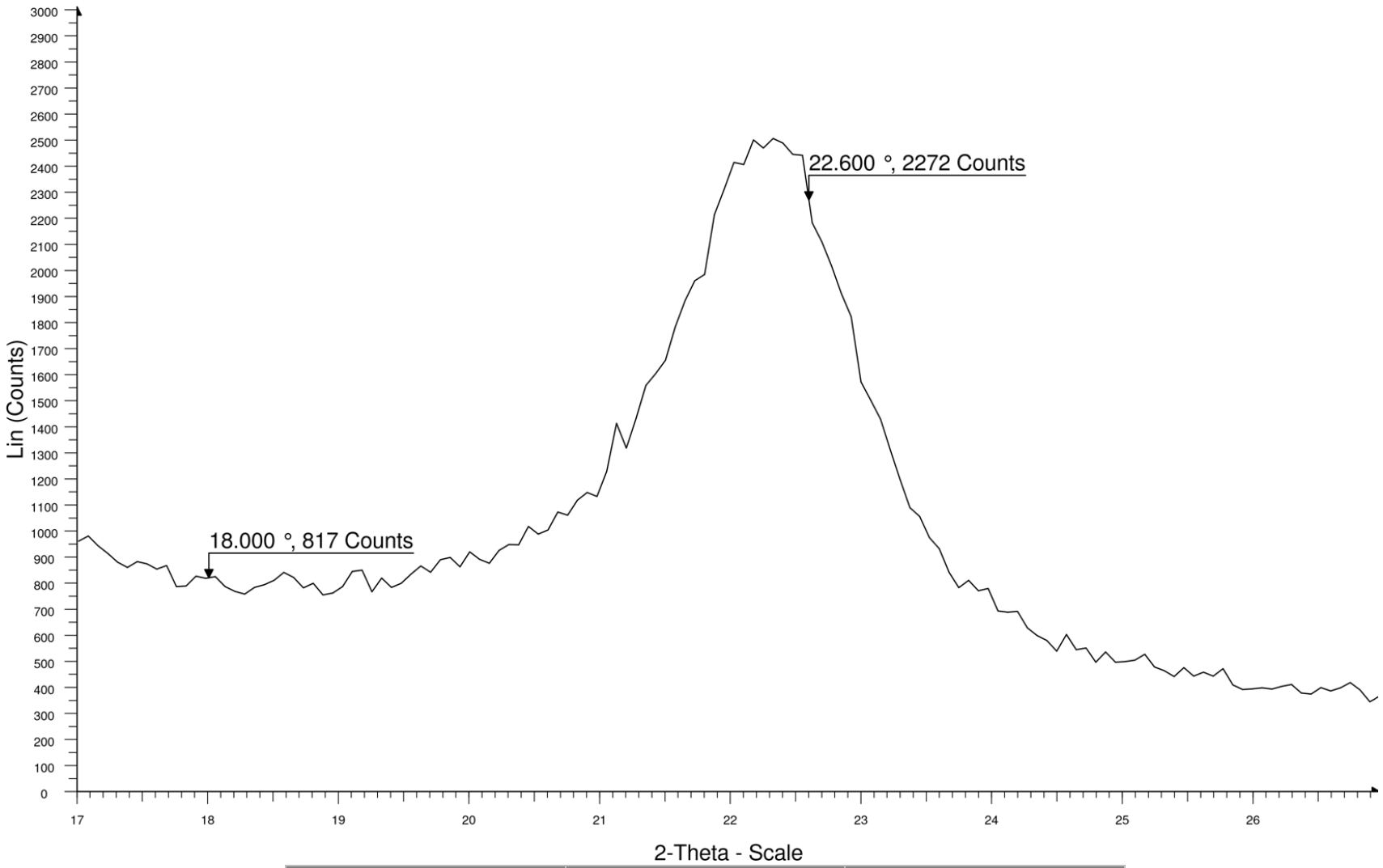

Density (g/cm³)	Crystallinity Index (%)	Multifibrillar angle (°)
1.319-1.419	39.67-43.07	1.179-1.560

Echinopsis spachiana

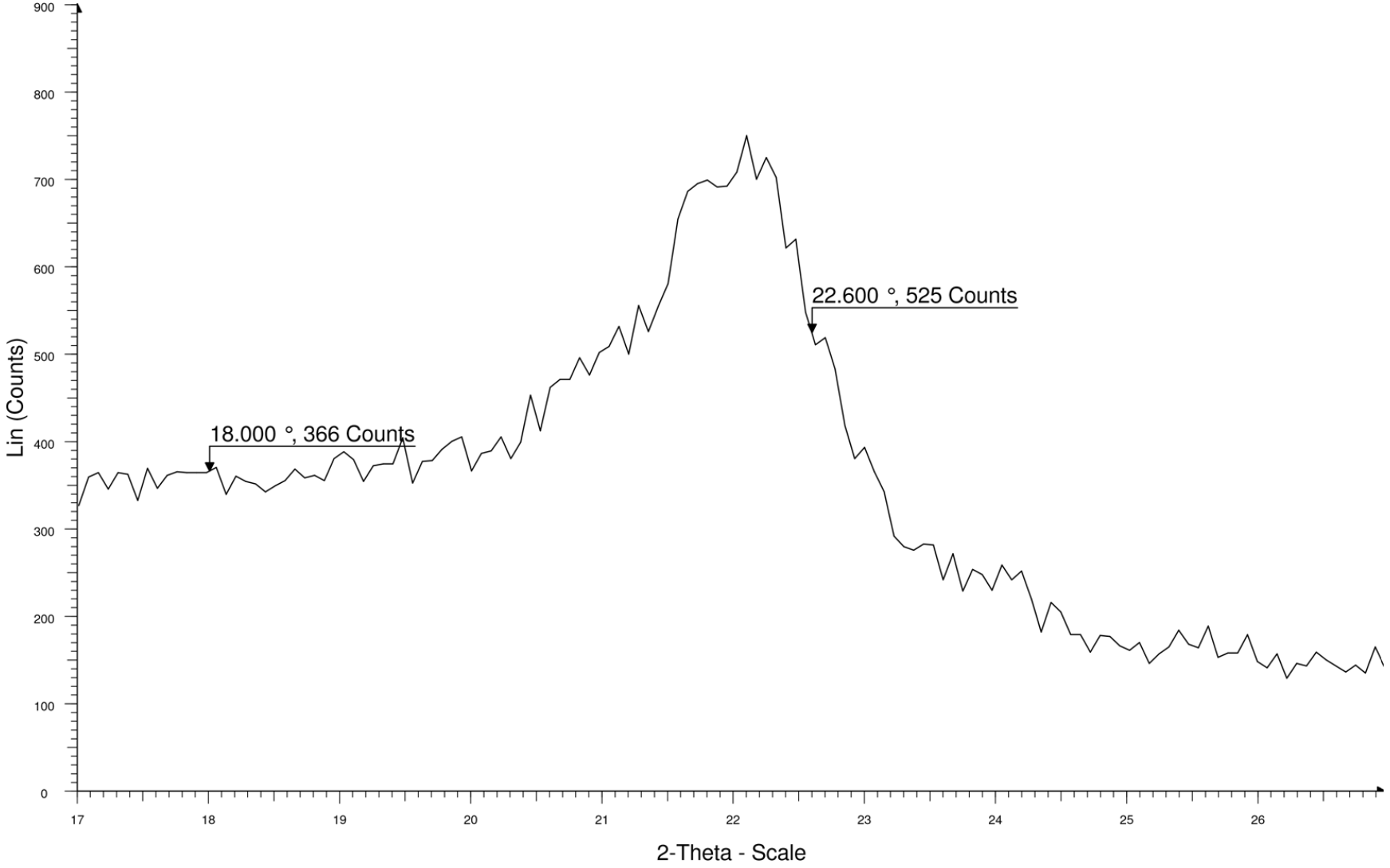

Density (g/cm3)	Crystallinity Index (%)	Multifibrillar angle (°)
1.259-1.359	26.99-33.46	1.110-1.710

Echinopsis terschekii

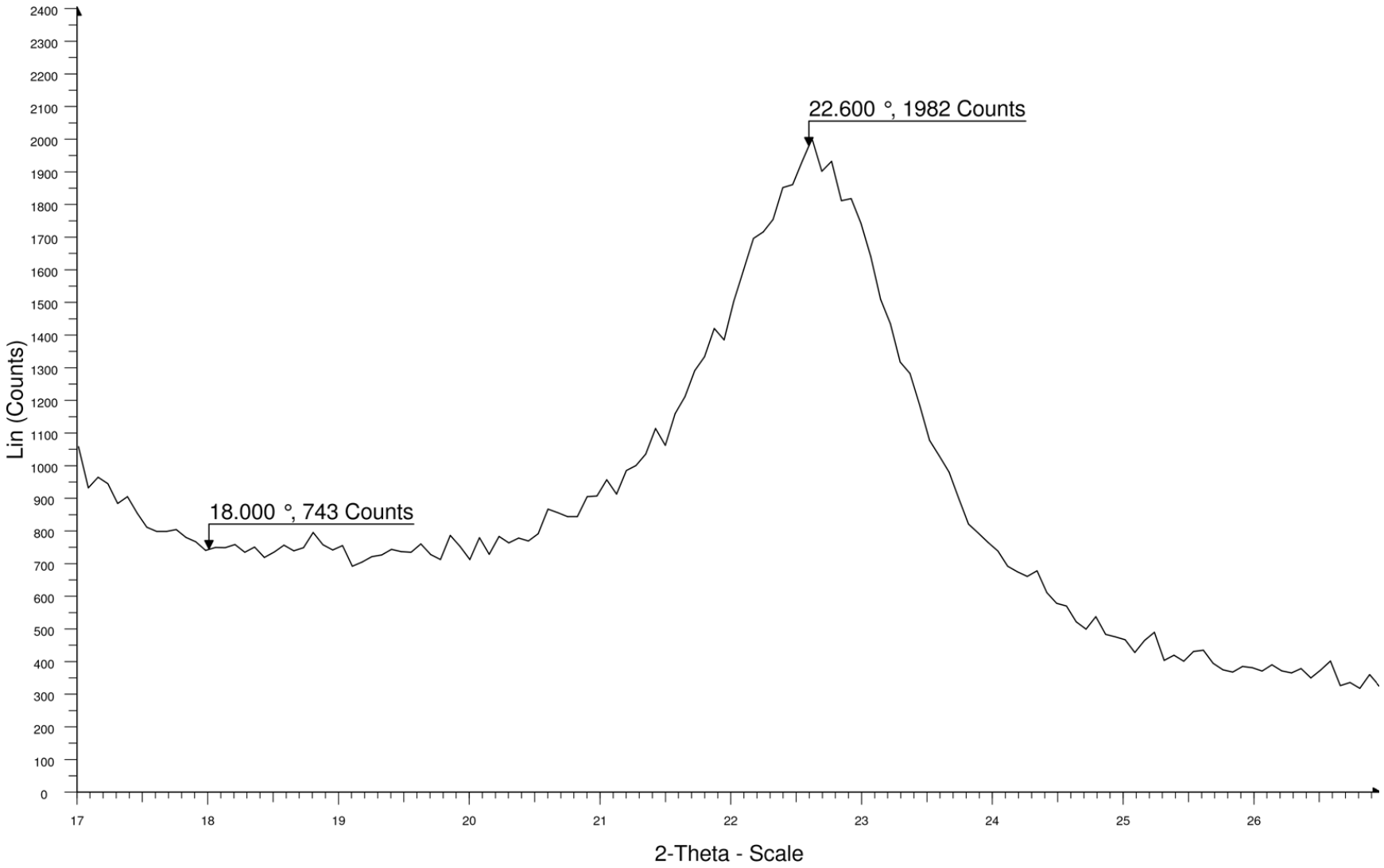

Density (g/cm3)	Crystallinity Index (%)	Multifibrillar angle (°)
1.259-1.359	58.95-65.90	1.230-1.530

Ferocactus chrysacanthus

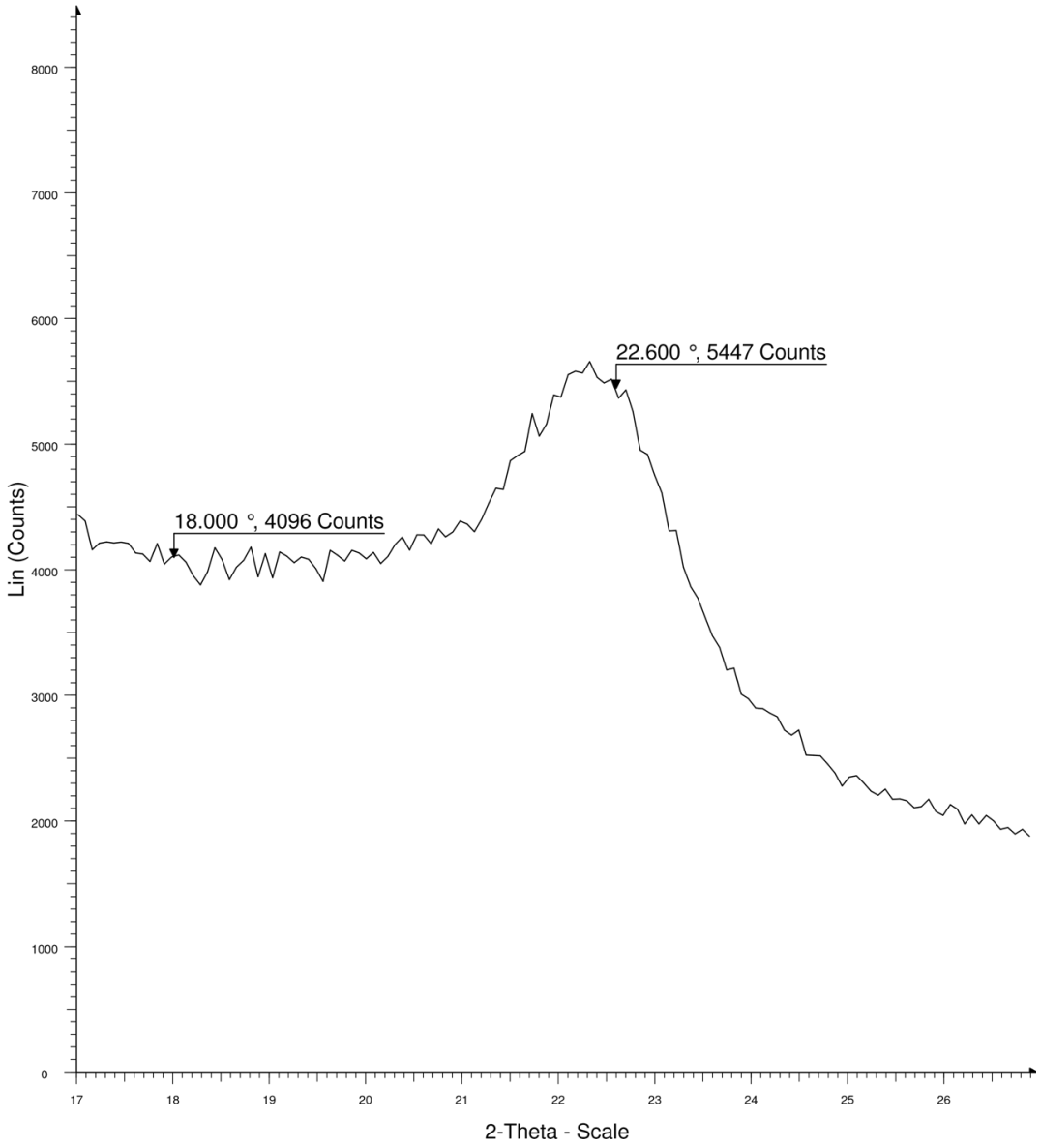

Density (g/cm^3)	Crystallinity Index (%)	Multifibrillar angle (°)
1.266-1.366	18.53-26.58	2.04-2.52

Ferocactus cylindraceus

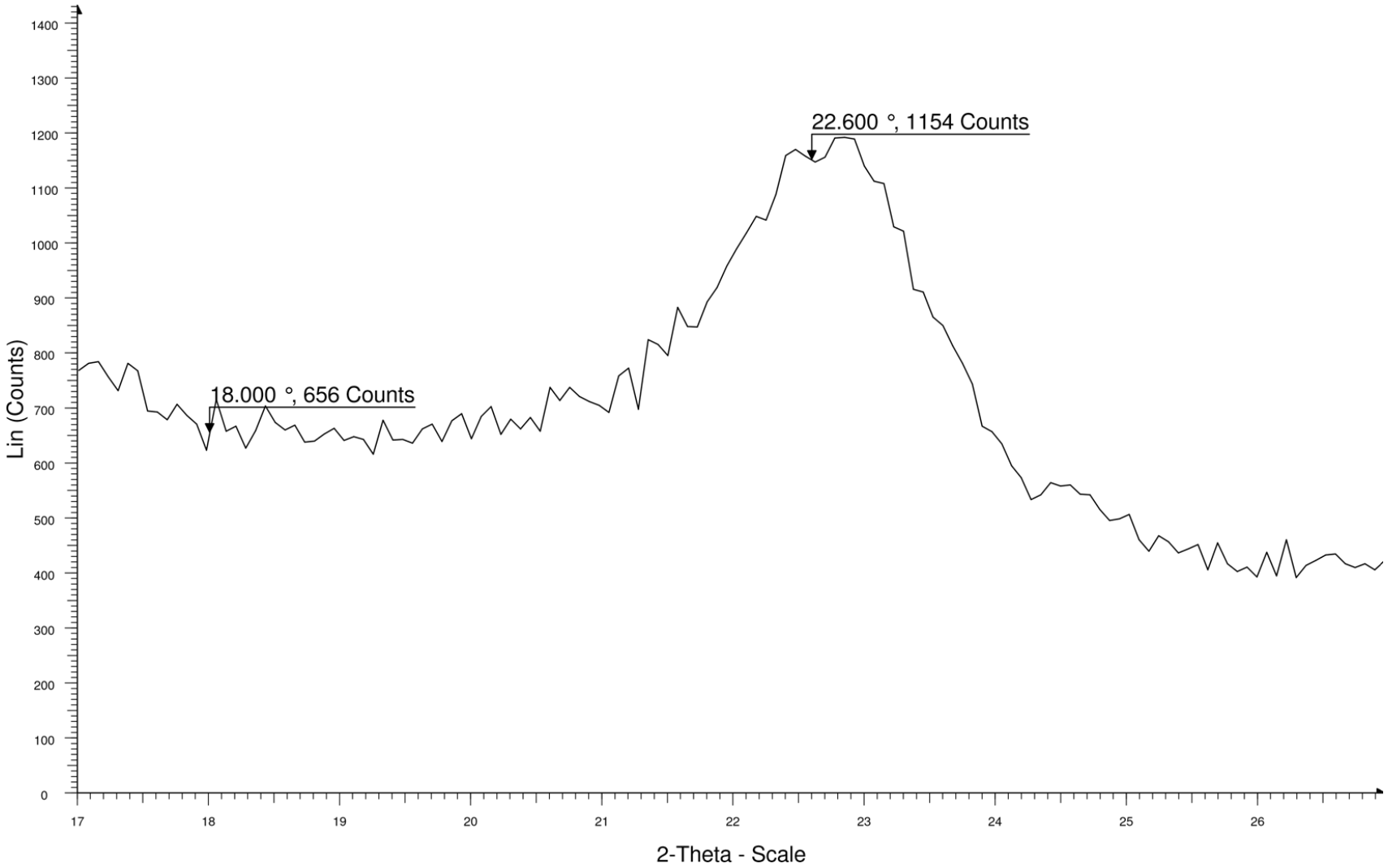

Density (g/cm^3)	Crystallinity Index (%)	Multifibrillar angle (°)
1.430-1.530	41.78-44.50	1.755-2.040

Ferocactus emoryi

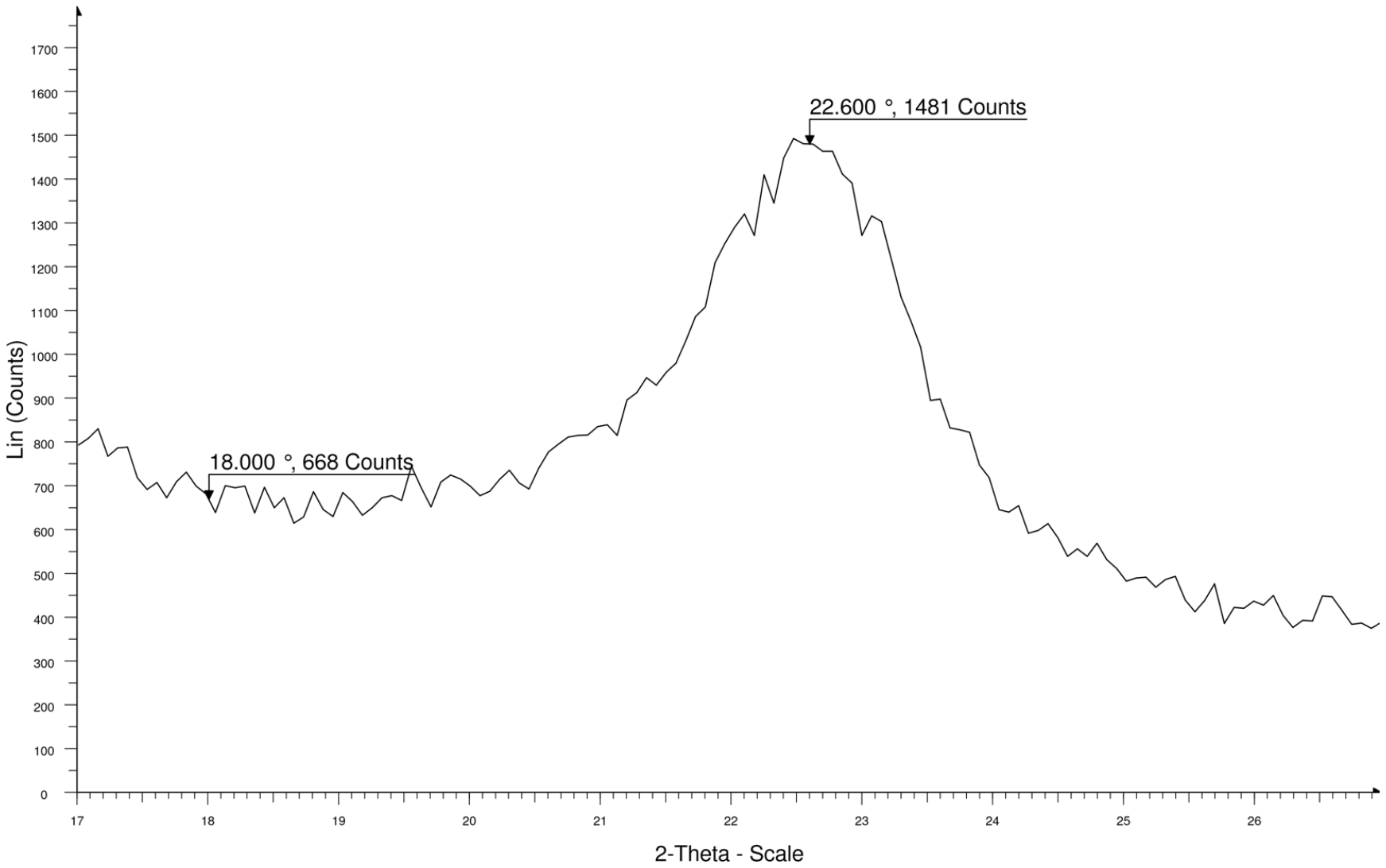

Density (g/cm3)	Crystallinity Index (%)	Multifibrillar angle (°)
1.446-1.546	49.83-59.63	1.485-1.980

Ferocactus pilosus

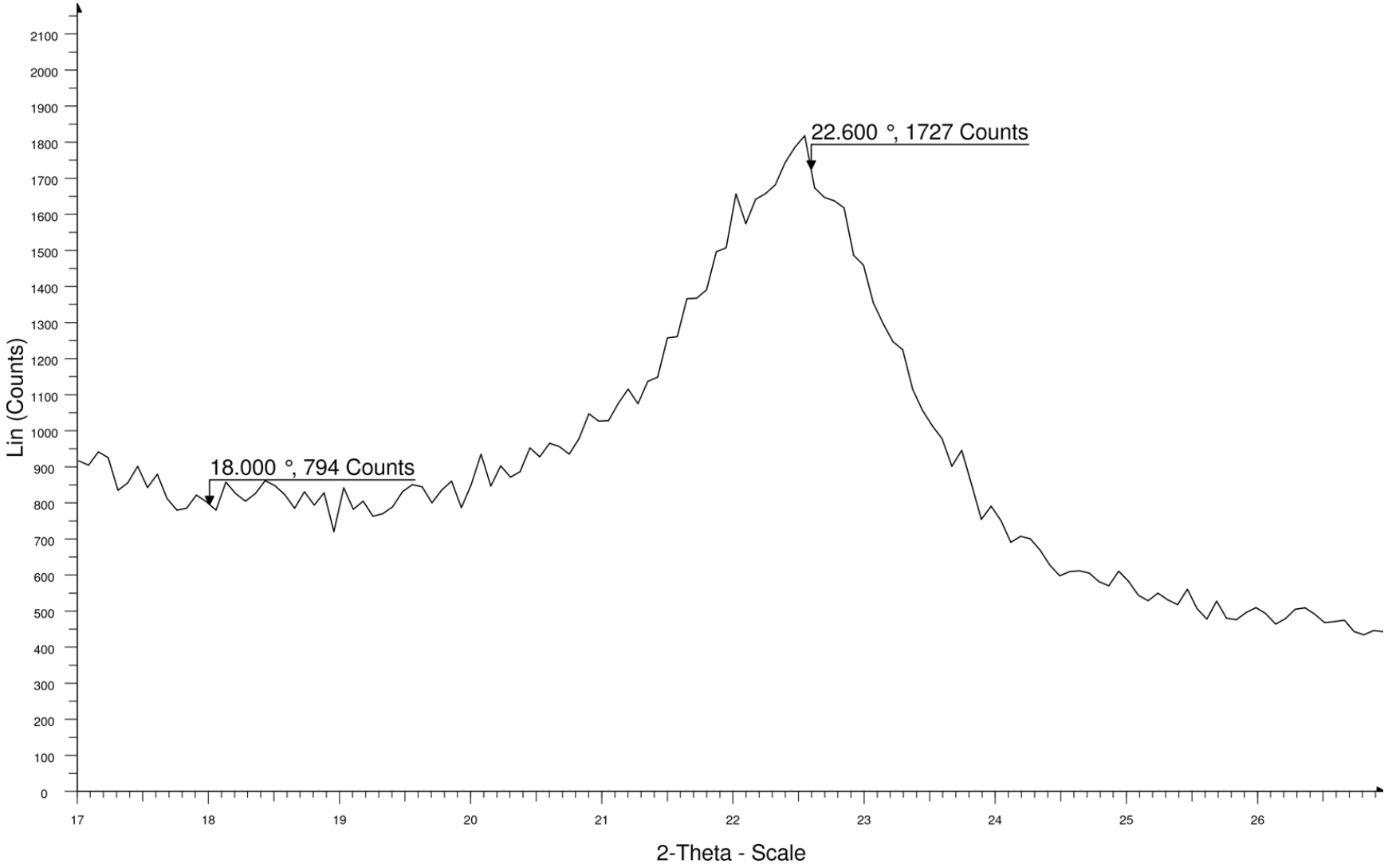

Density (g/cm3)	Crystallinity Index (%)	Multifibrillar angle (°)
1.446-1.546	49.67-58.13	1.545-1.830

Ferocactus viridescens

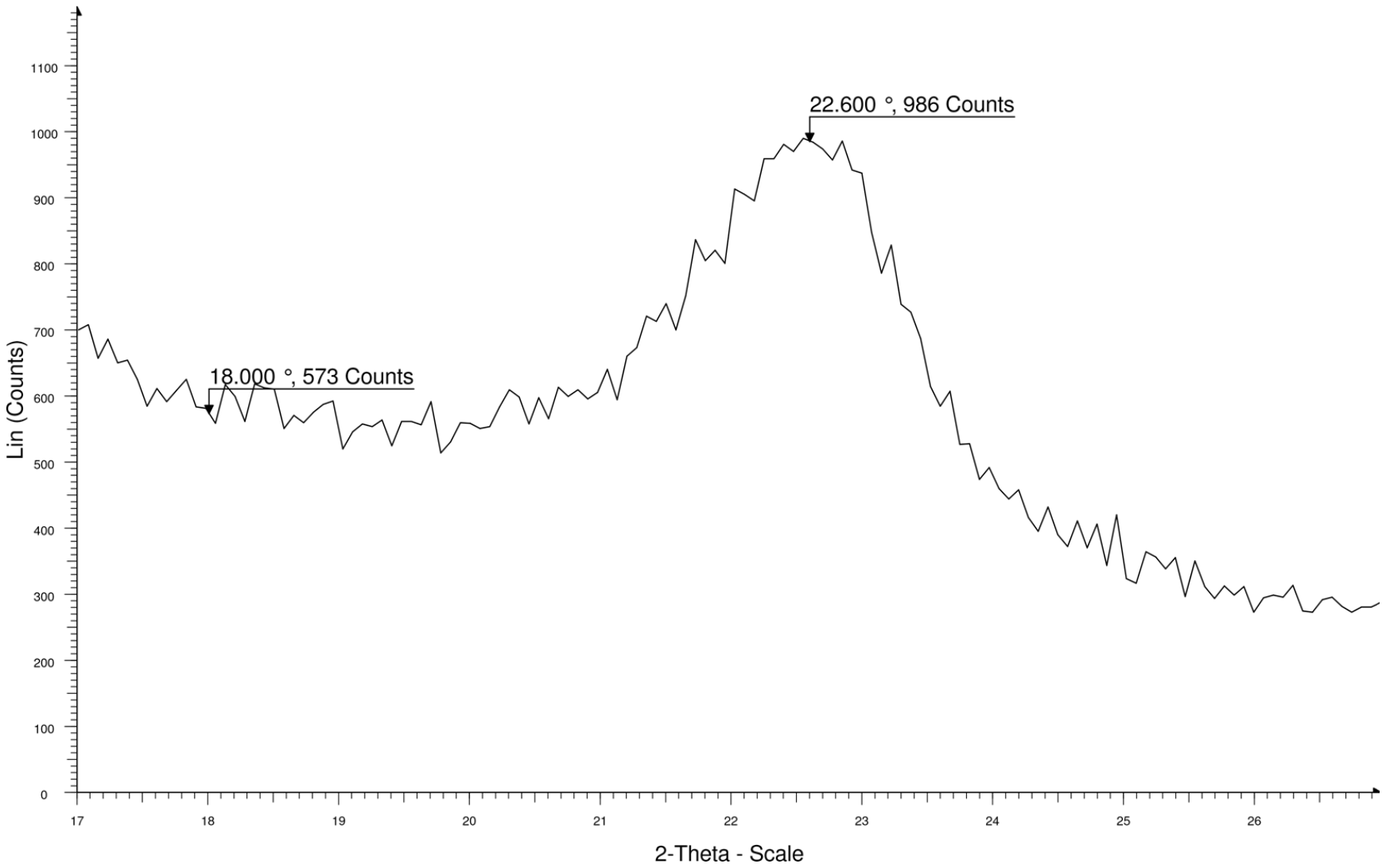

Density (g/cm3)	Crystallinity Index (%)	Multifibrillar angle (°)
1.300-1.400	40.27-43.47	1.665-2.115

Ferocactus wislizenianus

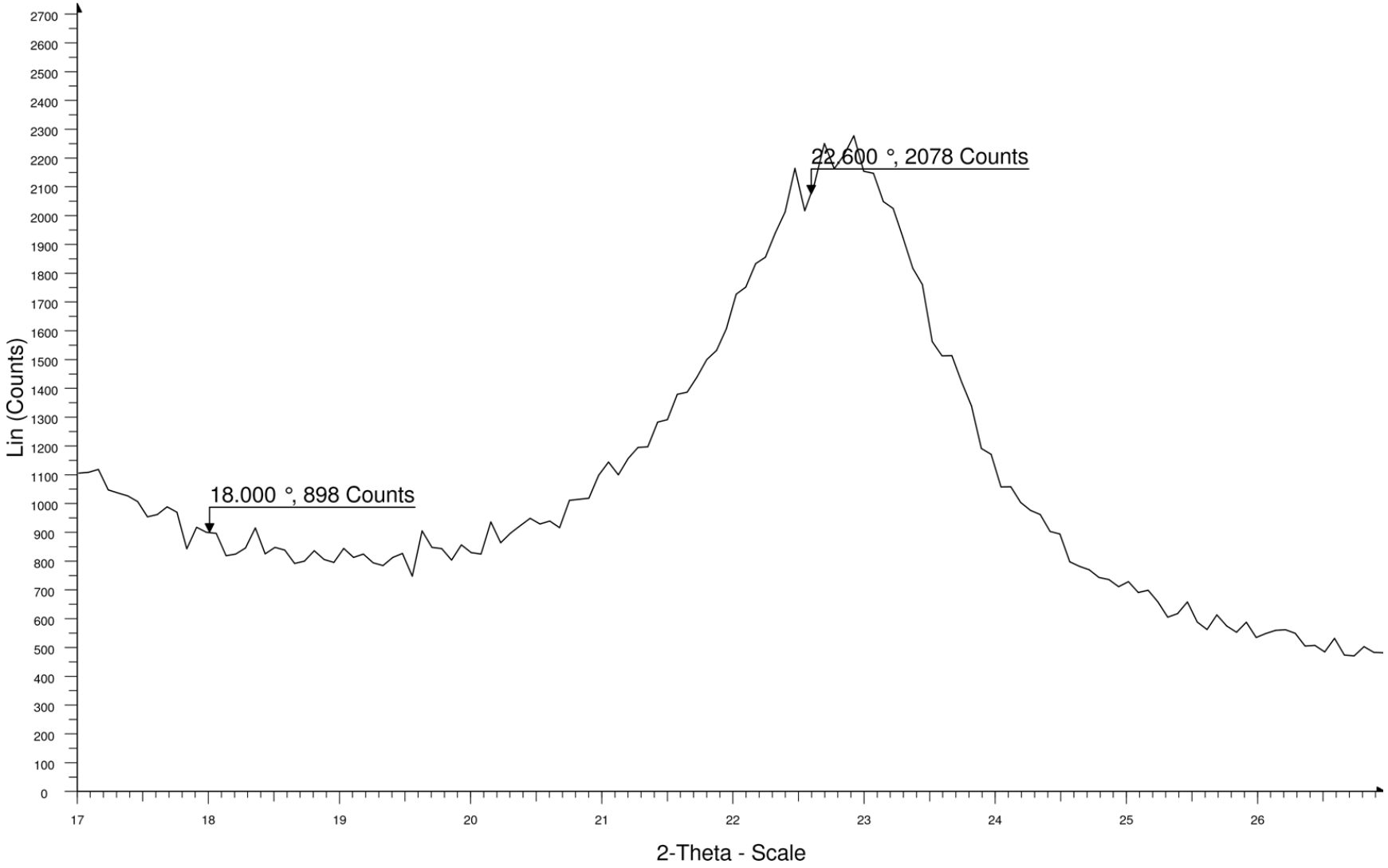

Density (g/cm3)	Crystallinity Index (%)	Multifibrillar angle (°)
1.387-1.487	53.25-60.15	1.449-2.010

Gruosnia emoryi

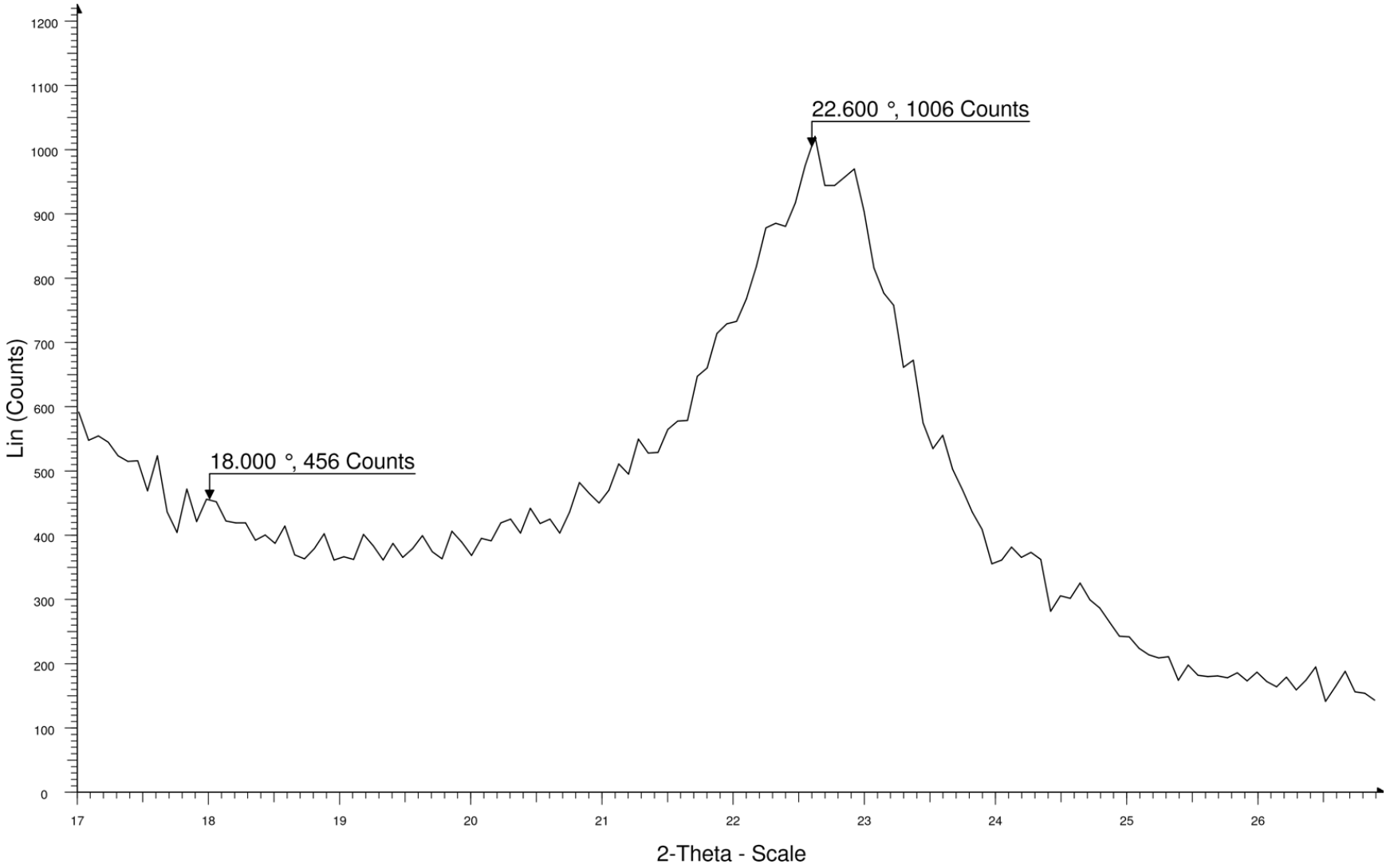

Density (g/cm3)	Crystallinity Index (%)	Multifibrillar angle (°)
1.101-1.201	53.21-56.10	1.155-1.620

Myrtillocactus geometrizans

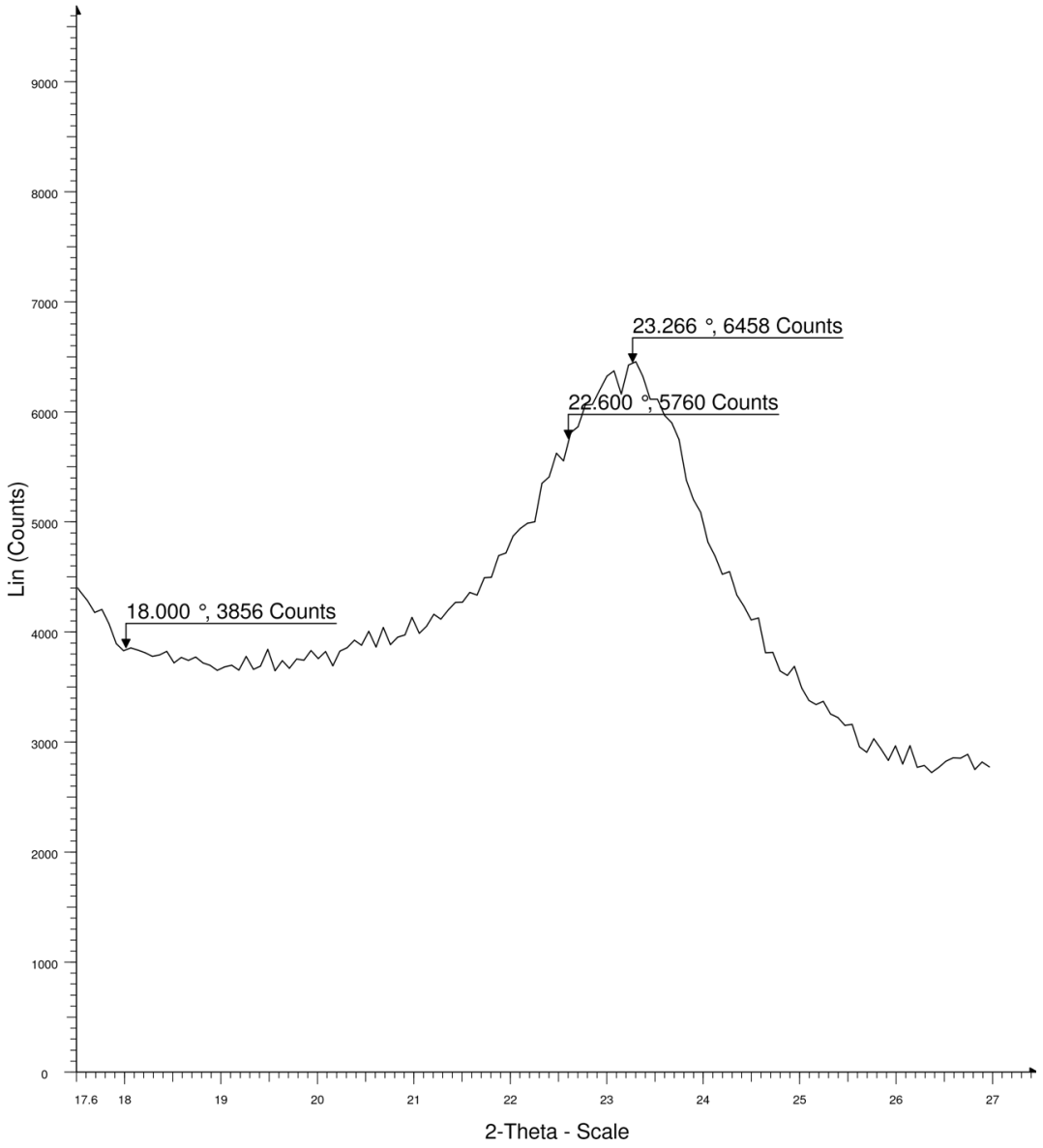

Density (g/cm^3)	Crystallinity Index (%)	Multifibrillar angle (°)
1.318-1.418	34.60-39.02	2.160-2.310

Oreocereus celsianus

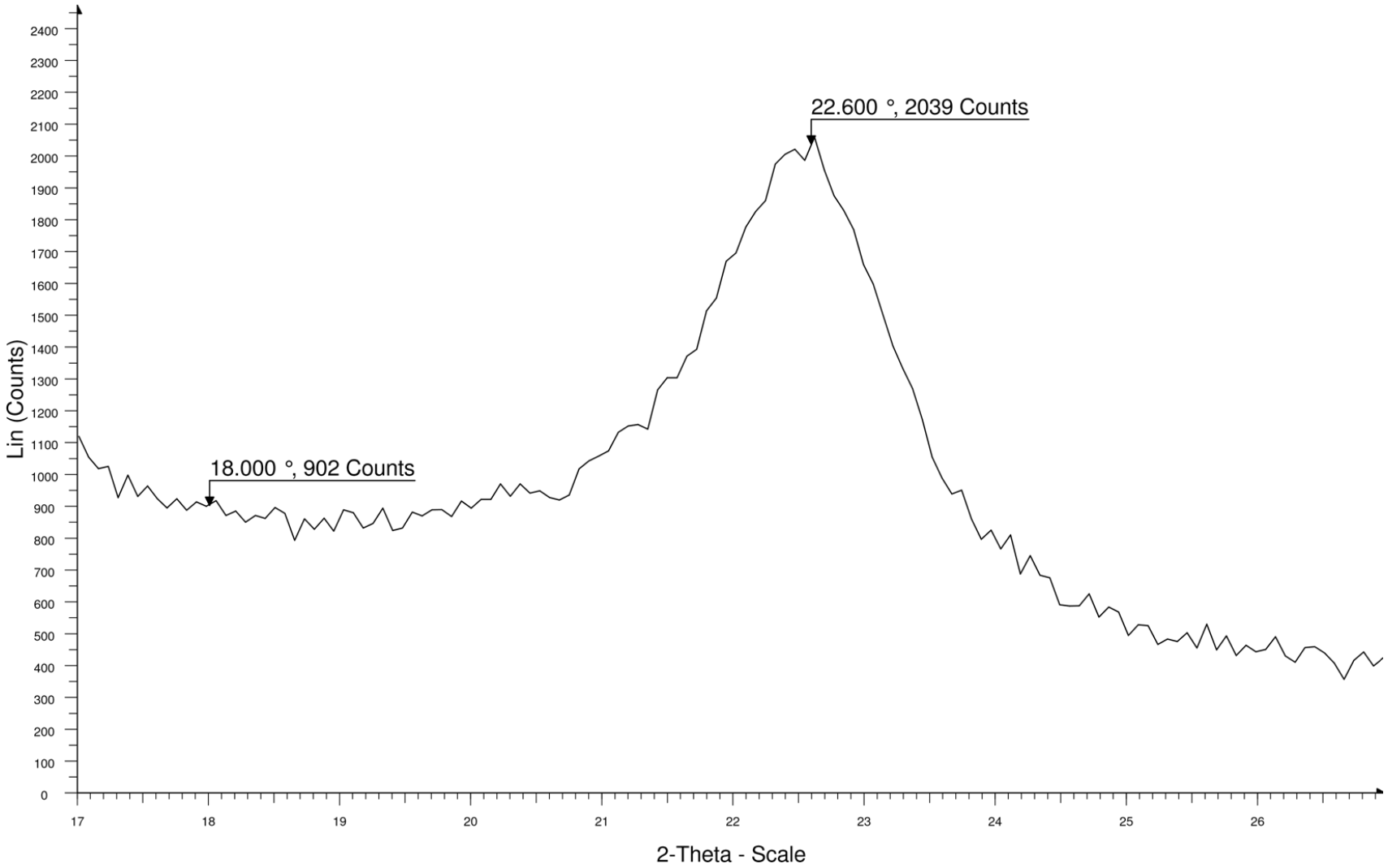

Density (g/cm^3)	Crystallinity Index (%)	Multifibrillar angle (°)
1.360-1.460	52.14-59.21	1.290-1.515

Pachycereus pringlei

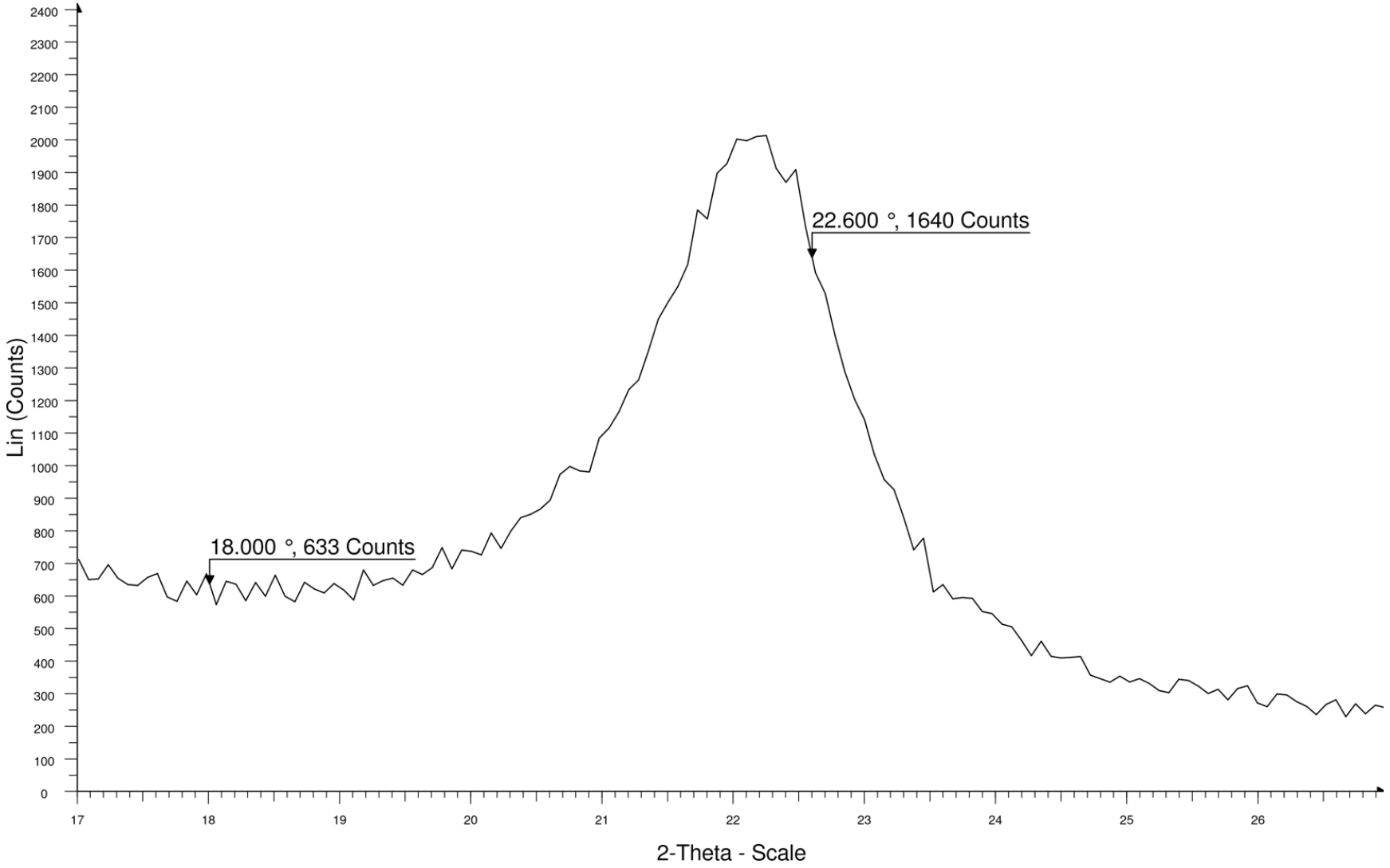

Density (g/cm3)	Crystallinity Index (%)	Multifibrillar angle (°)
1.195-1.295	57.04-65.50	1.230-1.530

Sclerocactus parviflorus

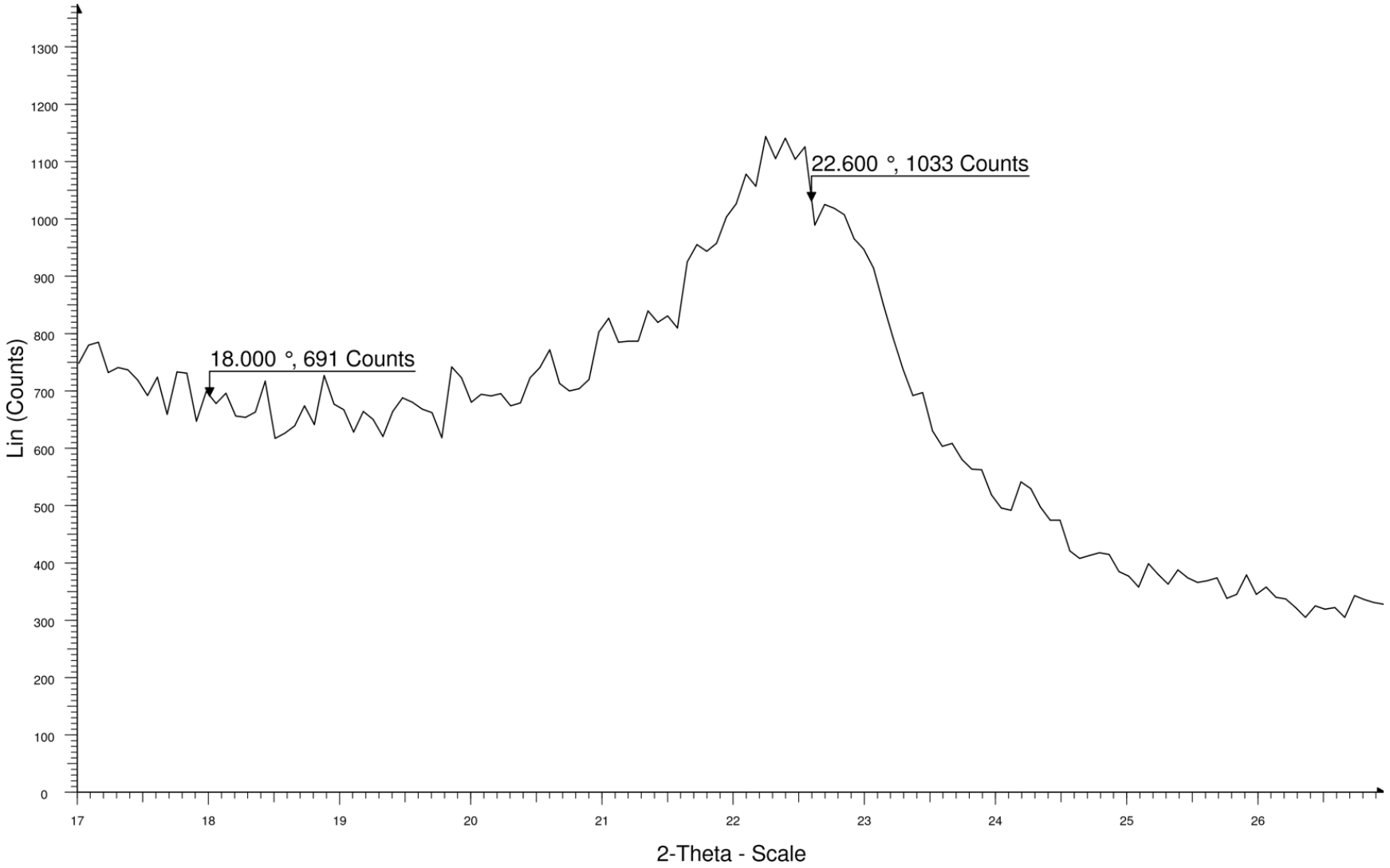

Density (g/cm3)	Crystallinity Index (%)	Multifibrillar angle (°)
1.258-1.358	40.59-43.64	1.425-2.040

Sclerocactus polyancistrus

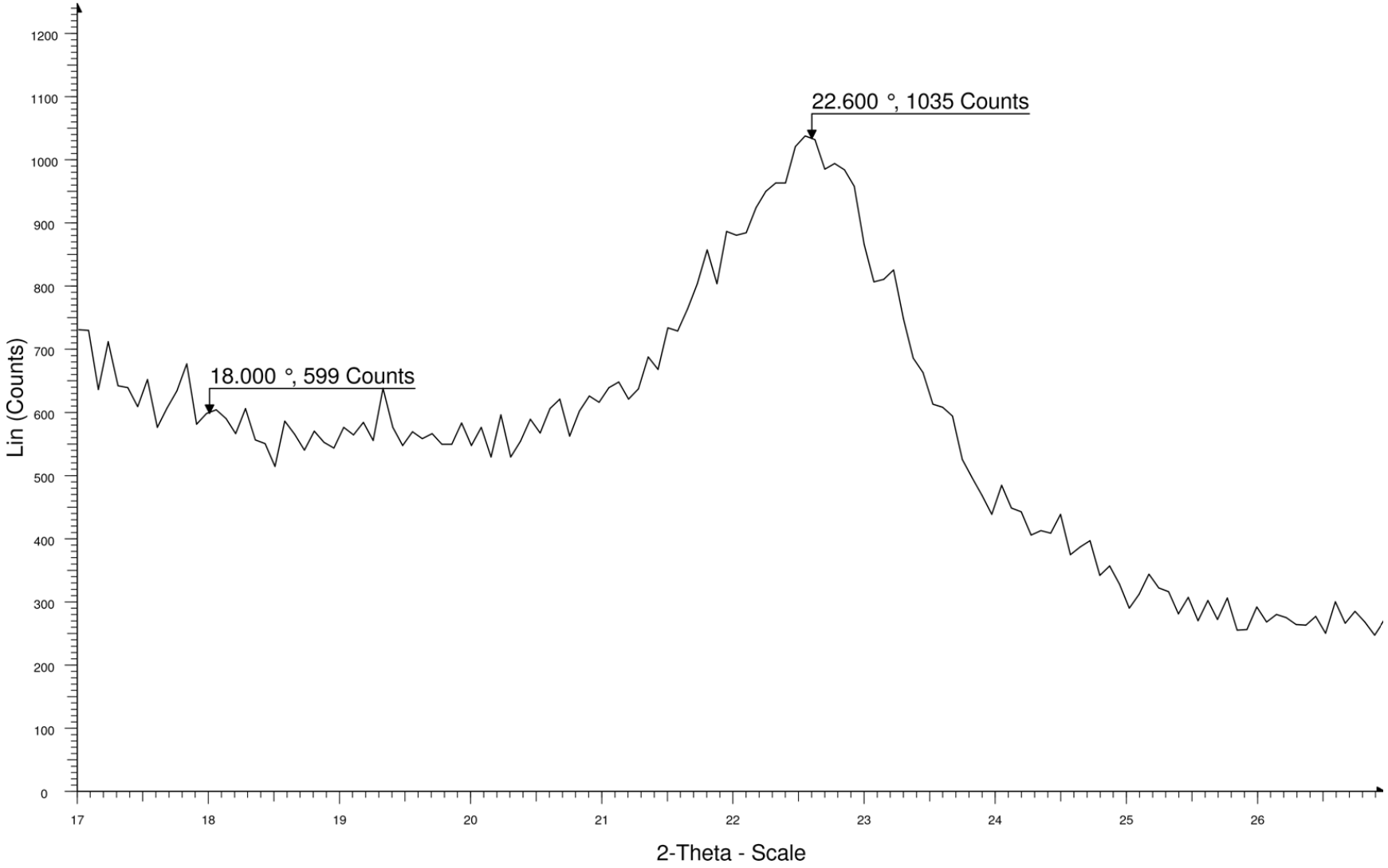

Density (g/cm3)	Crystallinity Index (%)	Multifibrillar angle (°)
1.308-1.408	31.48-34.71	1.530-1.890

Stenocactus crispatus

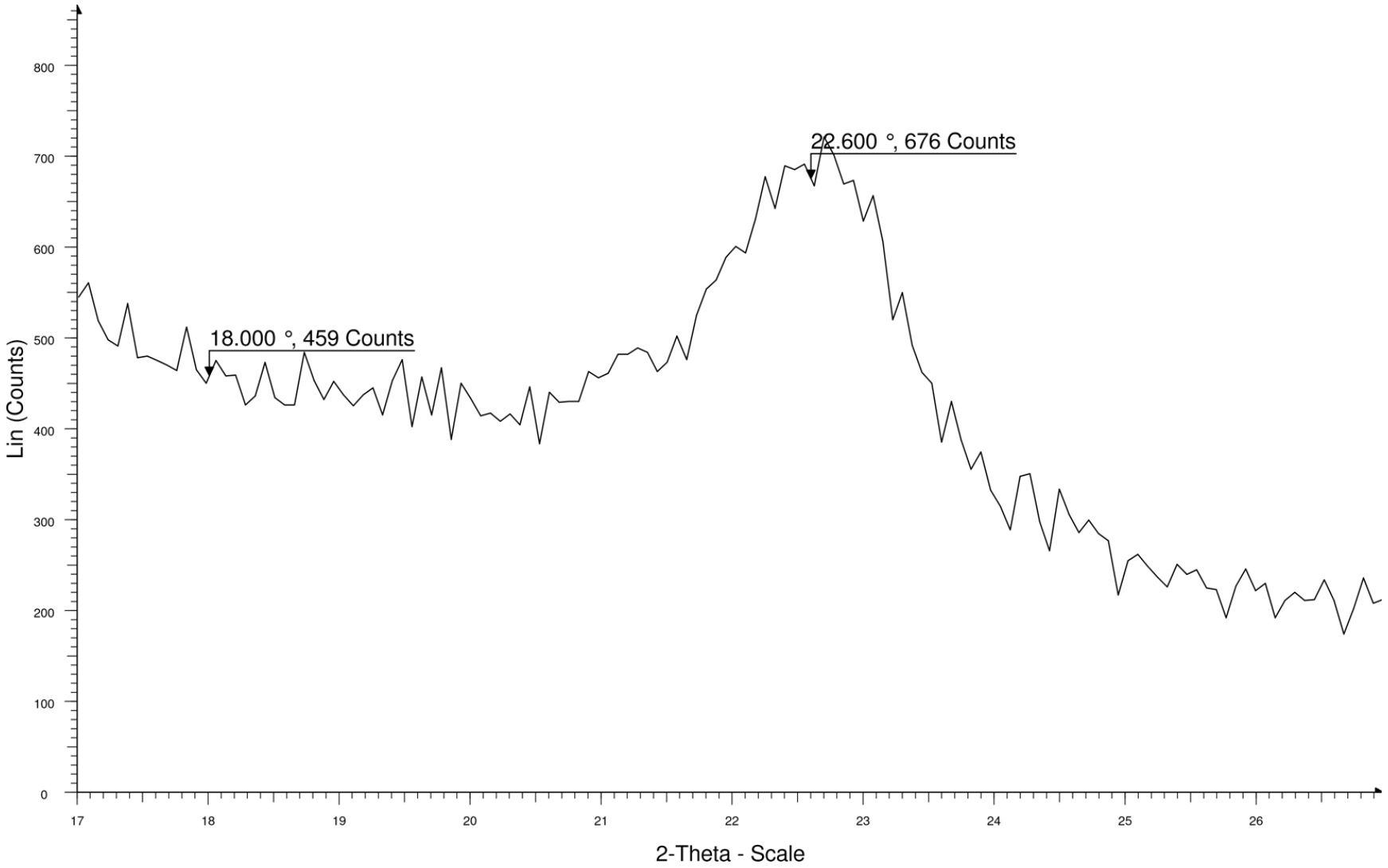

Density (g/cm3)	Crystallinity Index (%)	Multifibrillar angle (°)
1.271-1.371	29.58-34.55	1.515-1.920

Stenocactus multicostatus

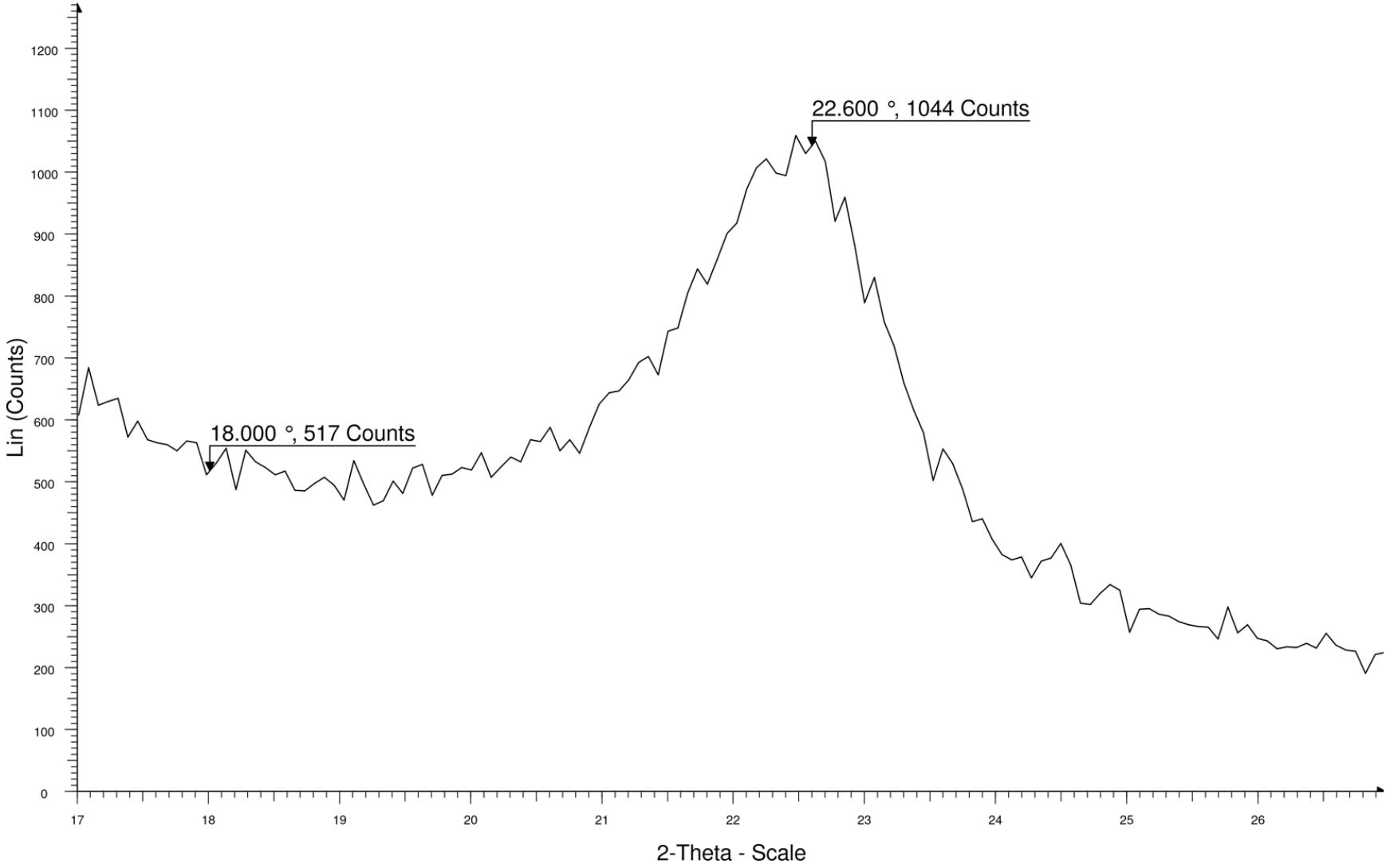

Density (g/cm3)	Crystallinity Index (%)	Multifibrillar angle (°)
1.313-1.413	49.03-51.90	1.485-1.740

Stenocereus thurberi

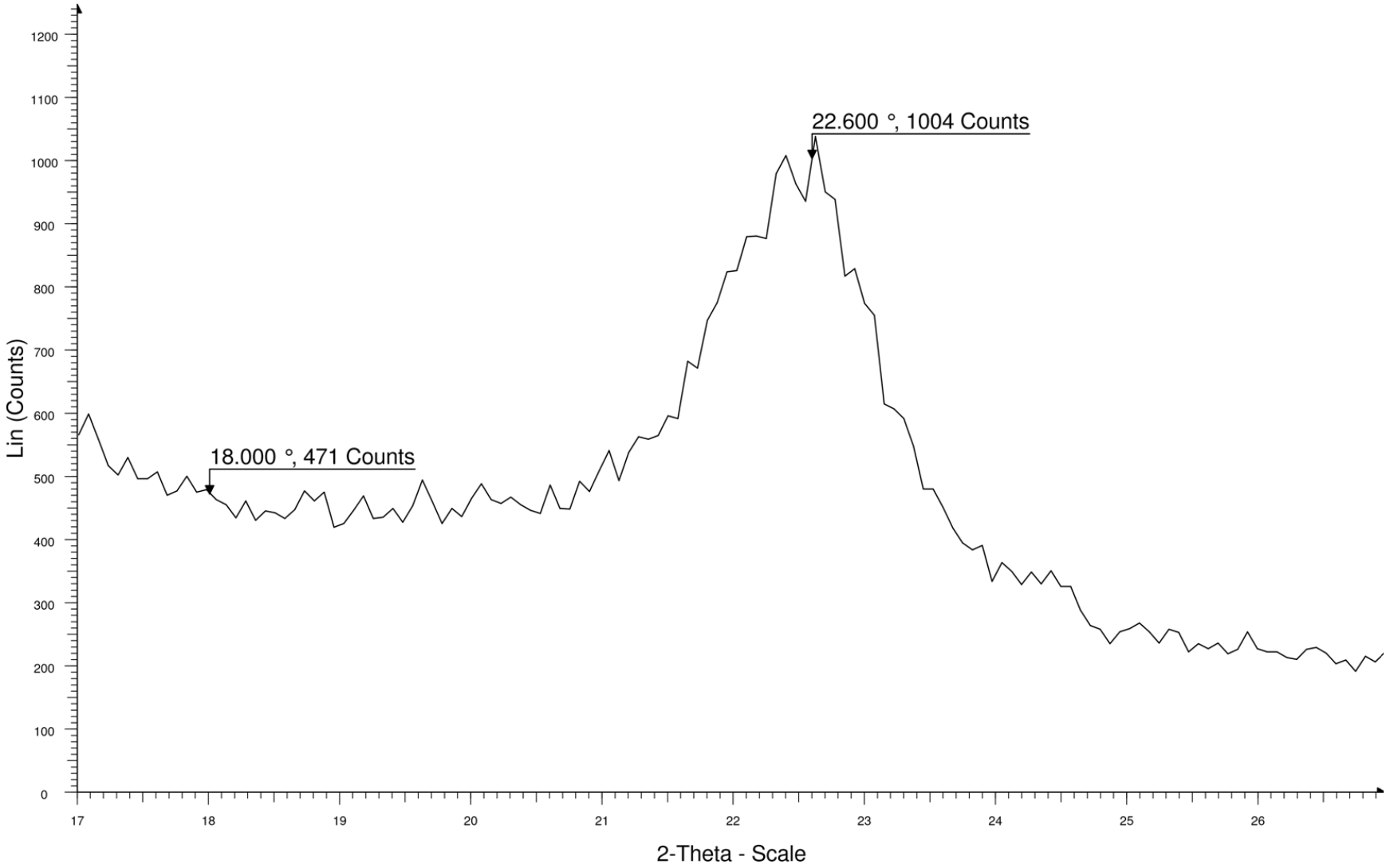

Density (g/cm3)	Crystallinity Index (%)	Multifibrillar angle (°)
1.313-1.413	51.61-54.54	1.125-1.560

Tephrocactus alexanderi

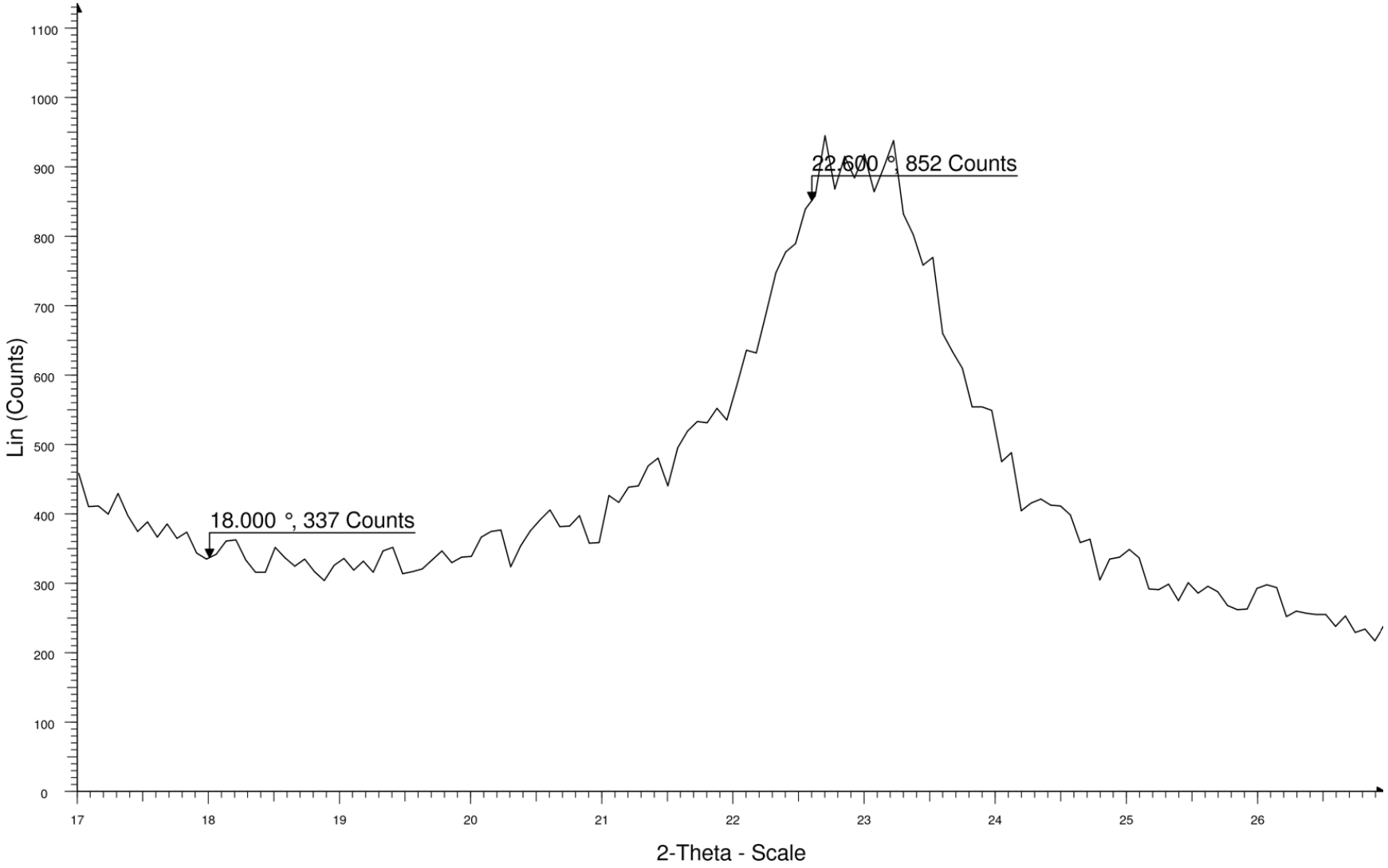

Density (g/cm3)	Crystallinity Index (%)	Multifibrillar angle (°)
1.397-1.497	58.79-62.06	1.155-1.620

Appendix D: Three-Point Bend Testing Results

Astrophytum ornatum

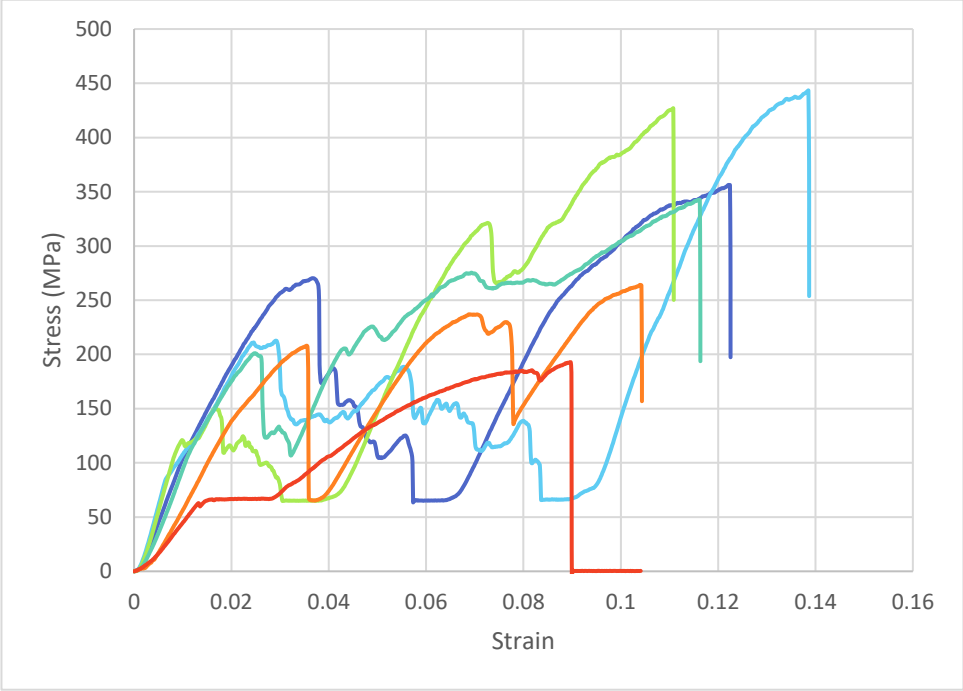

ε (%)	σ (MPa)	E (GPa)
0.122	357.4	9.20
0.138	444.9	8.78
0.111	428.1	4.83
0.116	344.0	8.30
0.104	265.2	6.71
0.090	193.5	2.82

Echinocactus grusonii

ε (%)	σ (MPa)	E (GPa)
0.051	158.9	4.19
0.044	246.4	9.91
0.039	367.2	17.29
0.034	286.4	13.39
0.035	298.2	13.40
0.036	347.3	15.96

Echinocactus polycephalus

ε (%)	σ (MPa)	E (GPa)
0.024	100.2	4.31
0.074	68.8	1.22
0.070	142.7	4.40
0.060	161.5	5.24
0.047	139.3	3.91
0.043	182.2	5.14

Echinocereus boyce-thompsonii

ε (%)	σ (MPa)	E (GPa)
0.019	235.3	26.8
0.021	311.9	21.8
0.023	276.2	30.0
0.025	236.1	25.4
0.020	200.8	17.3
0.024	220.4	23.8

Echinocereus englemanii

ε (%)	σ (MPa)	E (GPa)
0.072	149.0	7.33
0.046	179.5	8.99
0.037	332.2	19.35
0.037	224.4	10.33
0.037	344.6	18.16
0.036	270.0	16.00

Echinocereus triglochidiatus

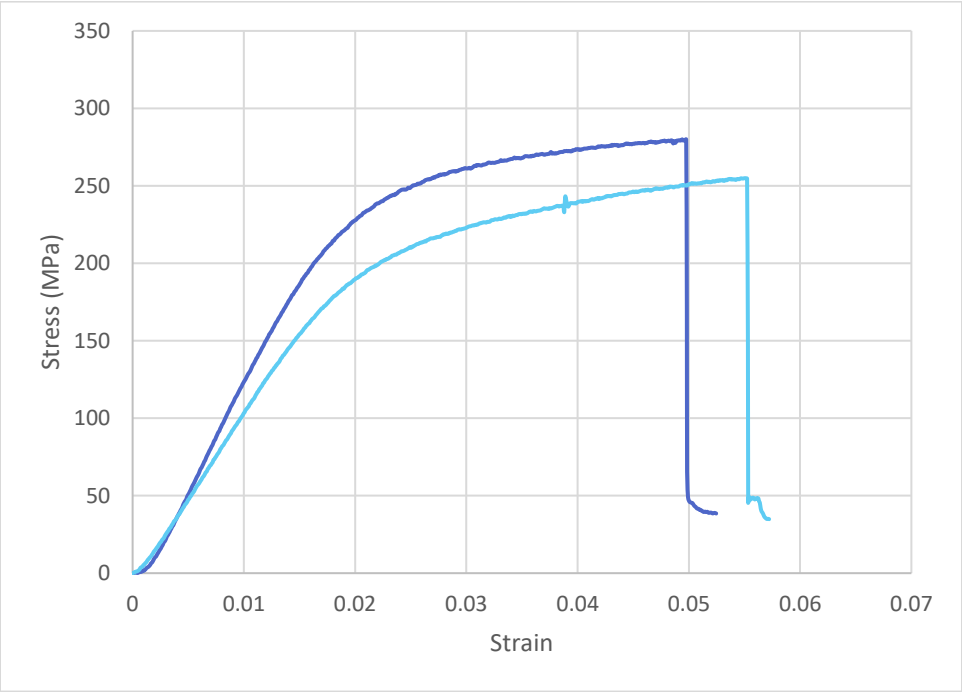

ε (%)	σ (MPa)	E (GPa)
0.048	94.3	6.90
0.047	211.7	12.56
0.055	200.0	17.15
0.045	133.4	8.91
0.050	281.3	12.30
0.055	256.1	10.20

Echinopsis spachiana

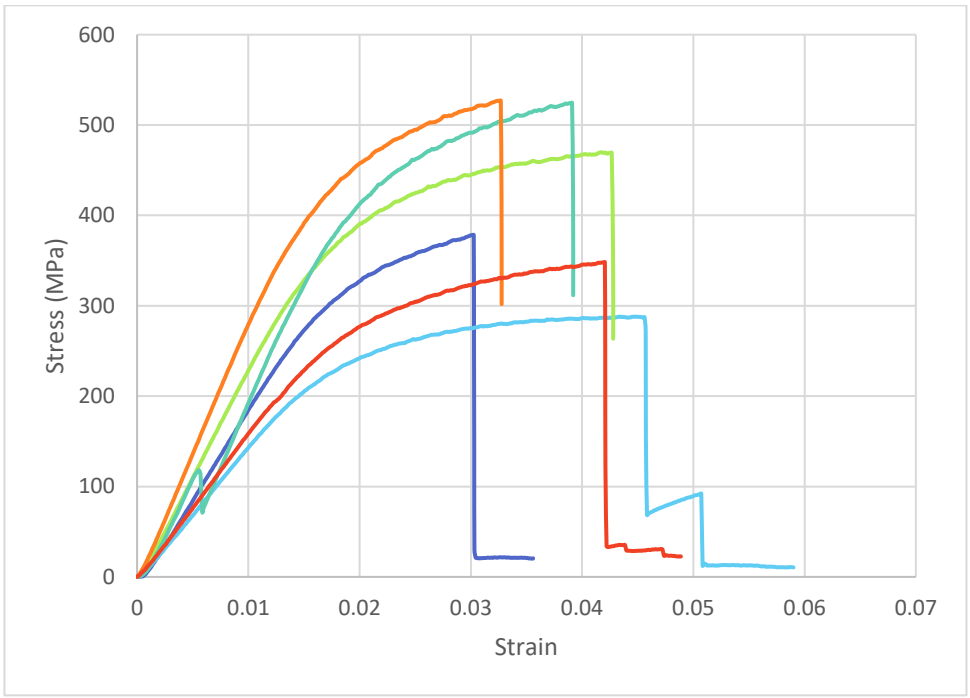

ε (%)	σ (MPa)	E (GPa)
0.030	379.0	18.55
0.046	287.7	14.18
0.043	470.0	22.62
0.039	525.1	21.04
0.033	527.9	27.30
0.042	348.9	15.51

Echinopsis terschekii

ε (%)	σ (MPa)	E (GPa)
0.027	288.9	17.60
0.018	208.8	14.08
0.037	259.0	14.54
0.033	198.5	10.75
0.033	229.8	16.57
0.032	116.5	4.83

Ferocactus emoryi

ε (%)	σ (MPa)	E (GPa)
0.028	223.9	11.76
0.021	208.8	12.45
0.052	220.5	4.56
0.033	280.9	13.19
0.033	188.4	7.05
0.040	222.1	10.91

Ferocactus pilosus

ε (%)	σ (MPa)	E (GPa)
0.030	369.1	17.60
0.025	266.8	11.47
0.031	283.4	12.94
0.023	277.1	13.27
0.028	310.0	15.16
0.033	349.8	15.15

Ferocactus chrysacanthus

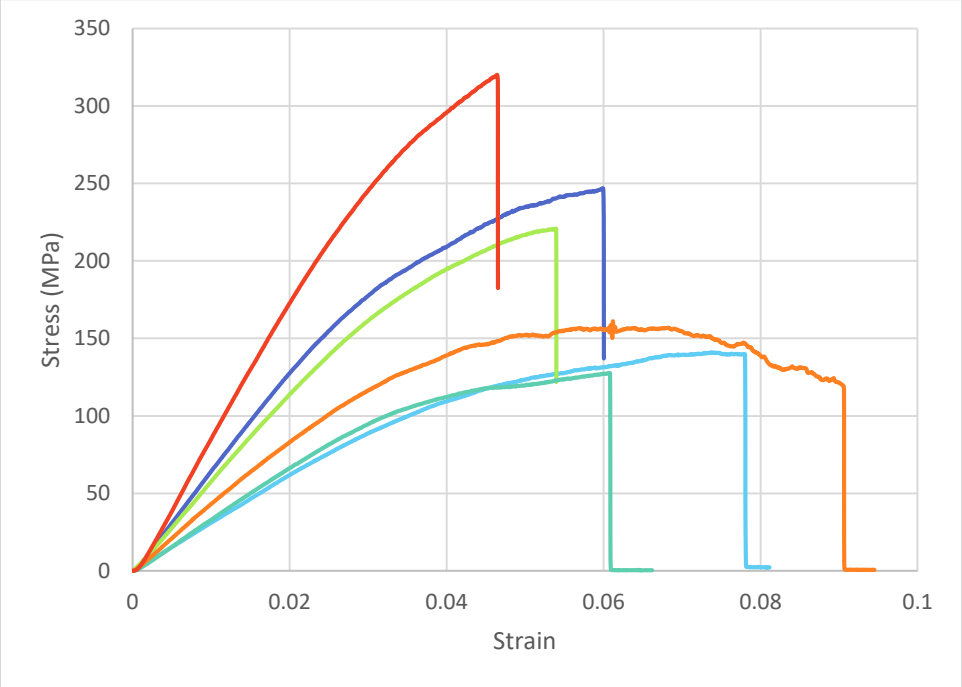

ε (%)	σ (MPa)	E (GPa)
0.060	246.9	6.42
0.074	141.2	3.11
0.054	221.2	5.72
0.061	128.1	3.29
0.061	161.5	4.31
0.046	322.2	8.43

Sclerocactus polyancistrus

ε (%)	σ (MPa)	E (GPa)
0.063	213.0	12.5
0.009	151.2	18.1
0.036	230.0	28.4
0.033	227.1	19.5
0.038	242.2	18.0
0.033	239.8	12.18

Stenocactus multicostatus

ε (%)	σ (MPa)	E (GPa)
0.075	206.5	8.51
0.130	114.7	4.17
0.093	259.4	11.12
0.082	157.2	6.83
0.086	175.2	7.38
0.098	64.7	2.58

Tephrocactus alexanderi

ε (%)	σ (MPa)	E (GPa)
0.066	172.5	14.28
0.041	245.6	23.00
0.046	261.9	19.46
0.057	209.6	15.13
0.018	218.1	17.34
0.040	216.8	12.37

Ferocactus cylindraceus

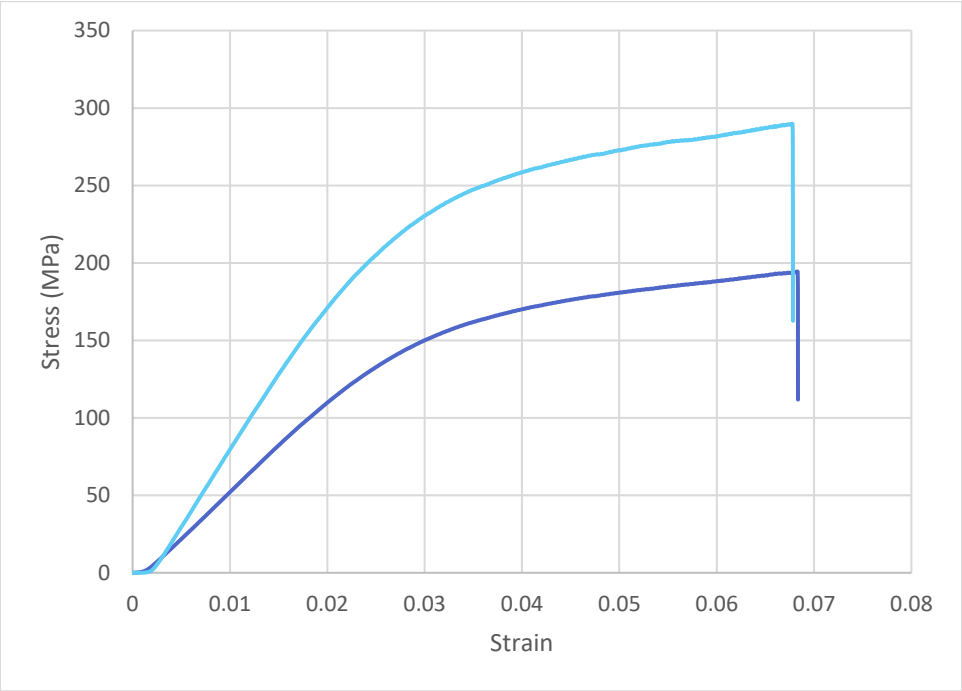

ε (%)	σ (MPa)	E (GPa)
0.069	194	5.46
0.046	233.7	8.13
0.049	232.1	7.58
0.045	211.7	9.06
0.047	227.8	10.38
0.068	289.4	8.51

Ferocactus viridescens

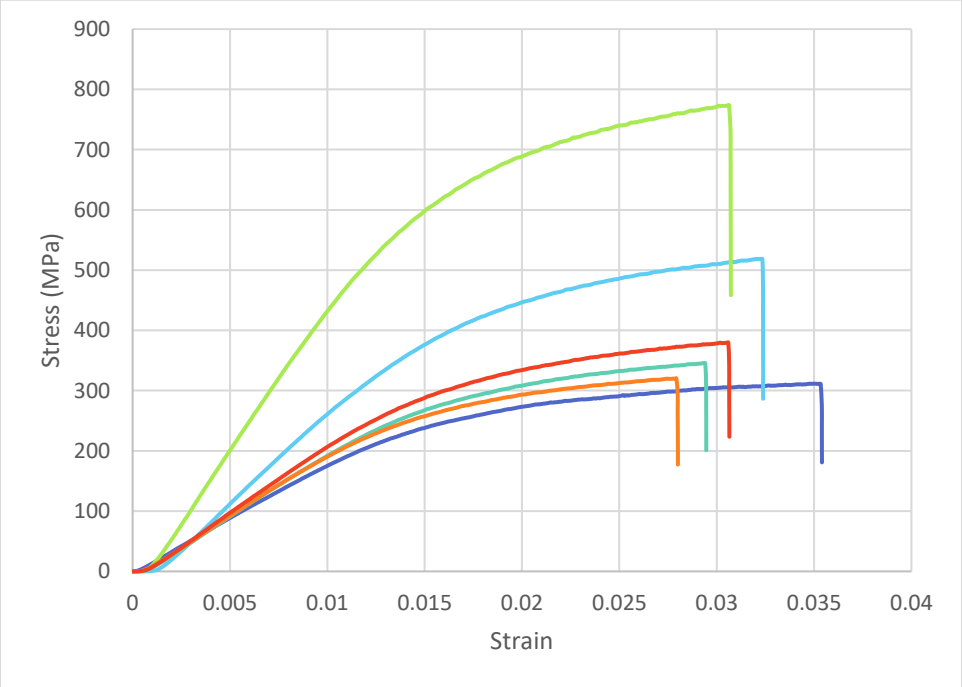

ε (%)	σ (MPa)	E (GPa)
0.035	311.5	17.79
0.032	518.9	25.52
0.031	774.2	43.03
0.029	346.0	19.18
0.028	320.7	19.14
0.031	380.0	20.56

Ferocactus wislizenianus

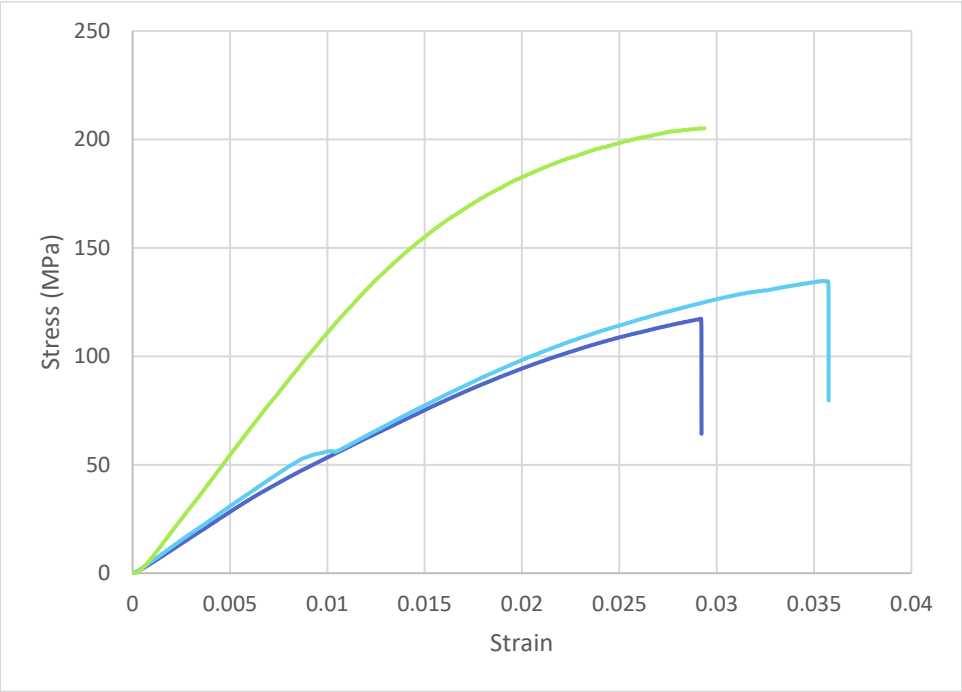

ε (%)	σ (MPa)	E (GPa)
0.031	378.2	24.83
0.038	267.1	12.38
0.038	264.8	12.54
0.046	271.2	11.47
0.049	246.2	11.09
0.047	218.5	11.08

Gruosnia emoryi

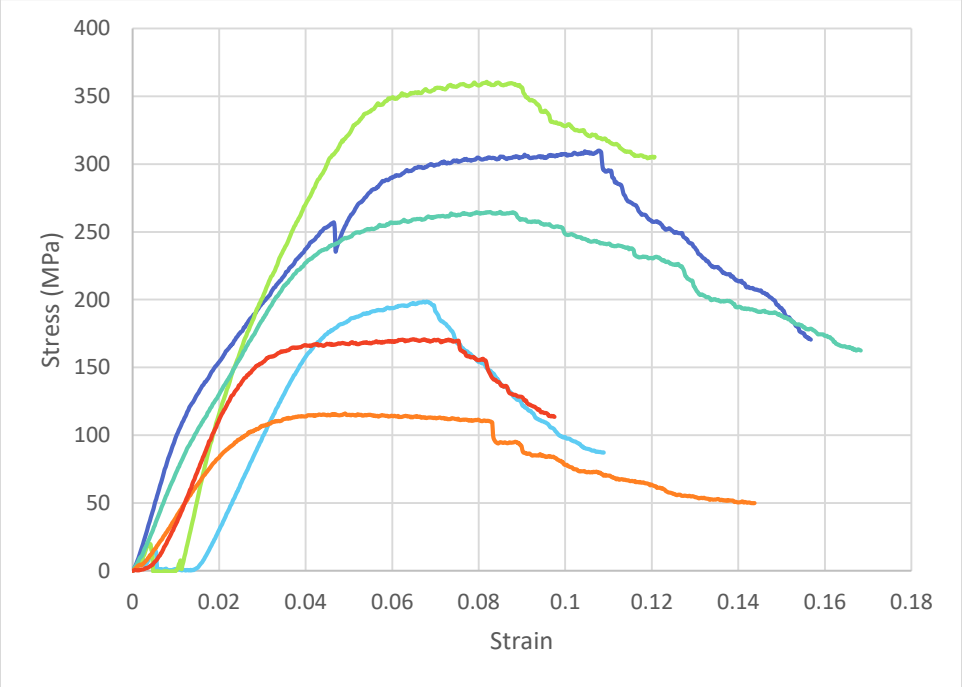

ε (%)	σ (MPa)	E (GPa)
0.108	310.2	6.13
0.068	199.5	3.82
0.087	360.8	6.75
0.088	265.1	5.93
0.055	115.5	3.11
0.075	172.7	4.51

Myrtillocactus geometrizans

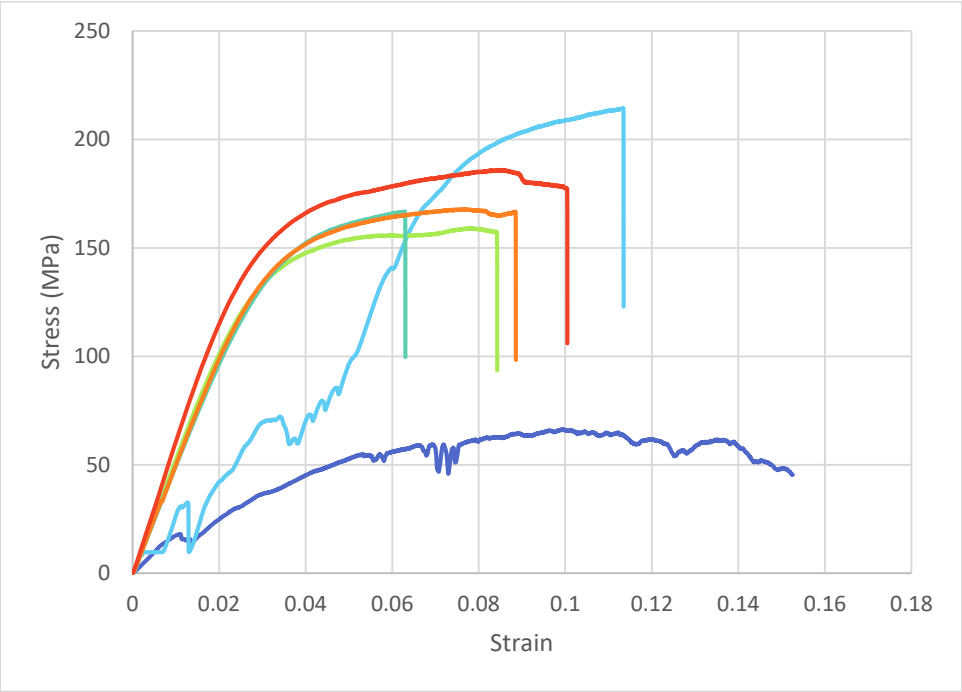

ε (%)	σ (MPa)	E (GPa)
0.102	66.5	1.37
0.113	214.5	2.63
0.078	159.2	5.23
0.063	166.8	4.94
0.076	167.8	5.02
0.086	185.9	6.04

Oreocereus celsianus

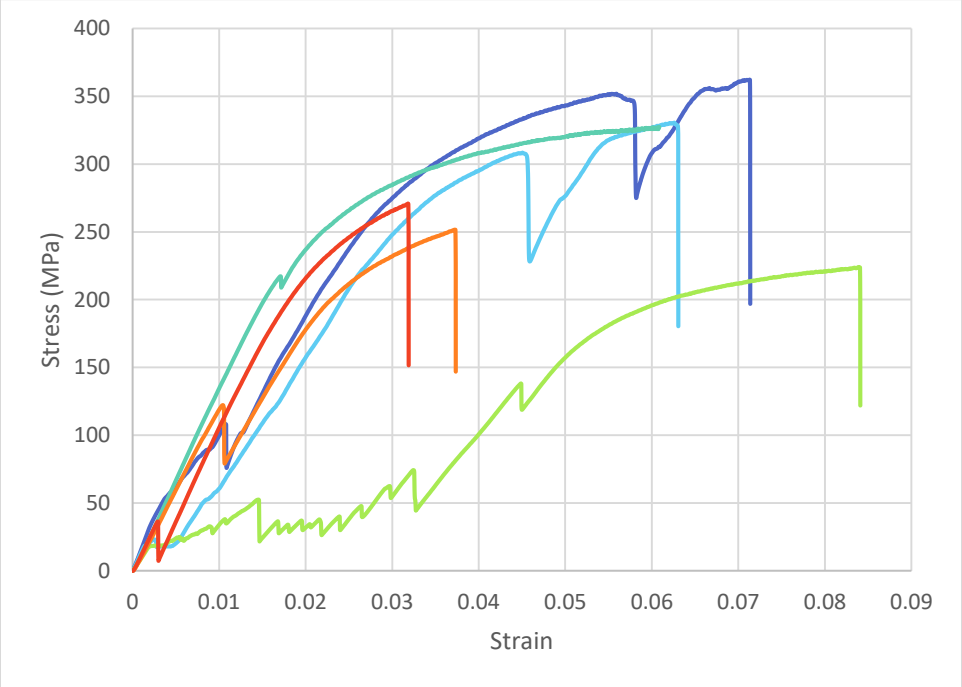

ε (%)	σ (MPa)	E (GPa)
0.056	352.1	9.93
0.045	308.8	6.03
0.084	224.1	3.29
0.061	327.4	13.44
0.047	251.6	11.92
0.032	270.9	10.47

Pachycereus pringlei

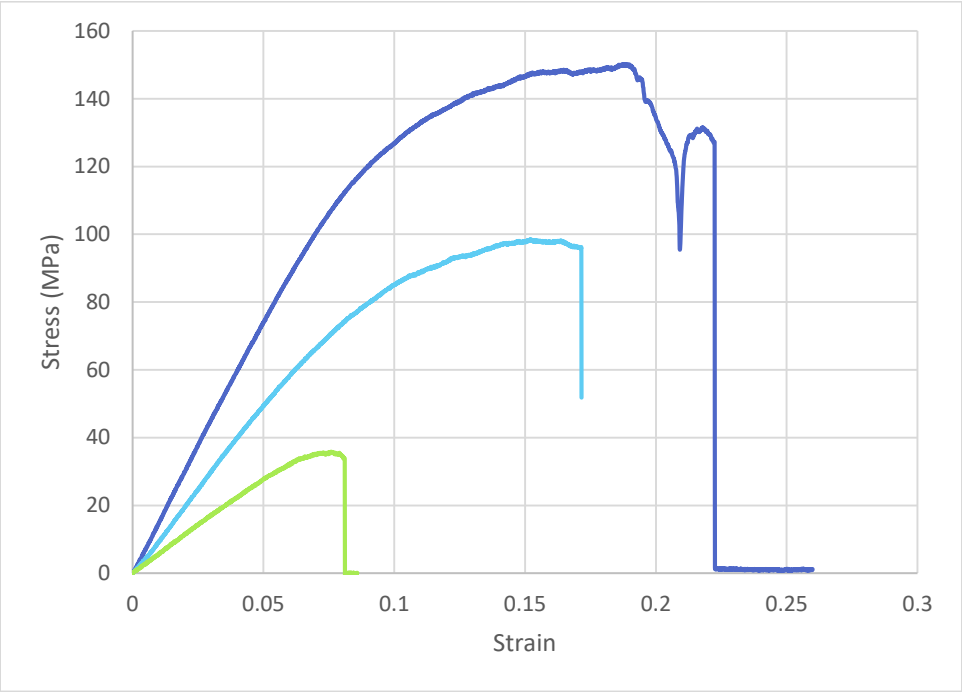

ε (%)	σ (MPa)	E (GPa)
0.046	359.1	26.16
0.027	296.1	21.00
0.015	118.6	14.66

Sclerocactus parviflorus

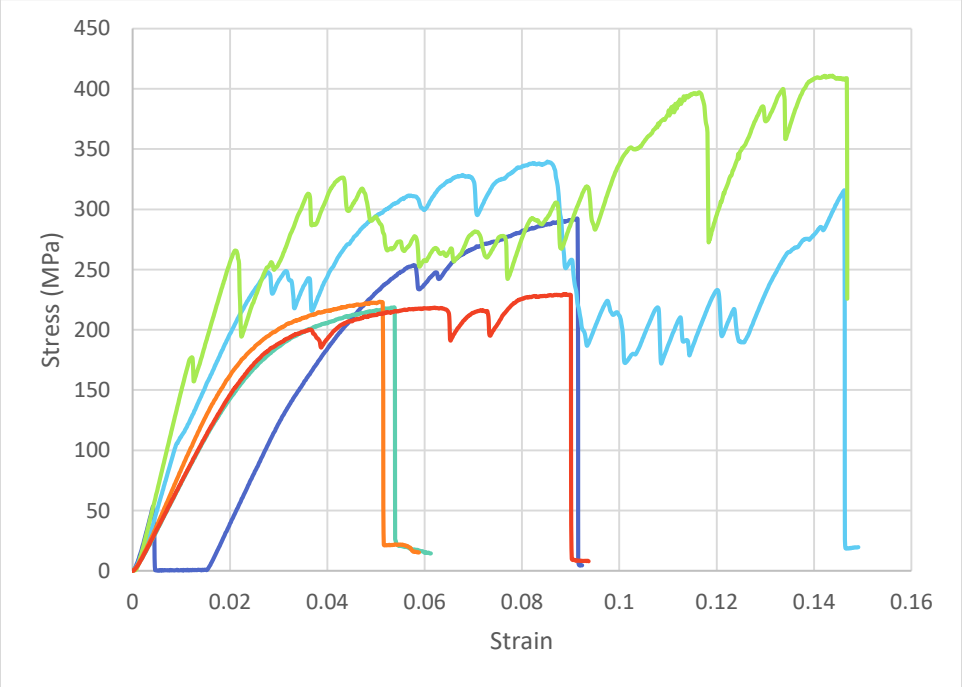

ε (%)	σ (MPa)	E (GPa)
0.091	294.7	3.33
0.146	318.0	9.26
0.147	412.9	9.04
0.054	219.8	6.68
0.051	224.1	7.38
0.090	229.5	6.84

Stenocactus crispatus

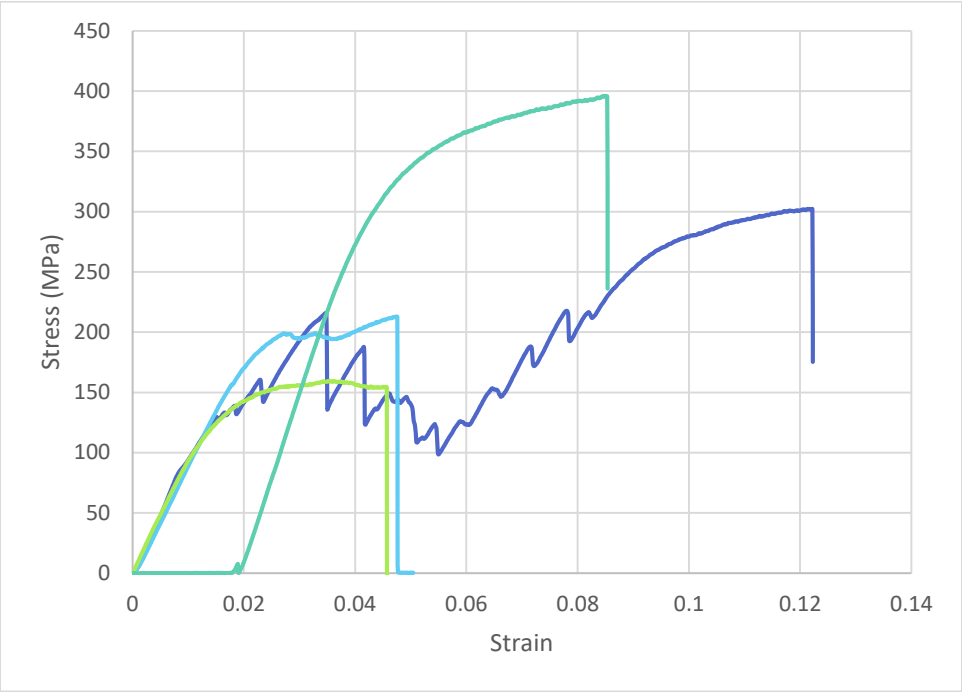

ε (%)	σ (MPa)	E (GPa)
0.122	302.8	6.21
0.048	213.2	7.78
0.101	300.7	6.80
0.037	160.1	5.02
0.051	242.7	8.33
0.044	243.9	9.28

Stenocereus thurberi

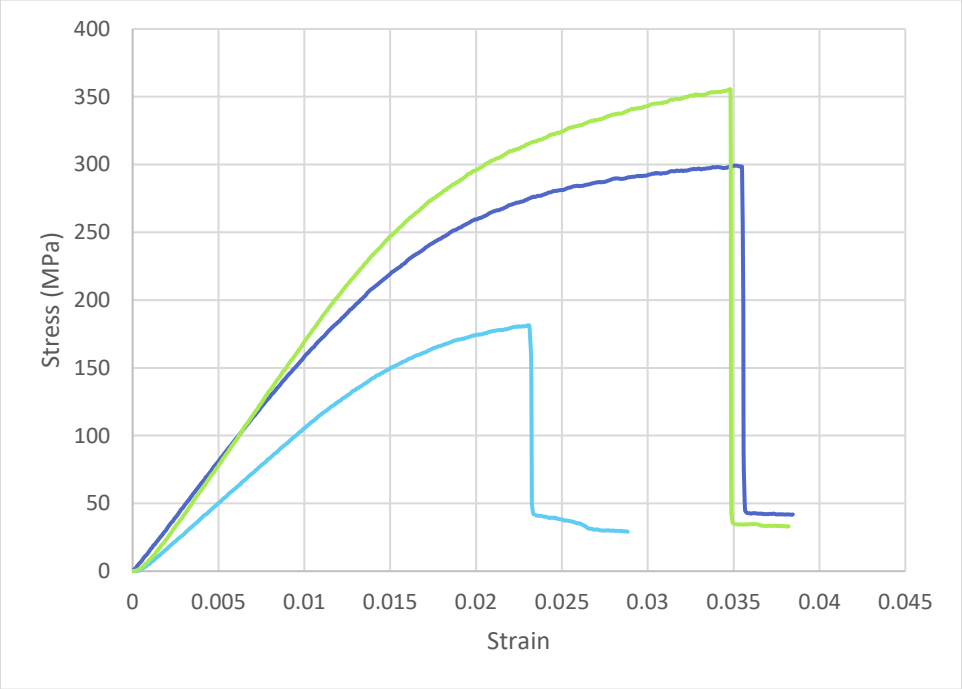

ε (%)	σ (MPa)	E (GPa)
0.066	172.5	14.28
0.041	245.6	23.00
0.046	261.9	19.46
0.057	209.6	15.13
0.018	218.1	17.34
0.040	216.8	12.37